THÈSE

En vue de l'obtention du

DOCTORAT DE L'UNIVERSITÉ DE TOULOUSE

Délivré par l'Université Toulouse 3 - Paul Sabatier

Présentée et soutenue par
Xu YANG
Le 19 septembre 2019

Titre: Une étude expérimentale de la photoréduction du mercure atmosphérique dans des eaux de pluie
Title: An experimental study of atmospheric mercury photoreduction in rainfall

Ecole doctorale : **SDU2E - Sciences de l'Univers, de l'Environnement et de l'Espace**
Unité de recherche : **GET - Géosciences Environnement Toulouse**
Spécialité : **Géochimie d'Environnement**

Jury

M. Jeroen SONKE-DR2, GET-OMP, CNRS, TOULOUSE (Directeur)

Mme Laurence MAURICE-DR1, GET-OMP, IRD, TOULOUSE (Examinatrice)

M. Jiubin CHEN-Professor, ISESS, Tianjin University, Chine (Rapporteur)

M. Xuewu FU-Professor, SKLEG, CAS, Guiyang, Chine (Rapporteur

M. Aurélien DOMMERGUE-MCF, IGE Grenoble (Rapporteur)

Thèse dirigée par **Jeroen SONKE**

Abstract

Mercury (Hg) is an ubiquitous heavy metal which is highly toxic and causes great concern all over the world. Once Hg is emitted to the atmosphere by natural sources, anthropogenic sources and re-emitted sources, it can experience a series of redox processes and deposit back to the Earth's surface. Early atmospheric Hg model simulations indicated that atmospheric elemental Hg(0) emissions are oxidized by OH, ozone or halogens to more reactive divalent Hg(II) forms. Recent reports suggest that Hg(0) is oxidized to Hg(II) by a Br-induced two-stage reaction and results in formation of a series of end products of Hg(II)XY complexes (e.g., $HgCl_2$, HgBrOH, $HgBr_2$, HgBrI, HgBrCl, $HgBrNO_2$, HgBrONO, HgBrOOH, HgBrOBr, HgBrOI, HgBrOCl). Photoreduction of atmospheric Hg(II) compounds back to Hg(0) competes with Hg(II) deposition and changes the magnitude and pattern of atmospheric Hg(II) deposition via rainfall and dry deposition. Hg(II) photoreduction is therefore important to understand. Photoreduction of atmospheric Hg(II) compounds can take place in both aqueous phase and gaseous phase. To balance fast oxidation of atmospheric Hg(0), a fast aqueous photoreduction of atmospheric Hg(II) complexes is assumed in cloud water and optimized in atmospheric Hg models. However, lab or field observation for this process is lacking. The objectives of this PhD research are to conduct aqueous phase photoreduction of atmospheric Hg(II) complexes in rainfall.

Photoreduction experiments of simulated rainfall solutions containing known amounts of Hg, halides (Cl, Br, I) and DOC (dissolved organic carbon) indicated that the presence of halides bound to Hg(II) inhibits Hg(II) photoreduction. Rainwater Hg(II) photoreduction rates, under fully sunlit conditions, are an order of magnitude slower than the optimized maximum in-cloud

photoreduction rate of > 1.0 h^{-1} in global Hg models. The ensemble of observations suggests that atmospheric gaseous $HgBr_2$, $HgCl_2$, $HgBrNO_2$, $HgBrHO_2$ forms, scavenged by aqueous aerosols and cloud droplets, are converted to Hg(II)-DOC forms in rainfall due to abundant organic carbon in aerosols and cloud water. Aqueous phase photoreduction of Hg(II)-DOC complexes is the dominant reduction pathway within clouds and rainfall and proceeds at reaction rates that are slower than in terrestrial and marine waters, likely due to different origin and molecular structure of atmospheric DOC. The model results based on the observed rainfall Hg(II) photoreduction rate constants indicated that photoreduction of Hg(II)-DOC in aqueous aerosols and clouds is too slow to balance fast oxidation of atmospheric Hg. Our collaborators have in parallel made theoretical estimates of the gas phase photolysis rates of Hg(II) compounds. The results of our combined studies show that gas phase photolysis of Hg(II) compounds can be fast, and is fast enough to rebalance the GEOS-Chem modeled atmospheric Hg cycle between Hg(0) oxidation and Hg(II) reduction.

Key words:

Mercury, redox reaction, rainwater, divalent speciation, photoreduction rate, halide, organic carbon, atmospheric model

Résumé

Le mercure (Hg) est un métal lourd omniprésent et hautement toxique, lequel suscite de vives inquiétudes dans le monde entier. Une fois que le Hg est émis dans l'atmosphère par des sources naturelles, des sources anthropiques et des sources réémises, il peut subir une série de processus d'oxydoréduction et se déposer à la surface de la Terre. Les premières simulations de modèles atmosphériques du Hg ont indiqués que le Hg(0) atmosphérique est oxydé par OH, l'ozone ou les halogènes. Un rapport récent propose que le Hg(0) est principalement oxydé en complexes de Hg(II) par une réaction en deux étapes induite par le Br et aboutit à la formation d'une série de produits finaux de complexes de Hg(II)XY (par exemple, $HgCl_2$, HgBrOH, $HgBr_2$, HgBrI, HgBrCl, $HgBrNO_2$, HgBrONO, HgBrOOH, HgBrOBr, HgBrOI, HgBrOCl). La photoréduction des composés atmosphériques de Hg(II) entre ensuite en compétition avec les dépôts de Hg(II) ce qui modifie l'ampleur et la variabilité des dépôts atmosphériques de Hg(II) par voie humide (pluie) et par voie sèche (poussières). La photoréduction des composés atmosphériques de Hg(II) pourrait avoir lieu à la fois en phase aqueuse et en phase gazeuse. Pour équilibrer l'oxydation rapide du Hg(0) atmosphérique, on suppose une photoréduction aqueuse rapide des complexes de Hg(II) dans les nuages et optimisée dans le modèle CTS. Cependant, l'observation en laboratoire ou sur le terrain de ce processus est manquante. Les objectifs de cette thèse sont de déterminer les vitesses de photoréduction en phase aqueuse de complexes atmosphériques de Hg(II) dans la pluie.

Des expériences de photoréduction des eaux de pluies simulées contenant des quantités connues de Hg, d'halogénures (Cl, Br, I) et de DOC (carbone organique dissoute) ont montré que la présence d'halogénures inhibe la photoréduction de Hg(II). Les taux de photoreduction des eaux de pluie, dans des conditions d'ensoleillement total, sont d'un ordre de grandeur inférieur au taux optimisé de photoreduction dans les nuages > 1,0 h^{-1} dans les modèles globaux de Hg. L'ensemble

des observations suggère que les formes $HgBr_2$, $HgCl_2$, $HgBrNO_2$, $HgBrHO_2$ gazeuses atmosphériques, absorbées par les aérosols aqueux et les gouttelettes de nuages, sont converties en formes Hg(II)-DOC dans les précipitations en raison de l'abondance de carbone organique dans les aérosols et les eaux de nuages. La photoréduction en phase aqueuse des complexes Hg(II)-DOC est la principale voie de réduction dans les eaux atmosphériques. Elle s'effectue à une vitesse de réaction plus lente que dans les eaux terrestres et marines, probablement en raison de l'origine et de la structure moléculaire différentes du DOC atmosphérique. Les résultats du modèle basés sur les constantes de vitesse de photoréduction du Hg(II) observées dans les précipitations ont indiqué que la photoréduction du Hg(II)-DOC dans les aérosols et les nuages aqueux est trop lente pour équilibrer l'oxydation rapide du Hg(0) atmosphérique. Nos collaborateurs ont estimés théoriquement les vitesses de photolyse du Hg(II) en phase gazeuse. Les résultats de nos études combinées montrent que la photolyse en phase gazeuse de composés de Hg(II) peut être rapide et suffisamment rapide pour rééquilibrer le cycle de Hg atmosphérique modélisé.

Mots clés:

Mercure, réaction redox, eaux de pluie, précipitation, spéciation, cinétique de réduction, halogènes, carbone organique, modèle atmosphérique

Acknowledgement

At the end of my Ph.D study, I foremost would like to express my deep appreciation to my supervisor, for the continuous guidance of my Ph.D study and research. I marveled at his immense knowledge on mercury science and talent on mercury research. His enthusiasm, patience and motivation in my daily life and research work encouraged me a lot. Without his help, I could not have imagined finishing my Ph.D study here and getting the final Ph.D degree. I really would like to thank Martin Jiskra who gave a lot of advice and assistance on my experiment scheme and work. My grateful thanks are also extended to our mercury group members, David Point, Nicolas Marusczak, Maxime Enrico, and Laure Laffont in the GET lab.

I would also like to thank the China Scholarship Council (CSC) for this PhD grant and European Union´s Horizon 2020 Research and innovation programme (ERC-2010-STG 258537) and H2020 ERA-PLANET (689443) iGOSP programme to support my Ph.D study.

Finally, I would like to thank my family members. They are all my strong support for my Ph.D study.

Table of contents

List of abbreviations

Hg	**Mercury**
MeHg	**Methylmercury**
GEM, Hg(0)	**Gaseous Elemental Mercury**
GOM and RGM, $Hg(II)_g$	**Gaseous Oxidized Mercury and Reactive Gaseous Mercury**
PBM, $Hg(II)_p$	**Particle-bound Mercury**
GEOS-CHEM	**Goddard Earth Observing System-Chemistry**
CTM	**Chemistry and Transport Model**

Chapter 1. Introduction

This Chapter is an overview of Hg characteristics and Hg transport and transformation mechanisms in the environment including Hg toxicity, atmospheric Hg sources and deposition, atmospheric Hg redox processes, and global atmospheric Hg model development.

1.1. Global Hg cycle

Mercury(Hg) is an unusual persistent and toxic heavy metal contaminant for human and ecosystem health damages that has been of great concern to the public and policy makers (Streets et al. 2017). Hg is released to troposphere mainly as Hg(0) (Gaseous Elemental Mercury, GEM), less as Hg(II) (including Gaseous Oxidized Mercury ($Hg(II)_g$) and Particulate Bound Mercury ($Hg(II)_p$)) by natural, anthropogenic and remitted sources (Horowitz et al. 2017b). Subsequently, a small fraction of Hg(0) will be vertically released to stratosphere and further oxidized to Hg(II), and finally deposited back to troposphere (Horowitz et al. 2017b). Different Hg species in the atmosphere result in different physicochemical properties (e.g., solubility, chemical activity, atmospheric lifetime) (Ariya et al. 2015a). Hg(0) is relatively insoluble, inert and has a long residence time of several months to a year in the atmosphere compared to Hg(II) (Schroeder and Munthe 1998, Lin and Pehkonen 1999b). It can undergo regional and worldwide transport by atmospheric circulation due to its long lifetime in the atmosphere, and be directly absorbed by plants and oceans (Jiskra et al. 2018b). Hg(0) can also be oxidized to Hg(II), which readily partitions into particles associated with aerosols and clouds and deposits to terrestrial and aquatic systems associated with dry and wet mechanisms. The oxidation of Hg(0) to Hg(II) results in reactive, soluble Hg species with shorter atmospheric residence times of a few days to a few weeks (Ariya et al. 2015a). Following atmospheric Hg deposition, a portion of Hg in the aquatic ecosystems will be transformed into neuro-toxic monomethyl-mercury (MeHg), which can be further bioaccumulated and biomagnified along aquatic food chains and poses a threat to human and wildlife health (Feng and Qiu 2008). A fraction of Hg circulates in the aquatic system and continues to deposit to deep-water sediment (Selin 2009). Hg(II) and Hg(II) compound existed in the atmosphere and deposited in the terrestrial and aquatic systems can be remitted to atmosphere after

reduction to Hg(0) (Si and Ariya 2018). Hg has been defined as a global pollutant due to its long-range transport and subsequent deposition, persistence in the environment, accumulation and magnification in the food chains, adverse effect on human and ecosystem health (Liu, Cai and O'Driscoll 2012).

The inventory of Hg emission to atmosphere by natural, anthropogenic and reemitted processes has been widely studied (Streets et al. 2017, UNEP 2013a). The major global atmospheric Hg reservoir is 3900Mg. $year^{-1}$ including 3500Mg. $year^{-1}$ Hg(0) and 400Mg. $year^{-1}$ Hg(II), which indicates that Hg(0) is the predominant form of atmospheric Hg emission (7490 Mg. $year^{-1}$, figure 2). Amounts of atmospheric Hg emission from all sources were defined in a wide range (5000-6000 Mg. $year^{-1}$) due to the uncertainties of Hg sources and poor understand of atmospheric Hg(0)/Hg(II) redox reactions (Horowitz et al. 2017b). As a result, Hg emissions were overestimated or underestimated in the model compared to the observed values. Emissions of natural, anthropogenic and reemitted sources account for 3%, 27% and 70% of total annual emission respectively (figure 3), which indicated that reemitted sources are the predominant pathways of atmospheric Hg emission, much larger than natural sources and anthropogenic sources.

Natural source of atmospheric Hg is an important sources for Hg(0) emission. The release of natural process is constituted by 250Mg. $year^{-1}$ including the weathering of Hg-containing rocks, geothermal activity and volcanism (Streets et al. 2017). Anthropogenic sources are widely distributed on the earth surface including artisanal and small-scale gold mining, coal burning, ferrous and non-ferrous metals production, cement production. Anthropogenic source is not only an important source for Hg(0) emission, but also a dominant source for Hg(II) emission. Total annual emission of anthropogenic Hg is about 2270Mg. $year^{-1}$, which consists of 1470Mg. $year^{-1}$ Hg(0) and 800Mg. $year^{-1}$ Hg(II). Emission of deposited mercury from oceans, lakes, rivers and soils is an important natural process, called re-emitted sources. Both natural and anthropogenic sources are potential re-emitted sources. Total annual emission of reemitted part is 6020Mg $year^{-1}$, which refers to 4600Mg $year^{-1}$ ocean sources, 1200Mg $year^{-1}$ vegetation, soil, and snow sources, 220Mg $year^{-1}$ forest or biomass

burning sources (Figure 1). Hg absorbed by plant can be reemitted to air by forest or biomass burning. Ocean is an important atmospheric Hg reservoir that contributes a large number of Hg(0) (54%, figure 1) and inputs large number of atmospheric Hg (Obrist et al. 2018). It has been reported that Hg(0) evasion from ocean is induced by reduction of dissolved Hg(II). But the detailed reduction pathway and mechanism of oceanic Hg is not very clear due to the low concentration of Hg and complicated physical-chemical properties in the ocean. More work is needed to conform reduction emission of oceanic Hg to atmosphere, to better establish database for global atmospheric Hg model development.

Deposition of atmospheric Hg(0) and Hg(II) to earth surface is an important process for Hg exchange between the atmosphere and terrestrial and aquatic systems (Ariya et al. 2015a). Hg(0) and Hg(II) (including $Hg(II)_g$ and $Hg(II)_p$) can be deposited to terrestrial and aquatic systems by wet and dry processes and absorption of plants and oceans (Jiskra et al. 2018b). Hg deposition is an important pathway for Hg input to ocean, which results in 54% Hg(II) deposition to ocean from atmosphere (Obrist et al. 2018). Hg(0) uptake by plants is a potential pathway for sink of atmospheric Hg to terrestrial environment (Jiskra et al. 2018b).

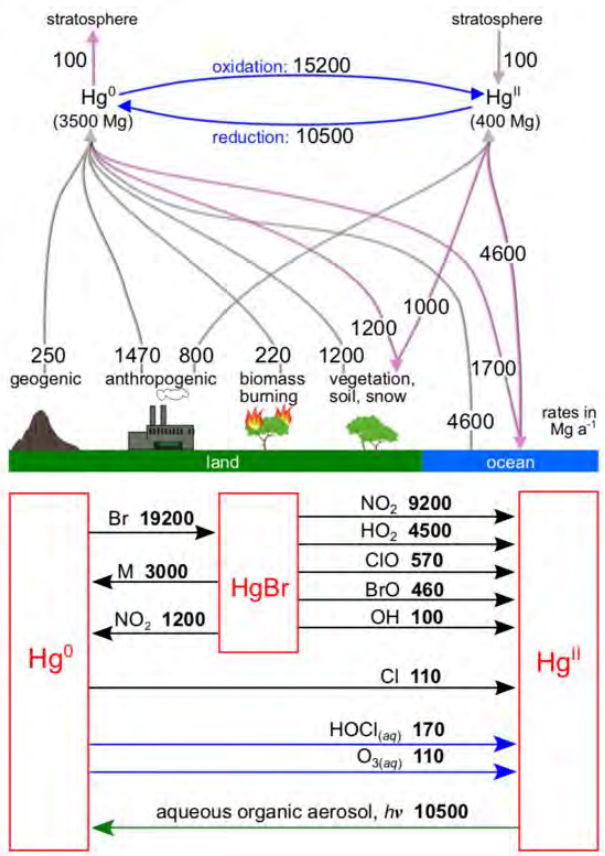

Figure 1 *Global budget of tropospheric mercury in the GEOS-Chem 3D Hg model. Hg^{II} includes gaseous and particulate forms in local thermodynamic equilibrium (Amos et al., 2012). The bottom panel identifies the major chemical reactions from Table 1 cycling Hg^0, Hg(I) and Hg^{II}. Hg masses are in Mg, and rates (fluxes) in Mg yr^{-1}. Reactions with global rates lower than 100 Mg yr^{-1} are not shown. (Figure from Horowitz et al., 2017)*

In the figure 1, the total input of Hg(0) and Hg(II) from atmospheric environment to terrestrial environmental is about 2200Mg.year^{-1}, which is much lower than the amount of 3200 Mg.year^{-1} achieved from recent research (Obrist et al. 2018). But the remission of Hg from terrestrial environmental to atmospheric environment is approximately 1420 Mg.year^{-1}, which is consistent with the range of 1700-2800 Mg.year^{-1} achieved from recent research (Selin 2009, Liu et al. 2012, Amos et al. 2013, Mason et al. 2012, Smith-Downey, Sunderland and Jacob 2010).

Hg, especially methylmercury is highly toxic on human and ecosystem health (Liu et al. 2012). Both inorganic Hg and MeHg can be accumulated and biomagnified through food chains (Figure 4). In the figure 4, the concentrations of Hg and MeHg in the aquatic system is in the range of 1-5ppt and 0.05-1.0ppt respectively. As a result, the concentrations of Hg and MeHg in the high trophic level of Bass have reached in the range of 500-5000ppb for both inorganic Hg and MeHg species. Inorganic Hg and MeHg have accumulated 10^5-$5*10^6$ and $5*10^5$-10^8 times respectively. Human history has experienced two notorious Hg poisoning events, which resulted in serious diseases and casualties. One

of them is the Minamata incident, which was caused by the release of highly toxic MeHg in industrial wastewater from the 1930s to the 1960s in Minamata, Japan. The other event is the Iraqi disaster in 1971, where organo-mercury fungicide treated seed grains were consumed by humans. Consumption of fish is a dominant pathway for human exposure to MeHg (Kessler 2013).

In order to reduce mercury emissions and limit mercury pollution, a global treaty named UNEP Minamata Convention was signed by 126 countries in 2013 (UNEP 2013b). This treaty calls for more research on the source, transport and transformation of Hg in the environment as well as the relationship between Hg exposure and environmental variables.

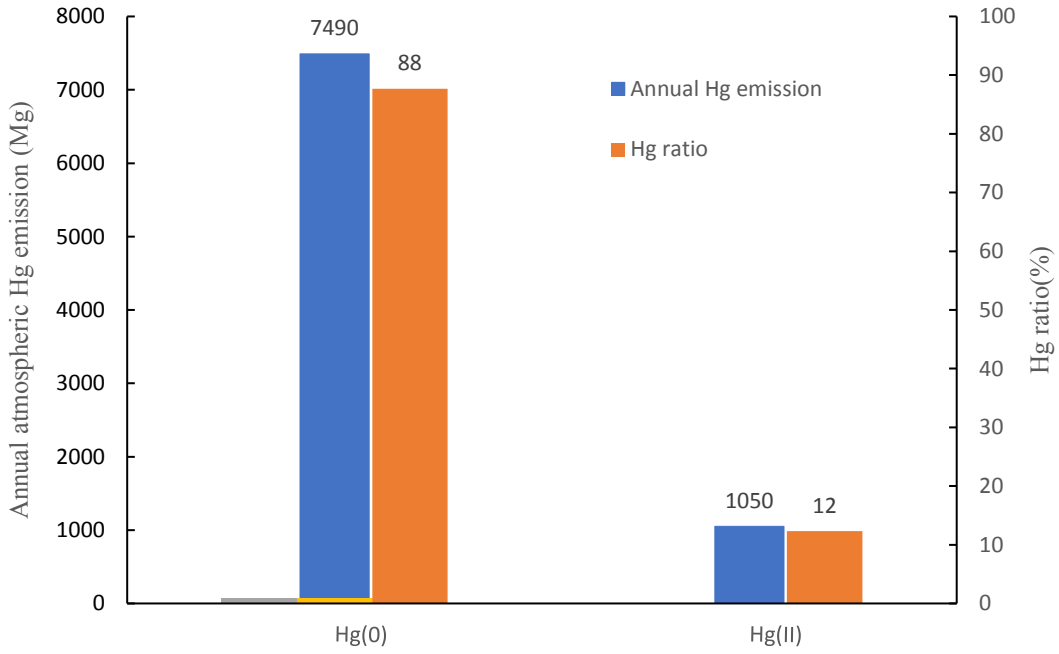

Figure 2 Amount and ratio of *annual global Hg(0)/Hg(II) emission. Data are from Horowitz et al., 2017 (Horowitz et al. 2017b). Hg(0) is emitted from anthropogenic and re-emitted sources, Hg(II) is emitted from natural and anthropogenic sources.*

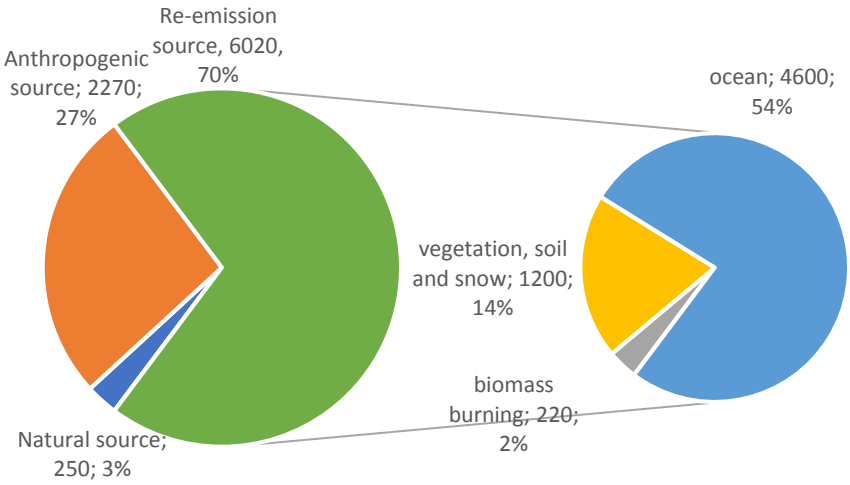

Figure 3 *Annual global atmospheric Hg emission from natural source, anthropogenic source, re-emission source. Data are extracted from Horowitz et al., 2017 (Horowitz et al. 2017b). Natural source is geogenic source, re-emitted sources refer to ocean, vegetation, soil, snow and biomass burning.*

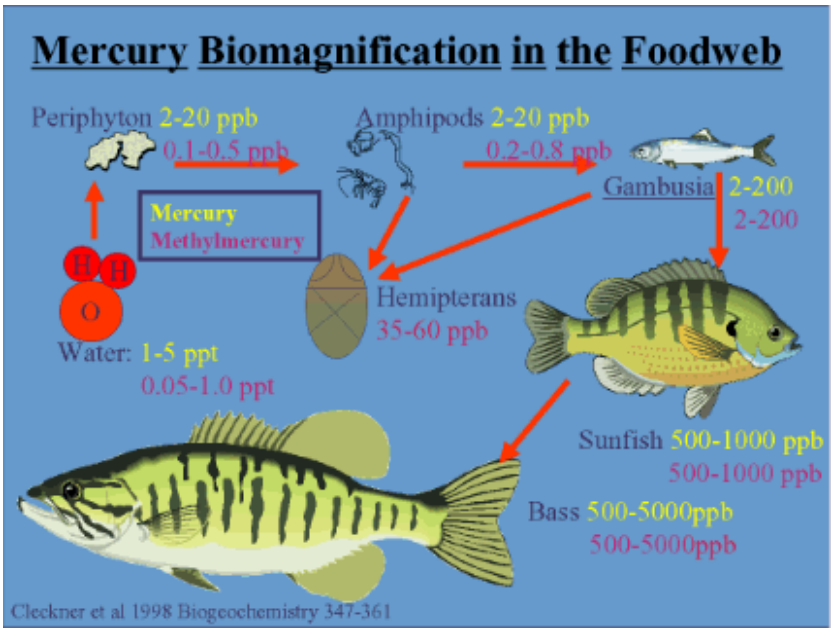

Figure 4 *Mercury biomagnification in the food web. From Cleckner et al., 1998. Trophic transfer of methylmercury in the northern Everglades. Biogeochemistry, vol40, pp.347-361.*

1.2. Redox reactions of atmospheric Hg

Once Hg is emitted to atmosphere, it can undergo a series of redox processes, modifying atmospheric Hg speciation, transport and deposition (Ariya et al. 2015a). Chemistry transport model (CTMs) is an important tool for understanding global Hg cycle and predicting Hg exposure, has drawn much attention on Hg(0) oxidation and Hg(II) reduction (Horowitz et al. 2017b, Dibble, Zelie and Mao 2012a, Lin and Pehkonen 1999b, Wang et al. 2014b). There are many potential Hg(0) oxidants, such as O_3, OH, HO_2, H_2O_2, NO_2, NO_3. But Hg(0) is thought to be oxidized to Hg(II) by a two-stage Br-induced reaction (Horowitz et al. 2017b, Wang et al. 2014b, Holmes, Jacob and Yang 2006b) (Figure 1). First, Hg(0) is oxidized to intermediate Hg(I)Br, which is very unstable, and can be readily dissociated back to Hg(0). Hg(I)Br can also be further oxidized to Hg(II) complexes by a series of atmospheric radicals (e.g., OH, Br, I, Cl, NO_2, HO_2, BrO, IO, ClO). As a result, a series of end products of Hg(II)XY complexes (e.g., $HgCl_2$, HgBrOH, $HgBr_2$, HgBrI, HgBrCl, $HgBrNO_2$, HgBrONO, HgBrOOH, HgBrOBr, HgBrOI, HgBrOCl, HgO) including halogen atoms and oxygen-containing species are produced (Horowitz et al. 2017b). Variations of Hg(0) oxidation has been implemented in the global Hg CTMs and resulted in a short residence time of atmospheric Hg, which is not matched to observations (Horowitz et al. 2017b).

Aqueous phase Hg(II) photoreduction has been widely observed in the earth surface water (Qureshi et al. 2011b). Reduction of Hg(II) to Hg(0) in the aquatic system is dominated by abiotic and biotic processes (Qureshi et al. 2011b, Amyot et al. 1994, Zhang and Lindberg 2001, Amyot et al. 2004, Mason, Morel and Hemond 1995, Siciliano, O'Driscoll and Lean 2002). Biotic processes include microbially mediated reduction, heterotrophic bacterial and algae reduction (Rolfhus and Fitzgerald 2004). Abiotic processes are dominated by photochemically mediated reactions (Amyot et al. 2000). Photoreduction of Hg(II) is strongly dependent on light wavelength and intensity (Garcia et al. 2005). Compared to visible light, ultraviolet radiation (UV) was reported to be more efficient for photoreduction of Hg(II) (Amyot, Gill and Morel 1997, Lalonde et al. 2004, O'Driscoll et al. 2006). Dissolved Organic Matter (DOM) is widely distributed in the aquatic environment and

can strongly bind with mercury (Ravichandran 2004). It has been reported that Hg must bind to dissolved organic matter (DOM) before photoreduction could take place (Costa and Liss 1999) (Allard and Arsenie 1991). Hg(II) could be photoreduced by two mechanisms. First, Hg(II) or Hg(I) is directly reduced by ligand metal charge transfer (LMCT). Second, Hg(II) is reduced by a formed reactive intermediate (e.g., $OH_2\cdot$).

Inorganic (e.g., halides) and organic ligands (e.g., DOM) are widely present in the aquatic system. Dissolved divalent Hg is readily bound to different kinds of inorganic and organic ligands and forms Hg-inorganic and Hg-organic complexes. The binding of Hg to different ligands and sites determines the amount of reducible form of Hg(II) complexes (O'Driscoll et al. 2006). The introduction of light wavelength and intensity would further influence photoreducible form of Hg(II) complexes. The process of Hg(II)-DOM photoreduction would be inhibited in the presence of halide ligands due to the binding competition between Hg-DOM complexes and Hg(II)-halide complexes (Allard and Arsenie 1991).

Reduction of atmospheric Hg(II) compounds is poorly understood. Little experimental observational resulted in the lack of reduction kinetics and mechanisms in the atmospheric liquid water (Pehkonen and Lin 1998a, Seigneur, Vijayaraghavan and Lohman 2006b). Aqueous SO_3 and HO_2 have been considered dominant reductants for atmospheric Hg(II) reduction (Pehkonen and Lin 1998a). But aqueous reduction of atmospheric Hg(II) by SO_3 and HO_2 are denied due to their irrelevance of global scale (Horowitz et al. 2017b). To balance fast Hg(0) oxidation in the model, a fast aqueous-phase photoreduction of atmospheric Hg(II) compounds has been assumed in cloud and the reduction rates are optimized in Global Hg CTMs (Selin et al. 2007a, Horowitz et al. 2017b) (Figure 1). Due to the fast reduction rate constants ($>\sim$1-3h^{-1}), the lifetime of in-cloud Hg(II) is <1h. Therefore, it is important to explore atmospheric aqueous Hg(II) reduction kinetics and mechanism and apply it for development of global Hg CTMs (Horowitz et al. 2017b, Seigneur et al. 2006b, Gardfeldt et al. 2003). In this PhD project we will address this data gap, by studying the

photoreduction rates of Hg(II) species in rainwater, and in experimental solutions containing halide ions (Cl, Br, I) and dissolved organic matter.

1.3. The objectives of this study

In order to validate fitted photoreduction rates of atmospheric Hg(II) in CTM models, photoreduction rate observations in rain water were made in this PhD research. Chapter 1 is an overview of Hg characteristics (atmospheric Hg transport and transformation, atmospheric Hg sources and deposition, Hg toxicity), redox reaction of atmospheric Hg (atmospheric Hg oxidation, dissolved Hg(II) reduction in the aquatic system, model development of aqueous phase reduction of atmospheric Hg(II)). The rainfall sampling and laboratory photoreduction experiments are detailed in Chapter 2. The results of these experiments are presented in detail in Chapter 3, and include additional, simulated rainwater experiments in the Hg – halide – DOC system, including thermodynamic equilibrium speciation calculations. In Chapter 4 we compare the photoreduction rates measured in the laboratory experiments (both simulated sunlight and real sunlight) with the photoreduction rate in Hg CTMs, and re-assess photoreduction fluxes of atmospheric aqueous Hg(II) and gaseous Hg(0) in these global Hg models. To do so, we collaborate with Spanish, American and Russian colleagues who are experts in Hg modeling, and who have performed all the model simulations. The rainfall photoreduction rates observed in Chapter 3, prove to be critical in revising modern atmospheric Hg models in Chapter 4. Chapter 5 closes this PhD thesis with a summary of conclusions and perspectives for future research.

Chapitre 1. Introduction

Il s'agit d'un aperçu des caractéristiques du mercure et des mécanismes de transport et de transformation du mercure dans l'environnement, notamment la toxicité atmosphérique du mercure, les sources et dépôts de mercure dans l'atmosphère, les processus d'oxydoréduction du mercure dans l'atmosphère et son fractionnement isotopique, ainsi que l'élaboration du modèle de mercure atmosphérique dans le monde.

1.1. Cycle global du mercure

Le mercure (Hg) est un contaminant persistant et toxique, responsable des dommages pour la santé de l'homme et des écosystèmes, qui préoccupe grandement le public et les décideurs (Streets et al. 2017). Le mercure est rejeté dans la troposphère principalement sous forme de Hg(0) (mercure élémentaire gazeux, GEM), et en une moindre fraction en Hg(II) (y compris le mercure oxydé gazeux ($Hg(II)_g$) et le mercure lié aux particules ($Hg(II)_p$)) par des origines naturelles, anthropiques et réémises (Horowitz et al. 2017). Les différentes espèces de mercure présentes dans l'atmosphère ont des propriétés physicochimiques différentes (par exemple, la solubilité, l'activité chimique, la durée de vie dans l'atmosphère) (Ariya et al. 2015). Le Hg(0) est relativement insoluble, inerte et a une longue durée de vie dans l'atmosphère de plusieurs mois à un an par rapport au Hg(II) (Schroeder et Munthe, 1998; Lin et Pehkonen, 1999). Le Hg(0) peut subir un transport régional et mondial par la circulation atmosphérique en raison de sa longue durée de vie dans l'atmosphère et être directement absorbé par les plantes et les océans (Jiskra et al. 2018). Le Hg(0) peut également être oxydé en Hg(II), qui se dépose dans les systèmes terrestres et aquatiques associés aux mécanismes de dépôt secs et humides. L'oxydation du Hg(0) en Hg(II) se traduit par la création d'espèces de mercure solubles réactives présentant des temps de séjour dans l'atmosphère plus courts, de quelques jours à quelques semaines (Ariya et al. 2015). À la suite des dépôts atmosphériques de mercure, une partie de celui-ci dans les écosystèmes aquatiques sera transformée en monométhyle-mercure (MeHg) neurotoxique, qui peut être bioaccumulé et bioamplifié le long des chaînes alimentaires aquatiques et constitue une menace pour la santé humaine et de la faune (Feng et Qiu 2008). Une fraction de mercure circule dans le

système aquatique et se déposera dans les sédiments marins profonds (Selin 2009). Les composés en Hg(II) présents dans l'atmosphère et déposés dans les systèmes terrestre et aquatique peuvent être remis dans l'atmosphère après réduction en Hg(0) (Si et Ariya 2018). Le mercure a été défini comme un polluant mondial en raison de son transport à longue distance et de ses dépôts ultérieurs, de sa persistance dans l'environnement, de son accumulation dans les chaînes alimentaires, et de ses effets néfastes sur la santé humaine et des écosystèmes (Liu, Cai et O'Driscoll 2012).

1.2. Réactions redox du Hg atmosphérique

Une fois que le mercure est émis dans l'atmosphère, il peut subir une série de processus rédox, modifiant la spéciation, le transport et le dépôt de mercure dans l'atmosphère (Ariya et al. 2015). Le modèle de transport chimique (CTM) est un outil important pour la compréhension du cycle global du mercure et la prévision de l'exposition au mercure. De nombreux travaux ont été réalisés sur l'oxydation du Hg(0) et la réduction du Hg(II) (Horowitz et al. 2017, Dibble, Zelie et Mao 2012, Lin et Pehkonen 1999, Wang et al. 2014). Il existe de nombreux oxydants potentiels pour le Hg(0), tels que O_3, OH, HO_2, H_2O_2, NO_2, NO_3. Cependant, on pense que le Hg(0) s'oxyde en Hg(II) par une réaction induite par le Br en deux étapes (Horowitz et al. 2017, Wang et al. 2014, Holmes, Jacob et Yang 2006). Premièrement, le Hg(0) est oxydé en un Hg(I)Br intermédiaire, qui est très instable et peut être facilement dissocié en Hg(0). Le Hg(I)Br peut également être oxydé davantage en complexes Hg(II) par une série de radicaux atmosphériques (par exemple OH, Br, I, Cl, NO_2, HO_2, BrO, IO, ClO). En conséquence, une série de produits finis de complexes Hg(II)XY (par exemple, $HgCl_2$, HgBrOH, $HgBr_2$, HgBrI, HgBrCl, $HgBrNO_2$, HgBrONO, HgBrOOH, HgBrOB, HgBrOI, HgBrOI, HgBrOI, HgBrOl, HgBrOl, HgBrIOH, HgBrOO) (Horowitz et al. 2017). Des mécanismes d'oxydation du Hg(0) ont été mises en œuvre dans les CTMs globaux pour le mercure et ont abouti à un court temps de séjour du mercure dans l'atmosphère, ce qui ne correspond pas aux observations (Horowitz et al. 2017).

La photoréduction en phase aqueuse de Hg(II) a été largement observée dans les eaux terrestres et marines (Qureshi et al. 2011). La réduction du Hg(II) en Hg(0) dans le système aquatique est

dominée par des processus abiotiques et biotiques (Qureshi et al. 2011, Amyot et al. 1994, Zhang et Lindberg 2001, Amyot et al. 2004, Mason, Morel et Hemond 1995, Siciliano, O'Driscoll et Lean 2002). Les processus biotiques comprennent la réduction à médiation microbienne, la réduction par des bactéries hétérotrophes et des algues (Rolfhus et Fitzgerald, 2004). Le processus abiotique est dominé par la médiation photochimique (Amyot et al. 2000). La photoréduction du Hg(II) dépend fortement de la longueur d'onde et de l'intensité de la lumière (Garcia et al. 2005). Comparativement à la lumière visible, le rayonnement ultraviolet (UV) serait plus efficace pour la photoréduction du Hg(II) (Amyot, Gill et Morel 1997, Lalonde et al. 2004, O'Driscoll et al. 2006). La matière organique dissoute (DOM) est largement répandue dans l'environnement aquatique et peut se lier fortement au Hg(II) (Ravichandran 2004). Il a été rapporté que le mercure doit se lier à la matière organique dissoute (DOM) avant que la photoréduction puisse avoir lieu (Costa et Liss, 1999). Le Hg(II) pourrait être photo-réduit par deux mécanismes. Premièrement, le Hg(II) ou le Hg (I) est directement réduit par transfert de charge de métal à ligand (LMCT). Deuxièmement, le Hg(II) est réduit par un intermédiaire réactif formé (par exemple, $OH_2^{\cdot}$).

Les ligands inorganiques (par exemple les halogènes) et les ligands organiques (par exemple les substances humiques) sont largement présents dans le système aquatique. Le Hg divalent dissous se lie facilement à différents types de ligands inorganiques et organiques et forme des complexes Hg-inorganiques et Hg-organiques. La liaison de Hg à différents ligands et sites détermine la quantité de la forme réductible de complexes de Hg(II) (O'Driscoll et al. 2006). La longueur d'onde et l'intensité de la lumière influencerait davantage la forme photoréductible des complexes de Hg(II). Il a été rapporté que le Hg(II) devait se lier à la matière organique dissoute (DOM) avant que la photoréduction puisse avoir lieu (Allard et Arsenie, 1991). Le processus de photoréduction par Hg(II) -DOM serait inhibé en présence de ligands halogénés en raison de la compétition de liaison entre les complexes Hg-DOM et les complexes Hg(II) -halogène (Allard et Arsenie, 1991).

La réduction des composés atmosphériques de Hg(II) est mal comprise. Peu d'observations expérimentales ont élucidés les mécanismes dominantes de réduction du Hg(II) dans l'eau liquide

atmosphérique (Pehkonen et Lin 1998, Seigneur, Vijayaraghavan et Lohman 2006). Le SO_3 et le HO_2 aqueux ont été considérés comme des réducteurs dominants pour la réduction atmosphérique du Hg(II) (Pehkonen et Lin, 1998). Mais la réduction aqueuse de Hg(II) atmosphérique par SO_3 et HO_2 a été remise en question en raison de leur manque de pertinence à l'échelle globale (Horowitz et al. 2017). Pour équilibrer l'oxydation rapide du Hg(0) dans le modèle, une photoréduction rapide en phase aqueuse de composés atmosphériques de Hg(II) a été supposée dans les eaux de nuages, et les taux de réduction sont optimisés dans les modèles globaux du Hg (Selin et al. 2007, Horowitz et al. 2017). En raison des constantes rapides du taux de réduction dans les modèles ($> \sim$ 1-3 h^{-1}), la durée de vie du Hg(II) dans le nuage est inférieure à 1h. Par conséquent, il est important d'explorer la cinétique et le mécanisme de réduction du Hg(II) aqueux dans l'atmosphère et de les appliquer au développement de CTMs globaux pour le mercure (Horowitz et al. 2017, Seigneur et al. 2006, Gardfeldt et al. 2003). Dans ce projet de thèse, nous étudierons les taux de photoréduction des espèces de Hg(II) dans les eaux de pluie et dans les solutions expérimentales contenant des ions halogénés.

1.3. Les objectifs de cette étude

Afin de valider les taux de photoréduction optimisés du Hg(II) atmosphérique dans les modèles CTM, des expériences de photoréduction du Hg(II) dans l'eau de pluie ont été effectuées. Le chapitre 2 décrit les expériences d'échantillonnage des précipitations et de photoréduction en laboratoire. Les résultats de ces expériences sont présentés en détail au chapitre 3 et incluent des expériences supplémentaires simulées sur l'eau de pluie dans le système Hg-halogénure-DOC, y compris des calculs de spéciation d'équilibre thermodynamique. En chapitre 4, nous comparons les taux de photoréduction mesurés dans les expériences de laboratoire (lumière solaire simulée et réelle) avec le taux de photoréduction dans les modèles CTM du mercure, et nous évaluons l'impact des flux de photoréduction sur les concentrations de Hg(II) et de Hg(0) dans l'atmosphère. Pour ce faire, nous collaborons avec des collègues espagnols, américains et russes, experts en modélisation du mercure. Les taux de photoreduction des précipitations observés en chapitre 3 se révèlent déterminants pour la révision des

modèles de Hg atmosphériques modernes en chapitre 4. Le chapitre 5 clôture cette thèse par un résumé des conclusions et des perspectives des recherches futures.

Chapter 2. Experimental methods

Both indoor and outdoor experiments were carried out for photoreduction kinetics and are described in detail in this chapter. Simulated sunlight was used for indoor experiments, and outdoor experiments were exposed to natural sunlight. The objective of this study is to evaluate aqueous phase photoreduction rate constants of atmospheric Hg(II) in the rainwater. The whole experiment was divided into two steps with 2 years from 25 October, 2015 to September, 2017. In the first step, we carried out 23 groups of photoreduction experiment of simulated rainwater in the Hg-halide-DOC system under xenon lamp light condition from October, 2015 to September, 2016 including thermodynamic equilibrium speciation calculation of dissolved Hg(II) compounds. In the second step, we conducted 13 groups of photoreduction experiment of rainfall Hg in the GET lab using xenon lamp light and outside the GET lab with natural sunlight from October, 2016 to September 2017.

2.1. A scheme for photochemical reduction experiment

In order to measure gross photoreduction rate constants of simulated rainfall Hg and rainfall Hg, an adapted apparatus from Bergquist et al. (2007) was used shown in figure 5 (Bergquist and Blum 2007). Photochemical experiments were carried out in a 60mm diameter, 0.5 L quartz reactor with both simulated and natural sunlight. Indoor photochemical experiments were conducted in a climatized room(20°C) under a 40mm diameter of focused beam of xenon lamp light. Outdoor photochemical experiments were exposed to the natural sunlight irradiation form 10-18h in a full sun of summer time. In order to eliminate the influence of other light sources and dissolved oxygen, the reactor was covered with aluminium foil and purged with Hg-free argon gas at 80 mL min^{-1} to remove product Hg(0) within minutes during the experiment (O'Driscoll et al. 2006). Higher flow rates of 300 mL min^{-1} were tested and gave identical results, suggesting that the flow rate had no effect on the observed gross photoreduction rate. Subsamples were collected at different intervals over the course of the experiments. The produced Hg(0) products were collected in Hg absorber in case of atmospheric Hg

pollution. Dark control experiments were carried out under the same conditions in the absence of light irradiation.

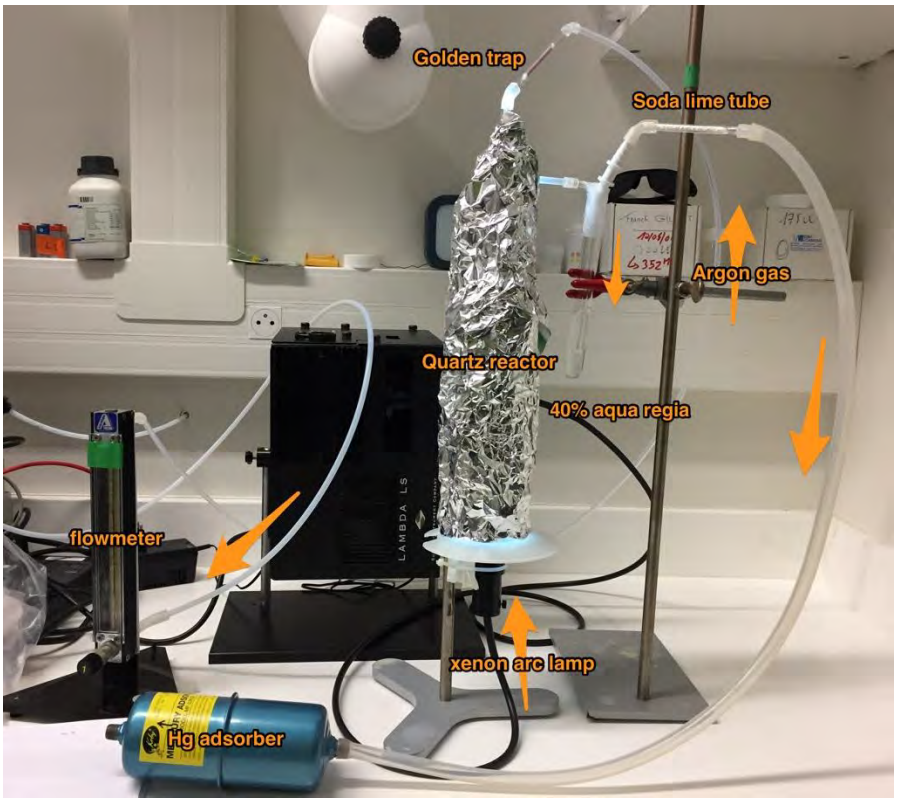

Figure 5 *Experimental apparatus used for photochemical reduction experiment*

2.2. Light source and light intensity measurement

For controlled indoor laboratory experiments, a Sutter Instruments Lambda LS solar simulator (Xenon lamp light) with Perkin Elmer 300W PE300BUV Xenon lamp was used to shine artificial solar light (in the UVA, UVB, UVC, VIS and IR range) in a 40mm focused beam through the reactor. Outdoor experiments were performed under natural sunlight (summertime, from 10-18h in full sun) outside the GET laboratory building in Toulouse, France. Two different light sources were intercompared with each other based on the experimental results. Light intensities of significant wavelengths of simulated and natural sunlight were measured with a solar light PMA 2200 radiometer, including PMA 2106, PMA 2110 and PMA 2130 for UV-B (280-320nm), UVA(320-400nm) and visible light(400-780nm) detector respectively.

2.3. Simulated and real rainfall samples

2.3.1. Simulated rain water preparation

Milli-Q water was used for the preparation of Hg solution, Hg and halogen solution, Hg, halogen and DOM solution with the addition of commercially available NIST 3133 $HgNO_3$, SRFA and halides (KCl, KBr, KI). The NIST SRM 3133 (10,000 μg g^{-1} Hg(II) in 10 vol.% HNO_3) was used as Hg standard, from which more diluted stock solutions were prepared. It is well known that NO_3^- can be photolyzed to form hydroxy radical (OH*) when light wavelength is greater than 290nm. OH* can further interact with DOM and halides to generate a variety of active radical, which can affect the photoreduction of dissolved Hg(II) compounds in the Hg-DOM-halide system. In order to check the influence of NO_3^- on photoreduction of dissolved Hg(II) compounds in the Hg-DOM-halide system, control experiment was conducted in the presence of 0.1mM KNO_3 or 5mM KNO_3 background electrolyte. As representative of natural DOC Suwannee river fulvic acid (SRFA) was obtained from the International Humic Substances Society and dissolved in MQ water for use a source of natural dissolved organic carbon (Maizel and Remucal 2017). KBr, KI and KCl salts were obtained from Sigma-Aldrich and diluted to 0.1 mM stock solutions. Experimental Hg/halide ratios were chosen to approximate the range of natural ratios.

2.3.2. Rainfall sampling, treatment, storage and preparation

There are 10 rainfall samples collected at two different sites in the summer of 2017 (July to August): 8 of them were collected in sub-urban Toulouse, France (43°33'41.10"N, 1°28'42.28"E) and the remaining two were collected at the high altitude (2877 m a.s.l.) Pic du Midi Observatory (PDM), France (42°56'10.85"N, 0° 8'32.76"E) (Fu et al. 2016b, Marusczak et al. 2017). Eight 36cm diameter x 40cm height acid-cleaned polypropylene buckets were used simultaneously following Enrico et al. (2016) for the collection of large volume of rain water from the beginning of a precipitation event to the end of the same precipitation event (Figure 6) (Enrico et al. 2016a). As a result, all the collected rainfall in 8 buckets were transferred to one bucket as a single rainfall event and stored in the 2L acid-cleaned pyrex bottles with GL45 caps as soon as possible. Each bucket was purified with 1%

HCl for 24h and sequently rinsed with MQ water for 3 times prior to precipitation sampling. The detailed information of collected rainfall from suburban Toulouse and Pic Du Midi Observatory is listed in table 1.

Figure 6 *Site A at suburban Toulouse, France and site B at high altitude (2877m.a.s.l) Pic du Midi Observatory (PDM) for rainfall sampling, and detailed sampling scheme of rain water*

Table 1 *detailed information of collected rainfall from suburban Toulouse and Pic Du Midi Observatory*

Label	type	date (time, dd/mm/yyyy)	event	site	volume (L)
Toulouse					
T-R1	rain	13:30, 3/6/2017-17:30, 3/6/2017	single	Surburban Toulouse (GET lab)	2.50
T-R2	rain	5:00, 9/6/2017-7:30, 9/6/2017	single	Surburban Toulouse (GET lab)	1.95
T-R3	rain	17:00, 26/6/2017-8:00, 27/6/2017	single	Surburban Toulouse (GET lab)	0.75
T-R4	rain	17:00, 27/6/2017-11:00, 28/6/2017	single	Surburban Toulouse (GET lab)	8.6
T-R5	rain	17:00, 28/6/2017-9:00, 29/6/2017	single	Surburban Toulouse (GET lab)	1.75
T-R6	rain	18:00, 19/7/2017-10:00, 20/7/2017	single	Surburban Toulouse (GET lab)	23.4
T-R7	rain	14:00, 24/7/2017-17:30, 24/7/2017	single	Surburban Toulouse (GET lab)	0.63
T-R8	rain	20:00, 30/8/2017-8:30, 31/8/2017	single	Surburban Toulouse (GET lab)	6.5
Pic du Midi					
PDM-R9	rain	5/9/2017-12/9/2017	multiple	Pic du Midi Observatory	1
PDM-R10	rain	26/9/2017-3/10/2017	multiple	Pic du Midi Observatory	1

Selected rainfall samples were filtered on pre-burnt 47mm quartz fiber filters (Millipore) in an acid-cleaned polycarbonate filtration unit (Fisher Scientific). Subsamples of filtered and unfiltered rainwater were taken for total Hg (THg, 10mL, acidified to 0.4 vol.% with bi-distilled 9N HCl, 0.5 vol% BrCl), TOC/DOC (20mL, acidified to 0.4 vol.% with 9N HCl), anions, pH (30mL,

unacidified), and major and trace metals (10mL, acidified to 2 vol.% 15.8N HNO3). Remaining rain samples were stored in the refrigerator in the dark at 4°C until analysis.

Rainfall experiments were done at both ambient Hg levels, and at 10× augmented Hg levels. Following sample addition, the reactor was wrapped with aluminum foil and equilibrated overnight. At the start of photoreduction experiment a sample aliquot (t=0) was taken and the reactor was exposed to natural sunlight outdoors (up to 8h) or to a solar simulator indoors (up to 48h).

2.3.3. pH measurement

The pH of all the rain samples and experimental solutions were measured as soon as possible after collection and preparation using an Orion pH electrode, calibrated against NIST traceable standards of pH 4 and 7 at GET, Toulouse, France.

2.3.4. Ions (cations and anions) measurement

Major cations in rainfall and experimental solutions were analyzed by high resolution ICP-MS (Thermo-Scientific Element-XR) at OMP, Toulouse, France. Anions were analyzed by ion exchange chromatography at EcoLab, Toulouse, France.

2.3.5. DOC measurement

DOC or TOC was measured on a total organic carbon analyzer (Shimadzu TOC VSCN) at GET, Toulouse, France.

2.3.6. Hg concentration measurement

Artificial rain water, rainfall and photochemical samples were analyzed for Hg concentration in duplicate following U.S. EPA method 1631 by cold vapor atomic fluorescence spectrometry (CV-AFS) (Agency 2002). All the samples were digested by $BrCl_2$ overnight for at least 24h and stored in the refrigerator until analysis. The digested samples would be taken out and reduced to Hg(0) by addition of $SnCl_2$ prior to analysis. The reduced Hg is absorbed on a gold trap to form an amalgam by sparging of Hg-free argon gas. Hg was desorbed from the gold trap when it was heating and transported to atomic fluorescence unit for quantification. Artificial rain water, rainfall and photochemical samples were divided into low and high Hg concentration samples and measured by

low and high concentration CV-AFS respectively. Samples with high Hg concentrations were diluted to 100 times and analyzed in 5 ml aliquots at fixed time steps. Diluted NIST 3133 was used for standard curve generation and CV-AFS calibration. 2-5ml low Hg concentrations samples were used for Hg measurement at fixed time steps. CV-AFS standard curve was made by diluted NIST 3133 and analysis accuracy was evaluated by regular analysis of the NRC ORMS-5 certified reference material (26.2 ng/L) with good results (25.2 ± 3.3, 1σ, n=79).

2.3.7. **kinetics of photoreduction**

In the photochemical experiments, The reactor was bubbled with 80mL.min^{-1} Hg-free argon gas for the removal of Hg(0) product and prevention of Hg(II) re-oxidation. So the whole reaction is defined as a gross photoreduction process (Qureshi et al. 2011b). Concentrations of DOM and halide were far excess of Hg concentration in the simulated and real rainfall samples, which would not limit Hg photoreduction. Dissolved Hg(II) is thought to be present as Hg(II)-ligand (Hg(II)L) complexes and reduced to Hg(0) in the presence of simulated solar light (Eq.1). The whole reduction process was assumed as a pseudo first-order reduction reaction with rate constant, k_{red} (Eq.2) (O'Driscoll et al. 2006).

$$Hg(II)L + hv \rightarrow Hg(0), \qquad \text{(Eq.1)}$$

$$\frac{d[Hg(II)L]}{dt} = k_{red} \times [Hg(II)L], \qquad \text{(Eq.2)}$$

where Hg(II)L is the complexed inorganic Hg(II) in the solution. Hg(0) is the produced dissolved gaseous mercury (DGM) during the photoreduction process, hv is the light irradiation including natural sunlight or xenon lamp light.

2.3.8. Aqueous Hg speciation modeling

The speciation of Hg compounds in simulated and real rain water was calculated using the geochemical equilibrium modeling software Visual Minteq Version 3.1. Calculation of Hg speciation of simulated rain water was based on measured pH, Hg, halide and DOM concentrations. Modelling of Hg speciation of real rain water was based on the measured pH, Hg, halide, DOM and ion concentrations. Trace metal, incl Hg(II), ion-DOC binding in Visual Minteq is based on the

Stockholm Humic Acid Model with the shmgeneric14.vdb database (Gustafsson 2001) and which has been validated for Hg(II) elsewhere (Richard, Bischoff and Biester 2016). Since atmospheric humic-likes substances are generally low molecular weight compounds, and we use SRFA as a surrogate, we simulate equilibrium Hg(II) binding to fulvic acids only with binding constant $\log K_{HgFA2}$ of 6.7, and Lk2 spread factor of 3.2. At our experimental rainfall Hg/DOC ratios of 0.5 to 6.8 $ng.mg^{-1}$, Hg(II) is coordinated to thiol groups on the DOC compounds (Haitzer, Aiken and Ryan 2002b), which is represented in visual Minteq by the Hg(II)-FA2 complexes in the database and equilibrium speciation results. The nominal pH was 4 in all experimental solutions, and ranged from 3.8 to 6.3 in rainwater samples. No buffer was used to stabilize pH, in order to avoid photochemical artifacts, and in general drift in pH was limited to not more than 0.2 units.

Chapter 3. Experimental rainwater divalent mercury speciation and photoreduction rates in the presence of halides and organic carbon (Science of the Total Environment)

3.1. Article

Title: Experimental rainwater divalent mercury speciation and photoreduction rates in the presence of halides and organic carbon

Xu Yang,[1] Martin Jiskra,[1,2] Jeroen E. Sonke[1]

[1]Géosciences Environnement Toulouse, Observatoire Midi-Pyrénées, CNRS/IRD/Université Toulouse III-Paul Sabatier, 31400 Toulouse, France

[2]Environmental Geosciences, University of Switzerland Basel, Bernoullistrasse 30, 4056 Basel, Switzerland

Abstract

Mercury (Hg) photochemical redox reactions control atmospheric Hg lifetime and therefore play an important role in global Hg cycling. Oxidation of Hg(0) to Hg(II) is currently thought to be a Br-initiated two-stage reaction with end-products $HgBr_2$, HgBrOH, HgBrONO, HgBrOHO. Atmospheric photoreduction of these Hg(II) compounds can take place in both the gas and aqueous phase. Here we present new experimental observations on aqueous Hg(II) photoreduction rates in the presence of dissolved organic carbon and halides and compare the findings to rainfall Hg(II) photoreduction rates. The pseudo first-order, gross photoreduction rate constant, k_{red}, for 0.5 μM Hg(II) in the presence of 0.5 mg L^{-1} of dissolved organic carbon (DOC) is 0.23 h^{-1}, which is similar to the mean k_{red} (0.15±0.01 h^{-1}(σ, n = 3)) in high altitude rainfall and at the lower end of the median k_{red} (0.41h^{-1}, n=24) in continental and marine waters. Addition of bromide (Br^-) to experimental Hg(II)-DOC solutions progressively inhibits Hg(II) photoreduction to reach 0.001 h^{-1} at total Br^- of 10 mM. Halide substitution experiments give $Hg(II)X_n^{(n-2)}$ photoreduction rate constants of 0.016, 0.004 h^{-1}, and <detection limit for X = Cl^-, Br^-, and I^- respectively and reflect increasing stability of the Hg(II)-halide complex. We calculate equilibrium Hg(II) speciation in urban and high-altitude rainfall using Visual Minteq, which indicates Hg(II)-DOC to be the dominant Hg species. The ensemble of observations suggests that atmospheric gaseous $HgBr_2$, $HgCl_2$, $HgBrNO_2$, $HgBrHO_2$ forms, scavenged by aqueous aerosols and cloud droplets, are converted to Hg(II)-DOC forms in rainfall due to abundant organic carbon in aerosols and cloud water. Eventual photoreduction of Hg(II)-DOC in aqueous aerosols and clouds is, however, too slow to be relevant in global atmospheric Hg cycling.

1. Introduction

Mercury (Hg) is a ubiquitous heavy metal found throughout the atmosphere, hydrosphere, biosphere, geosphere and anthroposphere (Selin 2009). Neurotoxicity of Hg to humans and wildlife is of global concern due to widespread exposure via seafood consumption (Wolfe, Schwarzbach and Sulaiman 1998). Emission of Hg to the atmospheric boundary layer occurs mainly in the form of gaseous elemental Hg(0), and to a lesser extent (10%) as gaseous oxidized Hg(II) and particle-bound Hg(P) from natural, anthropogenic and re-emitted sources (Schroeder and Munthe 1998, Futsaeter and Wilson 2013). Hg(0) is characterized by its low chemical reactivity and solubility, and long atmospheric lifetime of several months to over a year. Hg(0) is therefore fairly homogenously distributed throughout the atmosphere, and can be transported far from its emission sources and deposited to remote ecosystems (Horowitz et al. 2017b, Jiskra et al. 2018b, Saiz-Lopez et al. 2018). Oxidation of Hg(0) results in the formation of gaseous Hg(II) compounds, which are highly soluble, reactive and have a short atmospheric lifetime of days to weeks, and are readily scavenged by aerosols and clouds and returned to the Earth's surface by dry and wet deposition (Ariya et al. 2015a, Saiz-Lopez et al. 2018). Atmospheric Hg(II) compounds can also be reduced back to Hg(0) in both the aqueous and gas phase and results in a prolonged lifetime of atmospheric Hg(0) (Munthe, Xiao and Lindqvist 1991a, Si and Ariya 2008b, Saiz-Lopez et al. 2018). Redox processes of atmospheric Hg(0) and Hg(II) are considered as an important dynamic balance in global atmospheric Hg cycling and have been widely implemented in global atmospheric Hg chemistry and transport models (Travnikov and Ryaboshapko 2002, Selin et al. 2007a, Horowitz et al. 2017b). Therefore, quantifying the kinetics and identifying the pathways of these reactions is crucial to better understand transport and deposition of atmospheric Hg to aquatic and terrestrial systems (Bash et al. 2014b).

Production of atmospheric Hg(II) compounds is an important process in the atmosphere, as it is dominantly responsible for atmospheric Hg dry and wet deposition (Lin and Pehkonen 1999b, Selin et al. 2007a). Speciation of atmospheric Hg(II) is poorly understood, and has only identified as $HgCl_2$ and $HgBr_2$ in urban and indoor air and as $HgCl_2$ in power plant plumes (Ernest et al. 2014b, Deeds et al. 2015a). Previous research has indicated that gas phase oxidation of atmospheric Hg(0) potentially

involves various types of oxidants including O_3, OH, HO_2, H_2O_2, NO_3 and halogen species (Dibble et al. 2012a, Peleg et al. 2015, Horowitz et al. 2017b). Currently main oxidation of Hg(0) to Hg(II) is thought to be a Br-induced two-step reaction: first, Hg(0) is oxidized to Hg(I)Br by atomic bromide. Secondly, the relatively unstable Hg(I)Br is further oxidized to Hg(II) by other atmospheric radicals, such as OH, Br, I, Cl, NO_2, HO_2, BrO, IO and ClO, to produce dominant Hg-halide end products $HgBr_2$, HgBrOH, HgBrONO, HgBrOHO (Saiz-Lopez et al. 2018). These gaseous oxidized Hg(II) compounds are water soluble and therefore partition efficiently into cloud water and aqueous aerosols in general (Horowitz et al. 2017b).

Photoreduction of dissolved Hg(II) bound to inorganic and organic ligands as well as with humic substances in terrestrial and marine aquatic systems has been widely identified as an important emission source of Hg(0) to the atmosphere (Ariya et al. 2015a). Compared to direct photolysis of aqueous inorganic Hg complexes, the Hg-humics photoreduction process is considered to be induced by light energy absorption of dissolved humic substances followed by a primary or secondary reaction (Ravichandran 2004, Zhang 2006). The primary reaction is known as ligand to metal charge transfer: first, the dissolved Hg(II)-DOM complex is reduced to reactive and unstable Hg(I), second, the short-lived reactive intermediate Hg(I) quickly reduced to Hg(0) (Zheng and Hintelmann 2009). The secondary reaction has been proposed by Pehkonen and Lin (1998) via a two-step reduction process: first, dissolved Hg(II) is reduced to Hg(I) by $HO_2^{\cdot}$, second, Hg(I) is further reduced to Hg(0) by $HO_2^{\cdot}$ (Pehkonen and Lin 1998a). The Hg photoreduction rates in natural waters are consistent with pseudo-first-order reaction kinetics and have been reported in a wide range of variability of 0.00125 to 2.5 h^{-1} relative to different light irradiation and DOM (Xiao, Stromberg and Lindqvist 1995, O'Driscoll et al. 2006, Qureshi et al. 2011b).

Atmospheric Hg(II) photoreduction to Hg(0) in aqueous aerosols and clouds determines the lifetime of atmospheric Hg against wet deposition. The first global Hg chemistry and transport model (CTM) included Hg(II) reduction in the atmospheric aqueous phase by sulfite (SO_3^{2-}), with k_{red} of 0.6 s^{-1} (2160 h^{-1}) based on experimental work by Munthe et al. (Munthe et al. 1991a, Shia et al. 1999a).

A later study that directly measured the reactant $HgSO_3$ put into question the previously proposed reduction mechanism and rate constant, reporting k_{red} of 0.0106 s^{-1} (38.2 h^{-1}) (Van Loon, Mader and Scott 2000b). Shia et al.'s CTM also included aqueous phase reduction of Hg(II) by hydroperoxyl, HO_2, radicals, based on Pehkonen and Lin (1998) with 2nd order k_{red} of $1.7*10^4$ M^{-1} s^{-1} (Pehkonen and Lin 1998a, Shia et al. 1999a). This reaction, which proceeds by a Hg(I) intermediate step has been questioned by Gardfeldt and Jonsson based on the rapid oxidation of the Hg(I) form back to Hg(II) (Gardfeldt et al. 2001). These aqueous phase Hg(II) reduction mechanisms have been gradually abandoned in Hg CTMs, to adopt a fitting approach where aqueous phase Hg(II) photoreduction rates are optimized to balance fast Hg(0) oxidation and reproduce global variability in observed Hg(0). (Travnikov and Ryaboshapko 2002, Selin et al. 2007a, Horowitz et al. 2017b). The fitted k_{red} are typically on the order of 1.0 h^{-1}, which corresponds to Hg(II) lifetimes in clouds and aqueous aerosol of ~20 minutes (Selin et al. 2007a). Despite the long history of experimental and model studies on atmospheric aqueous Hg(II) photoreduction, the process has never been directly observed or quantified on natural samples. Recently, we conducted the first aqueous phase photoreduction experiments of Hg(II) in rainfall and observed slow values for k_{red} in sub-urban (0.05 ± 0.02 h^{-1}, 1σ, n=9) and high-altitude rain (0.15 ± 0.01 h^{-1}, 1σ, n=3) (Saiz-Lopez et al. 2018). We evaluated the upper value of k_{red} (0.15 h^{-1}) for atmospheric aqueous Hg(II) photoreduction in the GEOS-Chem and GLEMOS Hg CTMs, and found that the observation-based, slow k_{red} leads to a major redox imbalance in the models. Model results showed a strong negative bias in the size of the Hg(0) pool and a positive bias in Hg(II) wet deposition (Saiz-Lopez et al., 2018). Based on theoretical chemistry computation of k_{red}, we proposed that gas phase photoreduction of Hg(II)BrX to Hg(I)Br is an alternative and fast reduction pathway for atmospheric Hg(II).

In this study we perform cation, anion and DOC analyses on the rainwater samples used by Saiz-Lopez et al. (2018), in order to assess the equilibrium speciation of atmospheric aqueous Hg(II). We present new experimental observations on the photoreduction rate constants of Hg bound to different types and concentrations of halides (Cl, Br, I ions) and to 1mg.L^{-1}dissolved organic matter

(DOM), in the form of fulvic acids. The objective of the present study is to better understand Hg speciation and dynamics in atmospheric waters, from an equilibrium speciation and photoreduction kinetics perspective. We aimed to identify in particular the nature of the slow reducing Hg(II) complexes in rainfall.

2. Materials and methods

2.1. Sampling and experimental preparation

Twenty-three experimental solutions containing Hg(II), DOM and halogen were prepared from commercially available NIST 3133 Hg, SRFA and halides (KCl, KBr, KI). The NIST SRM 3133 (10,000 μg g^{-1} Hg(II) in 10 vol.% HNO_3) was used as Hg standard, from which more diluted stock solutions were prepared. Suwannee river fulvic acid (SRFA) was obtained from the International Humic Substances Society and dissolved in MQ water for use as a source of natural DOM (Maizel and Remucal 2017). KBr, KI and KCl salts were obtained from Sigma-Aldrich and diluted to 0.1 mM stock solutions. Collection of 12 rainfall events was previously detailed in Saiz-Lopez et al. (2018) (Saiz-Lopez et al. 2018). In brief, rainfall was collected at two different sites: in sub-urban Toulouse, France (n= 8, 1.479°E, 43.562°N) and at the high altitude (2877 m a.s.l.) Pic du Midi Observatory (PDM), France (n=2, 0.142°E, 42.937°N) in the summer of 2017 (Fu et al. 2016a, Marusczak et al. 2017). Large volume rain water was collected in 8 acid-cleaned polypropylene buckets simultaneously following Enrico et al. (2016) (Enrico et al. 2016a). Single event samples were transferred to 2L acid-cleaned pyrex bottles with GL45 caps. Selected samples were filtered on pre-burnt 47mm quartz fiber filters (Millipore) in an acid-cleaned polycarbonate filtration unit (Fisher Scientific). Subsamples of filtered and unfiltered rainwater were taken for total Hg (THg, 10mL, acidified to 0.4 vol.% with bi-distilled 9N HCl, 0.5 vol% BrCl), TOC/DOC (20mL, acidified to 0.4 vol.% with 9N HCl), anions, pH (30mL, unacidified), and major and trace metals (10mL, acidified to 2 vol.% 15.8N HNO_3). Remaining rain samples were stored in the refrigerator in the dark at 4°C until analysis.

2.2.Photoreduction experiments

Photochemical experiments were carried out in a 60mm diameter, 0.5 L quartz reactor. For controlled indoor laboratory experiments (Xenon lamp light) a Sutter Instruments Lambda LS solar simulator with Perkin Elmer 300W PE300BUV Xenon lamp was used to shine artificial solar light, corresponding to a solar light unit, (in the UVA, UVB, UVC, VIS and IR range) in a 40mm focused

parallel beam through the reactor. Light intensities of key wavelengths of artificial solar irradiation were measured with a solar light PMA 2200 radiometer, including PMA 2106, PMA 2110 and PMA 2130 for UV-B (280-320nm), UVA(320-400nm) and visible light (400-780nm) detector respectively (Supplementary Table S1). Outdoor experiments were performed under natural sunlight (summertime, from 10-18h in full sun) outside the GET laboratory building in Toulouse, France. No formal actinometric calibration of the experimental set-up was performed. Instead we inter-compared Xe lamp experiments to outdoors full sunlight experiments, which yielded similar Hg(II) reduction rates. Dynamic changes of natural UV and visible irradiation intensities of these experiment days were simultaneously measured once per hour and put in Supplementary Table S2. Rainfall experiments were done at both ambient Hg levels, and at 2-40× augmented Hg levels. Experiments on artificial Hg-halogen solutions were carried out at higher Hg concentrations (8-100 μg/L) with the goal to analyze Hg stable isotope fractionation (data not shown here). Although, the NIST3133 Hg standard solution is prepared in 10 vol.% HNO_3, the amounts of NO_3^- introduced into the reactor are relative small, ~ 16 μM. Since photoreaction of NO_3^- can generate a cascade of radical reactions, we compared NIST Hg additions to natural rainwater samples, and found no significant difference in Hg(II) reduction rate, suggesting absence of NO_3^- related bias. Experimental Hg/halide ratios were chosen to approximate the range of natural ratios. Following sample addition, the reactor was wrapped with aluminum foil and equilibrated overnight. At the start of photoreduction experiment a sample aliquot (t=0) was taken and the reactor was exposed to natural sunlight outdoors (up to 8h) or to a solar simulator indoors (up to 48h). During the experiment the reactor was continuously purged with Hg-free argon gas at 80 mL min^{-1} to remove product Hg(0) within minutes (O'Driscoll et al. 2006). Higher flow rates of 300 mL min^{-1} were tested and gave identical results, suggesting that the flow rate had no effect on observed the gross photoreduction rate. Subsamples were collected at different intervals over the course of the experiments. Dark control experiments were carried out under the same conditions in the absence of light irradiation. Analysis of the photoreduction product Hg(0) was attempted, but failed due to leaks on the quartz reactor cap, which is a common problem in these type of experiments.

2.3.Hg, pH, cations and anions, DOC measurement

Samples were measured for total Hg concentration in duplicate following U.S. EPA method 1631 by cold vapor atomic fluorescence spectrometry (CV-AFS) in 5 ml aliquots at fixed time steps. CV-AFS analysis accuracy was evaluated by regular analysis of the NRC ORMS-5 certified reference material (26.2 ng/L) with good results (25.2 ± 3.3, 1σ, n=79). The pH of all the rain samples and experimental solutions were measured as soon as possible after collection and preparation using an Orion pH electrode, calibrated against NIST traceable standards of pH 4 and 7. Major cations in rainfall and experimental solutions were analyzed by high resolution ICP-MS (Thermo-Scientific Element-XR) at OMP, Toulouse, France. Anions were analyzed by ion exchange chromatography at EcoLab, Toulouse, France. DOC or TOC was measured on a total organic carbon analyzer (Shimadzu TOC VSCN) at GET, Toulouse, France.

2.4. Gross photoreduction kinetics

The photoreduction experiments are considered as gross photoreduction due to the continuous purging of 80 mL min^{-1} Hg-free argon gas in the reactor, which removes product Hg(0) and prevents it from re-oxidation to Hg(II). Dissolved Hg(II) is thought to be present as Hg(II)-ligand (Hg(II)L) complexes and reduced to Hg(0) in the presence of simulated solar light (Eq.1). The whole reduction process is considered as a pseudo first-order reduction reaction with rate constant, k_{red} (Eq.2) (Xiao et al. 1995, O'Driscoll et al. 2006, Qureshi et al. 2011b).

$$Hg(II)L + hv \rightarrow Hg(0), \qquad \text{(Eq.1)}$$

$$\frac{d[Hg(II)L]}{dt} = k_{red} \times [Hg(II)L], \qquad \text{(Eq.2)}$$

where Hg(II)L is the complexed inorganic Hg(II) in the solution, Hg(0) is the produced dissolved gaseous mercury (DGM) during the photoreduction process, hv is the light irradiation including natural sunlight or xenon lamp light. In order to see whether our photoreduction reactions are pseudo first-order one, $\ln \frac{[Hg(II)L]_t}{[Hg(II)L]_0}$ is plotted as a function of time (h) shown in Supplementary Fig. S1a-e.

Result show that generally the data show strong linear relationships (r^2 of 0.69-1) and the pseudo-first order approach is therefore appropriate.

2.5. Aqueous Hg speciation modeling

The speciation of dissolved Hg in rain water and experimental solutions was calculated using the geochemical equilibrium modeling software Visual Minteq version 3.1 with default parameters. The input data were based on pH, temperature (22℃), Hg concentration, DOC concentration, cation types and concentrations (Rb, Mo, Cd, Ba, La, Tl, Pb, Th, U, Na, Mg, Al, Ca, V, Cr, Mn, Fe, Co, Ni, Cu, Zn, Sr and K), anion types and concentrations (F^-, Cl^-, $N\text{-}NO^{2-}$, Br^-, $N\text{-}NO_3^-$, $S\text{-}SO_4^{2-}$, $P\text{-}PO_4^{3-}$). Trace metal, incl Hg(II), ion – DOC binding in Visual Minteq is based on the Stockholm Humic Acid Model with the shmgeneric14.vdb database (Gustafsson 2001), and which has been validated for Hg(II) elsewhere (Richard et al. 2016). Since atmospheric humic-likes substances are generally low molecular weight compounds, and we use SRFA as a surrogate, we simulate equilibrium Hg(II) binding to fulvic acids only with binding constant $\log K_{HgFA2}$ of 6.7, and Lk2 spread factor of 3.2. At our experimental rainfall Hg/DOC ratios of 0.5 to 6.8 $ng.mg^{-1}$, Hg(II) is coordinated to thiol groups on the DOC compounds (Haitzer et al. 2002b), which is represented in visual Minteq by the Hg(II)-FA2 complexes in the database and equilibrium speciation results. The nominal pH was 4 in all experimental solutions, and ranged from 3.8 to 6.3 in rainwater samples. No buffer was used to stabilize pH, in order to avoid photochemical artifacts, and in general drift in pH was limited to not more than 0.2 units.

3. Results and Discussion

3.1. Photoreduction of aqueous Hg(II)-halide, $Hg(OH)_2$ and Hg(II)-DOC

Experimental photoreduction of Hg(II) in the presence of different types of halides and different ratios of Br^-/DOC were carried out to explore the influence of halide types and Br^-/DOC ratios on Hg(II) photoreduction rates (Table 2). The photoreduction kinetics are shown in Figure 7a-c indicate that different Hg(II) reduction rates occurred in all experiments including dark control and photo-induced conditions. Table 3 (exp. A3-A6) shows estimated equilibrium Hg(II) speciation at the start of the 0.1 mM halogen experiments, indicating that $HgCl_{2(aq)}$ (97%), $HgBr_{2(aq)}$ (98%) and $HgI_{2(aq)}$ (62%) + $HgI_{3(aq)}^-$ (37%) were dominant. Two types of Hg(II) control experiments were carried out: exp. A1, presence of light, in MQ water, suggesting $Hg(OH)_{2(aq)}$ as the dominant species (95%), and exp. A2, A3, two dark controls (i.e. no light), in MQ with 95% $Hg(OH)_{2(aq)}$, and in presence of 0.2mM KBr with 95% $HgBr_{2(aq)}$.

Table 2 *Compositions and conditions of experimental Hg and rainfall solutions of photoreduction experiments. A and R represent experimental Hg solution and rainfall solution. UF and F indicate unfiltered and filtered rainfall. Xe represents xenon solar simulator. TL and PDM indicate sub-urban Toulouse sample and high altitude (2877 m a.s.l.) Pic du Midi Observatory sample.*

Experiment no.	Figure legend	pH	light	Hg	DOC	Hg/DOC	halide	halide conc.	SRFA	Hg/halide	halide/DOC
				$ng.mL^{-1}$	$mg.L^{-1}$	$ng.mg^{-1}$		mM	$mg.L^{-1}$	$mg.mol^{-1}$	$mol.g^{-1}$
A1	Hg-Xe light	4.1	Xe light	100	/	/	/	/	/	/	/
A2	Hg-dark control	4.1	Dark control	100	/	/	/	/	/	/	/
A3	Hg-0.2mM KBr-dark control	4.1	Dark control	100	/	/	KBr	0.2	/	500	/
A4	Hg-0.1mM KCl-Xe light	4.2	Xe light	100	/	/	KCl	0.1	/	1000	/
A5	Hg-0.2mM KBr-Xe light	4.2	Xe light	100	/	/	KBr	0.2	/	500	/
A6	Hg-0.1mM KI-Xe light	4.0	Xe light	100	/	/	KI	0.1	/	1000	/
A7	Hg-1mg/L SRFA-Xe light	7	Xe light	100	0.5	200000	/	/	1	/	/
A8	Hg-0.001mM KBr-1mg/L SRFA-Xe light	4.1	Xe light	100	0.5	200000	KBr	0.001	1	100000	0.002
A9	Hg-0.01mM KBr-1mg/L SRFA-Xe light	4.1	Xe light	100	0.5	200000	KBr	0.01	1	10000	0.02
A10	Hg-0.1mM KBr-1mg/L SRFA-Xe light	4.1	Xe light	100	0.5	200000	KBr	0.1	1	1000	0.2
A11	Hg-1mM KBr-1mg/L SRFA-Xe light	4.1	Xe light	100	0.5	200000	KBr	1	1	100	2
A12	Hg-10mM KBr-1mg/L SRFA-Xe light	4.1	Xe light	100	0.5	200000	KBr	10	1	10	20
A13	Hg-0.1mM KCl-1mg/L SRFA-Xe light	4.2	Xe light	100	0.5	200000	KCl	0.1	1	1000	0.2
A14	Hg-0.1mM Kl-1mg/L SRFA-Xe light	7	Xe light	100	0.5	200000	KI	0.1	1	1000	0.2
							F^-	Cl^-	Br^-	I^-	
				$ng.L^{-1}$			$mg.L^{-1}$	$mg.L^{-1}$	$mg.L^{-1}$	$mg.L^{-1}$	
R1	Rain event 1-U-Xe light-TL	4.7	Xe light	8.98	2.14	4.2	0.02	0.8781	0.002	0.0011	
R2	Rain event 1-U-Xe light-TL	4.4	Xe light	82.22	2.14	38.4	0.02	0.8781	0.002	0.0011	
R3	Rain event 2-F-Xe light-TL	4.1	Xe light	88.98	2.10	42.3	0.02	0.2588	0.002	0.0011	
R4	Rain event 3-U-Xe light-TL	6.3	Xe light	88.93	3.47	25.6	0.02	0.1917	0.003	0.0011	
R5	Rain event 4-F-Natural light-TL	6.1	sunlight	87.93	1.42	61.7	0.01	0.091	0.001	0.0011	
R6	Rain event 5-F-Natural light-TL	6.3	sunlight	91.44	0.84	108.4	0.01	0.6257	0.002	0.0011	
R7	Rain event 5-F-Dark control-TL	6.3	dark control	92.41	0.84	109.5	0.01	0.6257	0.002	0.0011	
R8	Rain event 8-U-Natural light-TL	5.1	sunlight	2.57	2.46	1.0	0.01	0.1	0.001	0.0011	
R9	Rain event 8-U-Xe light-TL	5.1	Xe light	2.48	2.46	1.0	0.01	0.1	0.001	0.0011	
R10	Rain event 8-U-Xe light-TL	3.8	Xe light	102.53	2.46	41.6	0.01	0.1	0.001	0.0011	
R11	Rain event 9-U-Xe light-PDM	5.9	Xe light	2.26	0.75	3.0	0.01	0.0386	n.a.	0.0011	
R12	Rain event 10-U-Xe light-PDM	6.1	Xe light	2.00	0.28	7.1	0.01	0.0305	n.a.	0.0011	
R13	Rain event 10-U-Xe light-PDM	6.1	Xe light	1.99	0.28	7.1	0.01	0.0305	n.a.	0.0011	

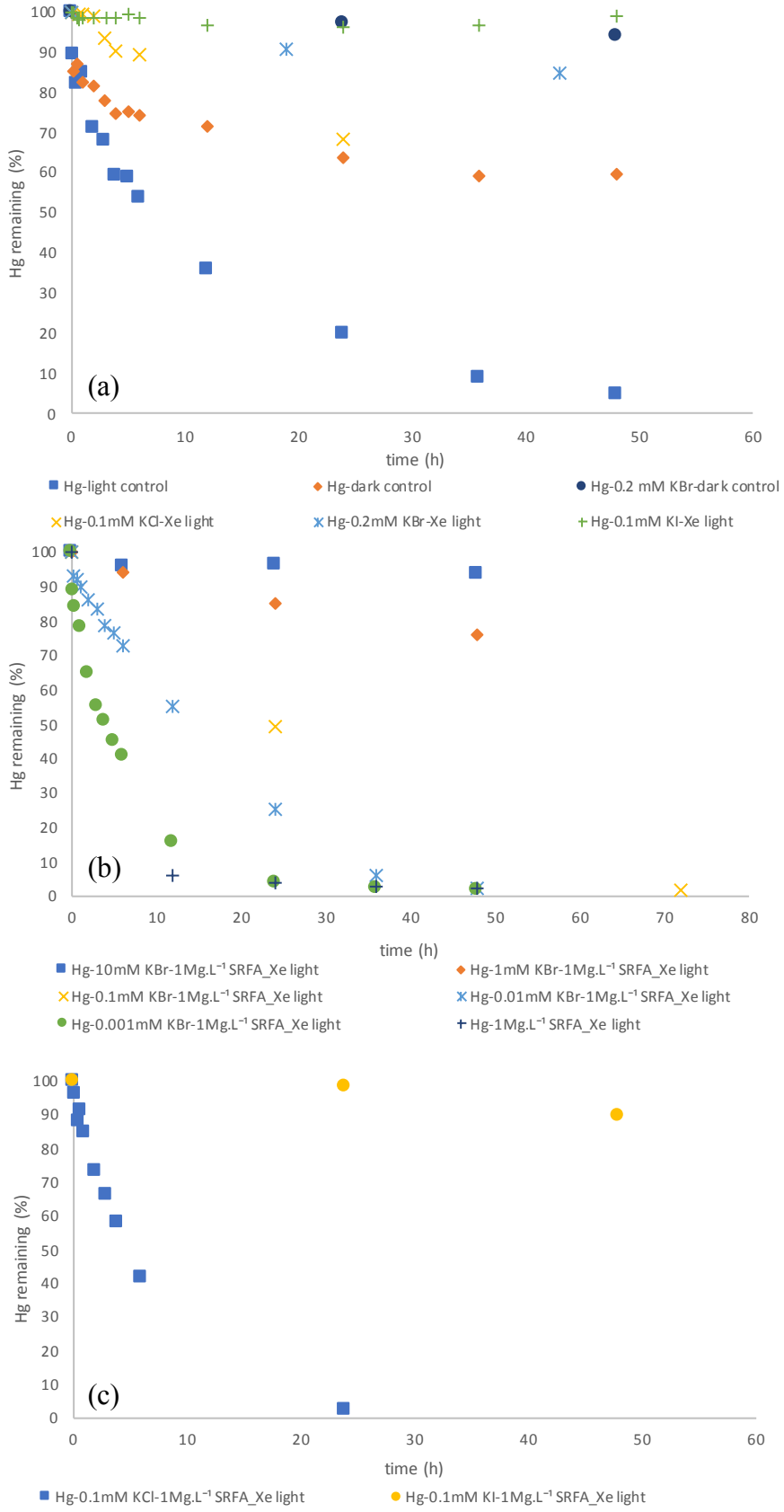

Figure 7a-c *Experimental photoreduction rates of 100ppb (0.5um) dissolved Hg(II) were carried out: a) in the presence of different types of halides (experiment nos. A4-A6, table 1) and for light and dark*

control experiments (experiments nos. A1-A3, table 1), b) in the presence of different Br^-/DOC ratios (experiment nos. A7-A12, table 1), c) in the presence of different types of halide/DOC (experiment nos. A13 and A14, table 1). SRFA, Suwannee river fulvic acid. Uncertainties on Hg concentrations were evaluated by regular analysis of the NRC ORMS-5 certified reference material (26.2 ng/L). Our analysis result had good results (25.2 ± 3.3, 1σ, n=79) and indicated that the uncertainty was 13.1% (1σ).

Table 3 *Equilibrium Hg(II) speciation of 100ppb experimental Hg solution and rainfall solution*

Experiment no.	Experiment name	Hg(II) species and percentage				
		species (%)	species (%)	species (%)	species (%)	species (%)
A1/A2	Hg+Xe light/dark control	Hg^{2+}	$HgOH^+$	$Hg(OH)_2$		
		0.96	4	95		
A3/A5	Hg+ 0.2mM KBr+dark control/Xe light	$HgBr_2$ (aq)	$HgBr_3^-$	$HgBr_4^{2-}$	HgBrOH (aq)	
		95	5	0.02	0.01	
A4	Hg+ 0.1mM KCl+Xe light	$HgCl^+$	$HgCl_2$ (aq)	$HgCl_3^-$	HgClOH (aq)	$Hg(OH)_2$
		0.21	97	0.10	3	0.02
A6	Hg+ 0.1mM KI+Xe light	HgI_2 (aq)	HgI_3^-	HgI_4^{2-}		
		62	37	0.33		
A7	Hg+ 1mg.L^{-1} SRFA	Hg^{2+}	/FA2Hg (aq)	$HgOH^+$	$Hg(OH)_2$	
		0.03	97	0.13	2.634	
A8	Hg+ 0.001mM KBr + 1mg.L^{-1} SRFA+Xe light	$HgBr^+$	$HgBr_2$ (aq)	/FA2Hg (aq)	HgBrOH	$Hg(OH)_2$
		0.28	46	52	1.45	0.014
A9	Hg+ 0.01mM KBr + 1mg.L^{-1} SRFA+Xe light	$HgBr^+$	$HgBr_2$ (aq)	$HgBr_3^-$	/FA2Hg (aq)	HgBrOH
		0.02	70	0.16	30	0.13
A10	Hg+ 0.1mM KBr + 1mg.L^{-1} SRFA+Xe light	$HgBr_2$ (aq)	$HgBr_3^-$	HgBrOH	/FA2Hg (aq)	
		90	2	0.02	7	
A11	Hg+ 1mM KBr + 1mg.L^{-1} SRFA+Xe light	$HgBr_2$ (aq)	$HgBr_3^-$	$HgBr_4^{2-}$	/FA2Hg (aq)	
		77	18	0.34	5	
A12	Hg+ 10mM KBr + 1mg.L^{-1} SRFA+Xe light	$HgBr_2$ (aq)	$HgBr_3^-$	$HgBr_4^{2-}$	/FA2Hg (aq)	
		25	60	13	2	
A13	Hg+ 0.1mM KCl + 1mg.L^{-1} SRFA	$HgCl^+$	$HgCl_2$ (aq)	$HgCl_3^-$	/FA2Hg (aq)	HgClOH (aq)
		0.10	48	0.05	50	1.42
A14	Hg+ 0.1mM KI + 1mg.L^{-1} SRFA	HgI_2 (aq)	HgI_3^-	HgI_4^{2-}	/FA2Hg (aq)	
		62	37	0.33	0.08	
		Species (%)	percentage (%)			
R1	Rain event 1-U-Xe light-TL	/FA2Hg (aq)	100			
R2	Rain event 1-U-Xe light-TL	/FA2Hg (aq)	100			
R3	Rain event 2-F-Xe light-TL	/FA2Hg (aq)	100			
R4	Rain event 3-U-Xe light-TL	/FA2Hg (aq)	100			
R5	Rain event 4-F-Natural light-TL	/FA2Hg (aq)	100			
R6	Rain event 5-F-Natural light-TL	/FA2Hg (aq)	100			
R7	Rain event 5-F-Dark control-TL	/FA2Hg (aq)	100			
R8	Rain event 8-U-Natural light-TL	/FA2Hg (aq)	100			
R9	Rain event 8-U-Xe light-TL	/FA2Hg (aq)	100			
R10	Rain event 8-U-Xe light-TL	/FA2Hg (aq)	100			
R11	Rain event 9-U-Xe light-PDM	/FA2Hg (aq)	100			
R12	Rain event 10-U-Xe light-PDM	/FA2Hg (aq)	100			
R13	Rain event 10-U-Xe light-PDM	/FA2Hg (aq)	100			

We observed low, but measurable, dark control reduction rates, k_{red}, of 0.009 h^{-1} for the $Hg(OH)_{2(aq)}$ complex in MQ water, and 0.001 h^{-1} for the $HgBr_{2(aq)}$ complex (Figure 7a, Table 2 experiments A2, A3). Dark reduction is generally attributed to abiotic, non-photochemical Hg(II) reduction and/or microbial Hg(II) reduction. Under full solar illumination by the Xe lamp, the stronger Hg-halide complexes resulted in progressively slower Hg(II) photoreduction rates, k_{red}, of 0.016 h^{-1}, 0.004 h^{-1}, for $HgCl_2$, $HgBr_2$, and undetectable for HgI_2/HgI_3^- (Figure 7b, Table 2 experiments A4, A5, A6). Experiments with F^- ion were attempted, but unsuccessful as F^- binds only weakly to Hg(II), resulting in dominant $Hg(OH)_2$ complexes under all environmentally relevant F^- concentrations. The light control experiment in absence of halides resulted in a fast photoreduction rate of the $Hg(OH)_{2(aq)}$ complex in MQ water with k_{red} of 0.022 h^{-1} (Figure 7a, Table 2 experiment A1). The fastest photoreduction was observed for Hg-DOC complexes with k_{red} of 0.23 h^{-1} (Figure 7a, Table 2 experiment A7), which is slightly lower than published rate constants under similar conditions: k_{red} = 0.47 h^{-1} (Bergquist and Blum 2007), and a literature review on aqueous Hg(II) photoreduction in continental and marine waters with median k_{red} = 0.41 h^{-1} (Qureshi et al. 2011b). Duplicate experiments on Hg-DOC and on $HgBr_2$ species resulted in typical uncertainties of 30% (1σ) on k_{red}. The dark control experiment with $Hg(OH)_2$ (Figure 7a, exp.A2) shows in fact a k_{red} that is faster (0.009 h^{-1}) than some of the Hg-halide photoreduction experiments, e.g. $HgBr_2$ at 0.004 h^{-1}. We suggest that the absence of stabilizing halide or DOC ligands in solution renders this dark control not representative of the true experimental or environmental dark Hg(II) reduction rates. The low dark control k_{red} of 0.001 h^{-1} of Hg(II) in the presence of Br is likely more representative (exp. A3).

Previous studies on Hg(II)-halide photochemistry suggested that ligand to metal charge transfer due to UVC absorption in the 200-300nm wavelength range can result in Hg(0) or Hg(I) products depending on Hg/halide ratio and presence of oxygen (Horvath and Vogler 1993). At our experimental conditions, under low UVC irradiation, and with molar Hg/halide ratios >100 and in absence of oxygen, Hg(0) should be the product. Xiao et al. (1994), performed similar experiments on

$Hg(OH)_{2(aq)}$ photoreduction at a higher pH of 7, finding k_{red} of 0.43 h^{-1} which is 7x faster than our observations (Xiao et al. 1994). The difference is likely due to a different experimental set-up, possibly due to their use of a more powerful (450W) medium pressure Hg vapor lamp. Compared to a Xe lamp which reproduces a solar light spectrum, medium pressure Hg vapor lamps emit primarily in the 200-600nm region, with a particularly strong UVA line at 365.4 nm.

3.2. Photoreduction of Hg(II) in the presence of both halides and DOC

Photoreduction kinetics of Hg vary at different Br^-/DOC ratios in the presence of halide and DOC (Figure 7b). The pseudo first-order reduction rate constant k_{red} reached a high value of 0.23 h^{-1} in the absence of Br^- (Table 2, exp.A7). Addition of Br^- at a low Br^-/DOC ratio of 0.002mol.g^{-1} resulted in a decreased k_{red} to 0.14h^{-1}, and approximately 98% of Hg(II) was reduced during 48h (Table 2, exp.A8). The continuous increase in Br^-/DOC ratio further inhibits Hg photoreduction to reach 0.001h^{-1} at a Br^-/DOC ratio of 20mol.g^{-1} and results in only about 7% of Hg(II) loss in the solution (Table 2, exp.A9-A12). Our experiments revealed that k_{red} had a strong linear correlation with the Br^-/DOC ratios during 48h (Figure 8).

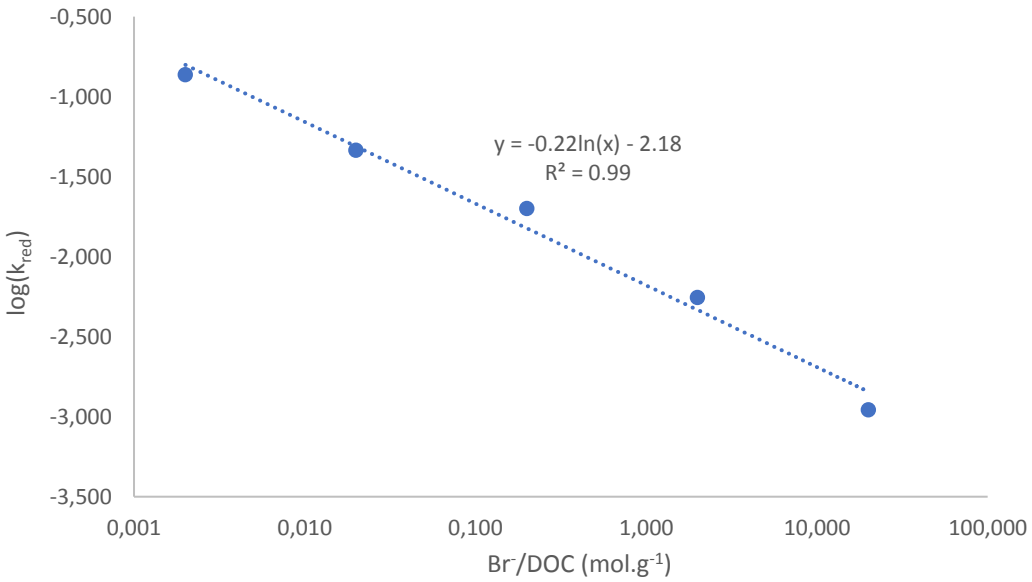

Figure 8 *Hg(II) photoreduction rates are plotted against different Br^-/DOC ratios (experiment nos. A7-A11, table 1). Br^-/DOC ratio is shown on a common logarithmic scale. k_{red} was evaluated by*

duplicate experiments on Hg-DOC and on $HgBr_2$ species and resulted in typical uncertainties of 30% (1σ).

Composition calculation of the dominant Hg(II) species in the Br^- + DOC system are shown in Table 3 and show a progressive change from DOC dominated to Br^- dominated Hg(II) coordination with the increase of Br^-/DOC from 0.002mol.g^{-1} to 20mol.g^{-1}. When Br/DOC >0.2 mol g^{-1}, $HgBr_{2(aq)}$ is the dominant species (84%), whereas at Br/DOC <0.2 mol g^{-1}, Hg-DOC dominates. These mixed ligand experiment show coherent behavior of Hg(II) photoreduction rates, varying between the fast (Hg-DOC) and slow ($HgBr_2$) end-members (Figure 8). Additional experiments at Cl^-/DOC of 0.2 mol g^{-1}, with calculated speciation of $HgCl_2$ (48%) and Hg-DOC (50%), resulted in a k_{red} of 0.16 h^{-1}. An I^-/DOC = 0.2 mol g^{-1} experiment resulted in a slow k_{red} of 0.0023 h^{-1} during the first 72h, followed by insignificant Hg(II) photoreduction from 72 to 168h (Figure 7c). The decrease in k_{red} from 0.16 to 0.011 to 0.0023 h^{-1} for the Cl^-, Br^-, I^- mixed ligand experiments in the presence of constant DOC concentration corroborates the role of the halide ion in stabilizing Hg(II) in solution (K_{eql} increasing from Cl^- to Br^- to I^-) , and effectively inhibiting photoreduction relative to Hg-DOC species. The inhibitory effect of halogen ligands on photoreduction can be explained by different photosensitizer properties of the halogens and DOC ligands. DOC contains chromophore moieties such as aromatic rings and conjugated double bonds which efficiently absorb UV-light at multiple wavelengths (Del Vecchio and Blough 2002). On the contrary, the ionic single bond of Hg(II)-X has more restricted UV absorption properties, likely leading to lower photoreduction yields (Saiz-Lopez et al. 2018).

3.3.Photoreduction of rainfall Hg(II)

We previously published experimental rainfall Hg(II) gross photoreduction rates, which ranged from 0.016 to 0.072 h^{-1} (mean 0.051 ± 0.019 h^{-1}, σ, n = 10) in suburban Toulouse, and from 0.14 to 0.19 h^{-1} (mean 0.15 ± 0.01 h^{-1}, σ, n = 3) at the remote high-altitude PDM (Saiz-Lopez et al. 2018). Here we complete this dataset with rainfall chemistry data for the same samples, including major cations, anions (including Cl^-, Br^- and F^-, but not I^-), pH and DOC (Table 2, experiments R1-R13). We use V.

Minteq to estimate the Hg(II) species distribution among inorganic (F^-, Cl^-, Br^-, NO_3^-, SO_4^{2-}, OH^-) and organic, DOC ligands, assuming that equilibrium conditions are met, and that the rainfall is saturated in CO_2 with respect to an atmospheric pCO_2 of 400 ppmv. Particulate Hg(II) forms are ignored in the speciation calculations based on the low (<5%) particulate Hg detected by filtration . For I^-, we assume a total concentration of 1.1 µg L^{-1}, identical to the mean rainfall total I observed at PDM (Suess et al. 2019). In the V. Minteq speciation model we assumed atmospheric DOC to be in the form of strong fulvic-type acids (FA2). Speciation calculation results are summarized in Table 3, and indicate that in all rainfall samples Hg is bound to DOC, notably to the stronger FA2 type sites that represent phenolic, thiol and bidentate complexes with Hg(II). The Hg/DOC concentration ratios we observe in rainfall range from 0.5 to 6.8 ng.mg^{-1}, indicating that Hg(II) is likely coordinated to thiol groups on the DOC compounds (Haitzer et al. 2002b). Observed Cl^-/DOC, Br^-/DOC and estimated I^-/DOC levels in rainfall range from 0.02 to 6 x 10^{-7} mol/g, corroborating that the photoreduction kinetics should be dominated by the Hg(II)-DOC experimental end-member.

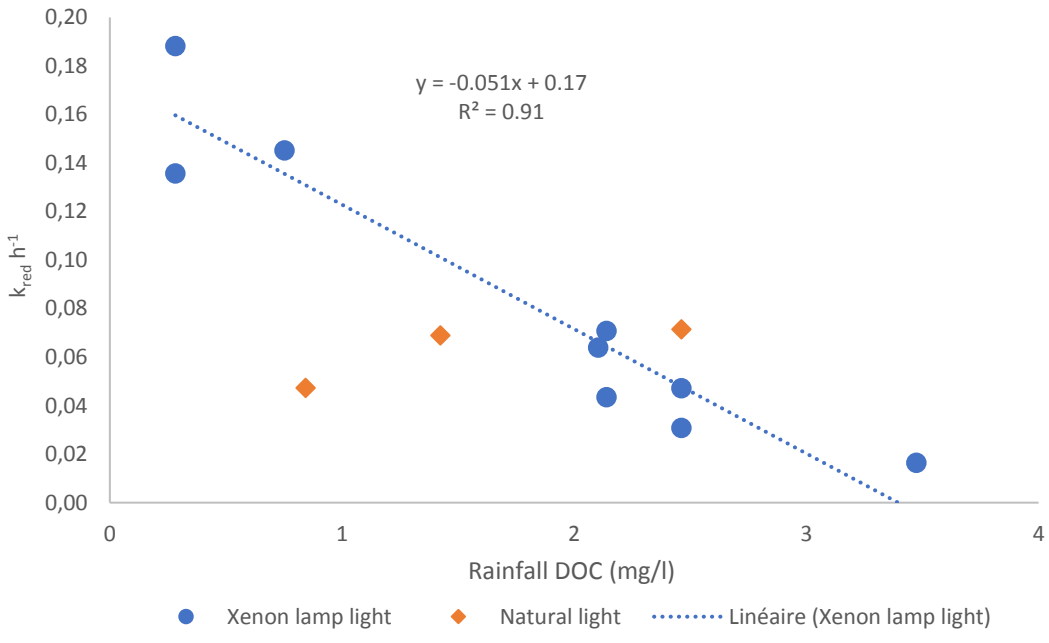

Figure 9 *Rainfall DOC (mg.L-1) plotted as a function of Hg(II) photoreduction rate (h-1) in the presence of xenon lamp light and natural sunlight. k_{red} was evaluated by duplicate experiments on Hg-DOC and on $HgBr_2$ species and resulted in typical uncertainties of 30% (1σ).*

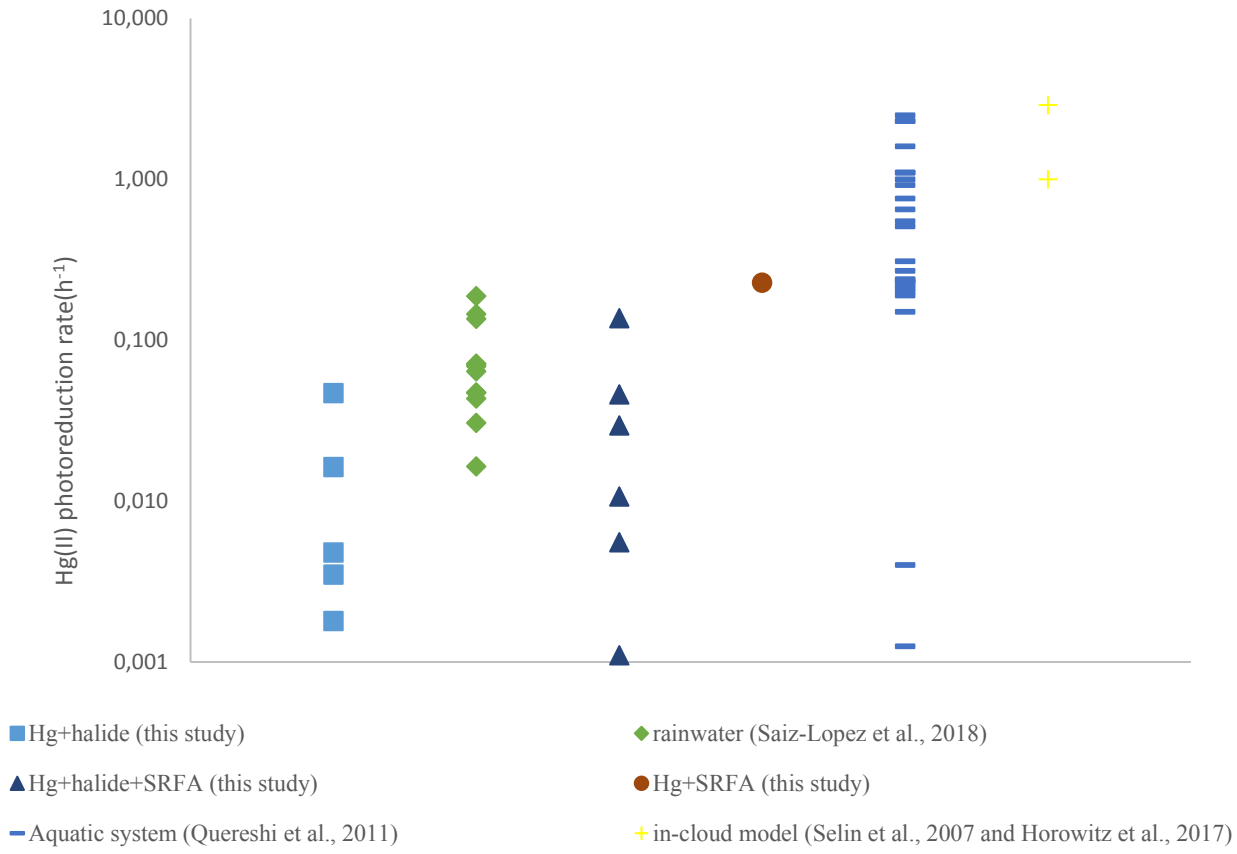

Figure 10 *Comparison of experimental and model photoreduction rates of Hg(II) in different media.*

Figure 9 shows a negative relationship between rainfall DOC and Hg(II) photoreduction rate (k_{red}, h^{-1}; $r^2 = 0.91$). The relationship is driven by the PDM data which has lower DOC and faster k_{red}. Within the urban rainfall data, the DOC vs k_{red} relationship remains significant, but less pronounced ($r^2 = 0.24$) (Supplementary Fig. S2). The variation in rainfall k_{red} is not driven by Hg/DOC ratio ($r^2 = 0.14$) (Supplementary Fig. S3). We observed no statistically significant ($p>0.05$) differences between rainfall Hg(II) reduction rates under natural ($0.063 \pm 0.026\ h^{-1}$, 2σ, n=3) and simulated sunlight ($0.037 \pm 0.032\ h^{-1}$, 2σ, n=5). We suggest that the overall DOC vs. k_{red} trend in Fig. 3 is possibly driven by rainfall DOM molecular properties, likely to be different in the urban boundary layer and free troposphere. One possible reason may be the partial oxidation of thiol groups in atmospheric DOC at the remote PDM site (Tyndall and Ravishankara 1991). A lower availability of the high-affinity thiol ligands should result in weaker complexation of Hg(II) by low affinity O/N ligands and therefore

faster photoreduction rates (Jiang et al. 2015). A more detailed characterization of DOC is needed to understand this observation. Fig. 4. summarizes published k_{red} and our experimental and rainfall k_{red} observations. Rainfall k_{red} are of similar magnitude as the lower (slower) end of k_{red} in terrestrial and marine waters. Once more this points to differences in OM, Hg-OM properties and trace metal : OM ratios in atmospheric, terrestrial and marine waters. Understanding the influence of aquatic geochemistry on Hg photoreduction rates requires investigating all three water types with the same experimental and analytical techniques.

4. Conclusions

In this study we performed Hg(II) photoreduction experiments in the presence of halides (Cl, Br, I) and DOC. The Hg(II) photoreduction rates observed in rainwater (0.05 h^{-1} in urban to 0.15 h^{-1} in remote rainfall) are faster than those of isolated $HgBr_2$ complexes (0.004 h^{-1}), and resemble more the rates of Hg(II)-DOC compounds (0.23 h^{-1}). Our observations on experimental and rainfall Hg(II) photoreduction rates and on estimated Hg(II) speciation in rainfall lead to a number of suggestions on cloud water Hg chemistry. Previous research on gas-phase Hg chemistry has shown that elemental Hg emissions are partially oxidized by a two-step mechanism, involving Br radicals in step 1, and NO_2, HO_2 radicals in step 2, to produce Hg-halide end products $HgBr_2$, HgBrOH, HgBrONO, HgBrOHO (Horowitz et al. 2017b, Saiz-Lopez et al. 2018). These gaseous oxidized Hg(II) compounds are water soluble and therefore partition efficiently into aqueous aerosols and eventually in cloud water and rain (Amos et al. 2012b, Horowitz et al. 2017b). Aerosols contain abundant organic carbon, in large excess over halide ions, which is reflected in the low halide/DOC ratios of rainfall observations (0.04 – 0.75 g g^{-1}). Despite the strong binding properties of halide ions towards Hg(II), our equilibrium Hg(II) speciation calculations, and experimental photoreduction rate observations suggest that scavenged Hg-halide complexes are rapidly transformed into aqueous Hg-DOC complexes in rainfall, and by extension in cloud-water.

Acknowledgements

This study has received funding from the European Research Council Executive Agency under the European Union´s Horizon 2020 Research and innovation programme (ERC-2010-STG 258537) and from the H2020 ERA-PLANET (689443) iGOSP programme to JES. XY thanks the China Scholarship Council (CSC) for this PhD grant. MJ received funding through the H2020 Marie Sklodowska-Curie grant agreement 657195 and Swiss National Science Foundation grant PZ00P2_174101. We thank the UMS 831 Pic du Midi Observatory team for help with rainwater sampling, Franck Gilbert at EcoLab for use of the solar simulator, and Laure Laffont for management of the Hg labs at GET.

3.2. Supporting Information

Supplementary information for:

Experimental rainwater divalent mercury speciation and photoreduction rates in the presence of halides and organic carbon

Xu Yang, Martin Jiskra, Jeroen E. Sonke

This file contains:

1. supplementary Fig. 1-3

2. supplementary table 1-2

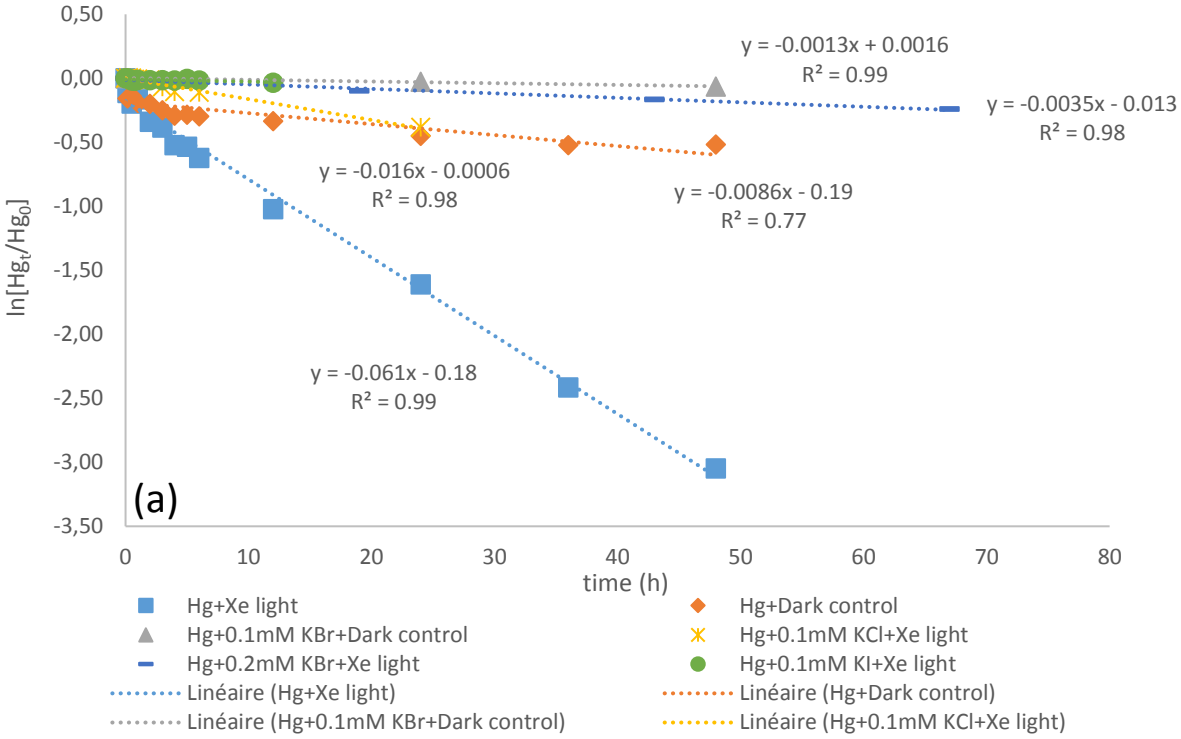
y = -0.0013x + 0.0016
R² = 0.99
y = -0.0035x - 0.013
R² = 0.98
y = -0.016x - 0.0006
R² = 0.98
y = -0.0086x - 0.19
R² = 0.77
y = -0.061x - 0.18
R² = 0.99
(a)
ln[Hgt/Hg0]
time (h)
Hg+Xe light
Hg+Dark control
Hg+0.1mM KBr+Dark control
Hg+0.1mM KCl+Xe light
Hg+0.2mM KBr+Xe light
Hg+0.1mM KI+Xe light
Linéaire (Hg+Xe light)
Linéaire (Hg+Dark control)
Linéaire (Hg+0.1mM KBr+Dark control)
Linéaire (Hg+0.1mM KCl+Xe light)

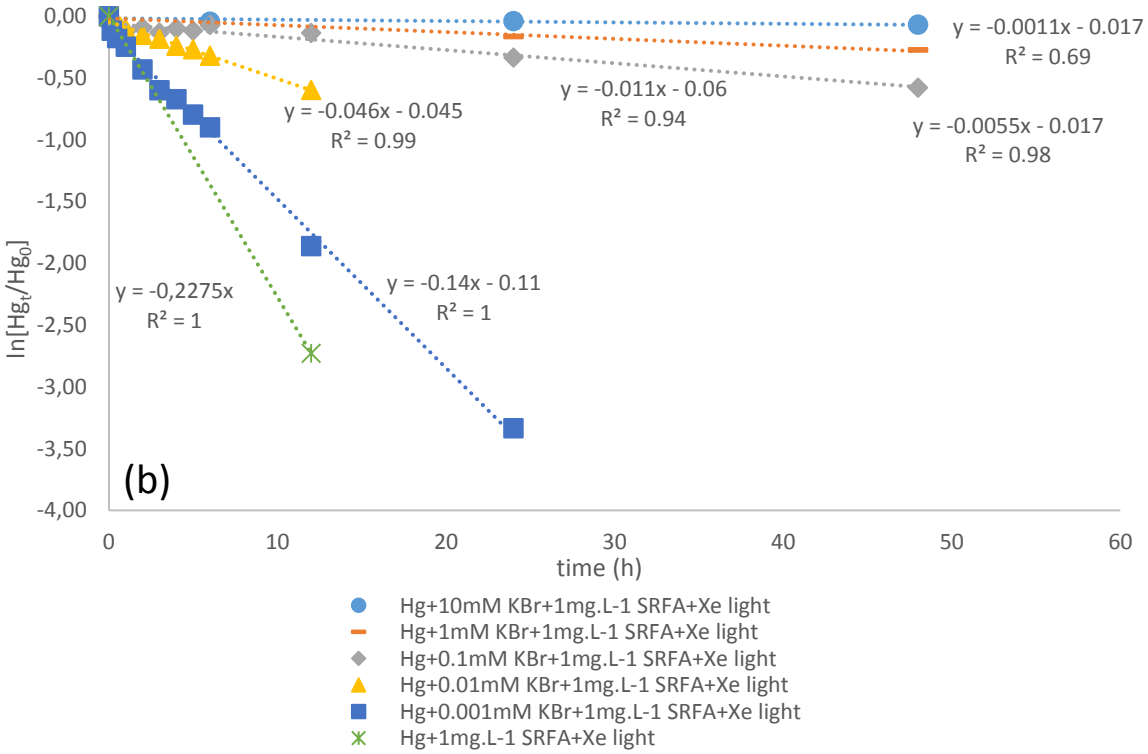
y = -0.0011x - 0.017
R² = 0.69
y = -0.011x - 0.06
R² = 0.94
y = -0.0055x - 0.017
R² = 0.98
y = -0.046x - 0.045
R² = 0.99
y = -0,2275x
R² = 1
y = -0.14x - 0.11
R² = 1
(b)
ln[Hgt/Hg0]
time (h)
Hg+10mM KBr+1mg.L-1 SRFA+Xe light
Hg+1mM KBr+1mg.L-1 SRFA+Xe light
Hg+0.1mM KBr+1mg.L-1 SRFA+Xe light
Hg+0.01mM KBr+1mg.L-1 SRFA+Xe light
Hg+0.001mM KBr+1mg.L-1 SRFA+Xe light
Hg+1mg.L-1 SRFA+Xe light

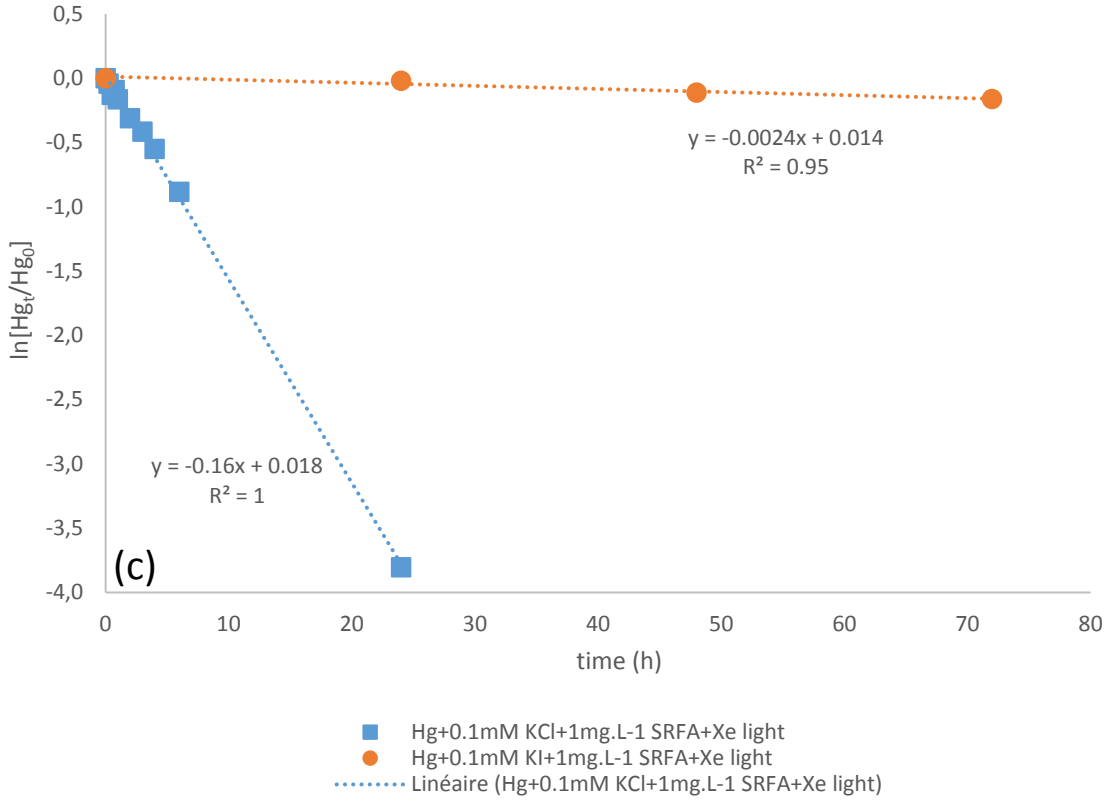
0,5
0,0
-0,5
-1,0
-1,5
-2,0
-2,5
-3,0
-3,5
-4,0
ln[Hgt/Hg0]
y = -0.0024x + 0.014
R² = 0.95
y = -0.16x + 0.018
R² = 1
(c)
0
10
20
30
40
50
60
70
80
time (h)
Hg+0.1mM KCl+1mg.L-1 SRFA+Xe light
Hg+0.1mM KI+1mg.L-1 SRFA+Xe light
Linéaire (Hg+0.1mM KCl+1mg.L-1 SRFA+Xe light)

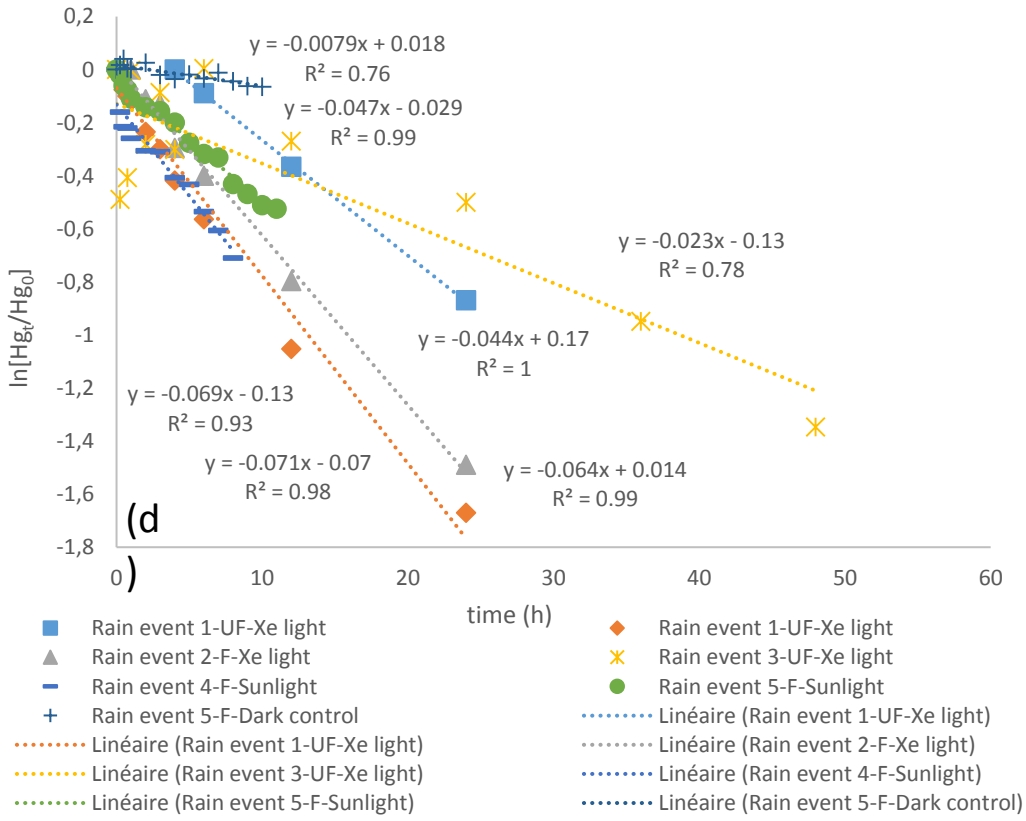
0,2
0
-0,2
-0,4
-0,6
-0,8
-1
-1,2
-1,4
-1,6
-1,8
ln[Hgt/Hg0]
y = -0.0079x + 0.018
R² = 0.76
y = -0.047x - 0.029
R² = 0.99
y = -0.023x - 0.13
R² = 0.78
y = -0.044x + 0.17
R² = 1
y = -0.069x - 0.13
R² = 0.93
y = -0.071x - 0.07
R² = 0.98
y = -0.064x + 0.014
R² = 0.99
(d
)
0
10
20
30
40
50
60
time (h)
Rain event 1-UF-Xe light
Rain event 2-F-Xe light
Rain event 4-F-Sunlight
Rain event 5-F-Dark control
Linéaire (Rain event 1-UF-Xe light)
Linéaire (Rain event 3-UF-Xe light)
Linéaire (Rain event 5-F-Sunlight)
Rain event 1-UF-Xe light
Rain event 3-UF-Xe light
Rain event 5-F-Sunlight
Linéaire (Rain event 1-UF-Xe light)
Linéaire (Rain event 2-F-Xe light)
Linéaire (Rain event 4-F-Sunlight)
Linéaire (Rain event 5-F-Dark control)

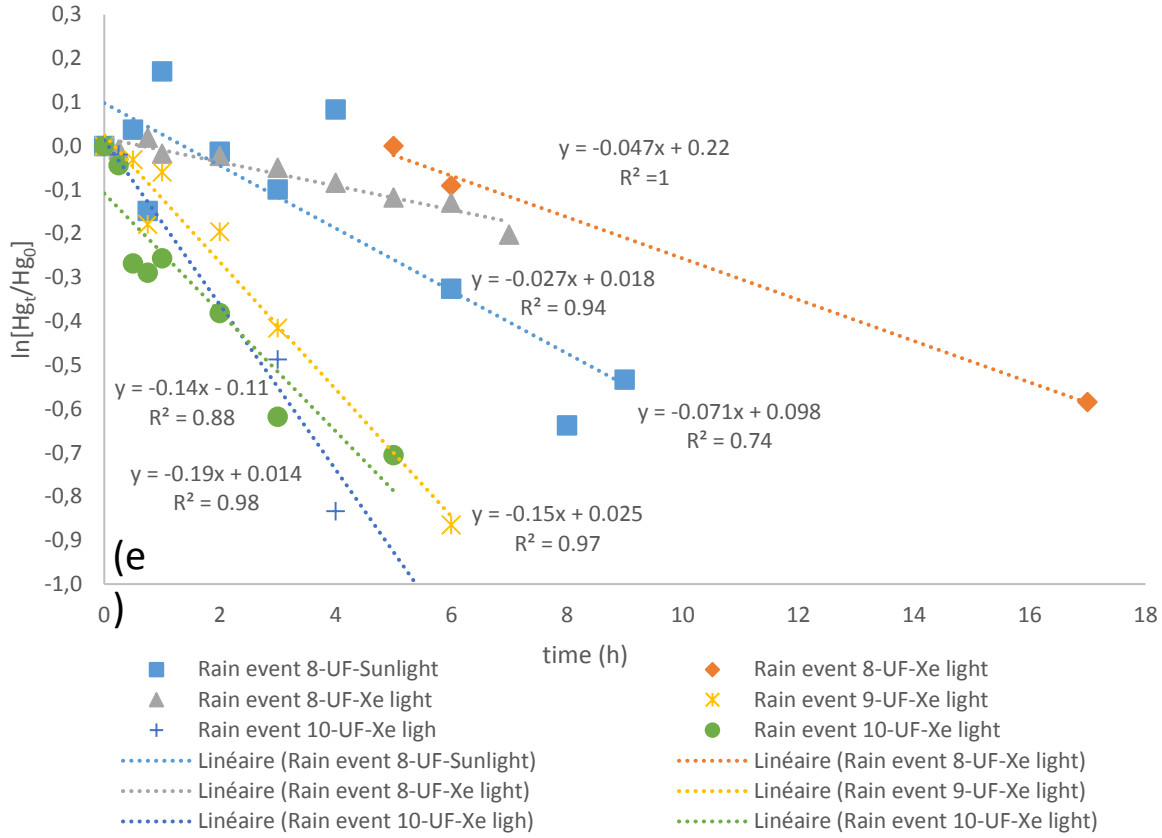

Figure 11a-e *Pseudo first-order photoreduction rate constants (k_{red}) of Hg(II) was plotted as the slope of ln[Hg_t/Hg_0] versus time (h), a) in the presence of different types of halides and for light and dark control experiments, b) in the presence of different Br^-/DOC ratios, c) in the presence of different types of halide/DOC, d) and e) in the rainfall sample.*

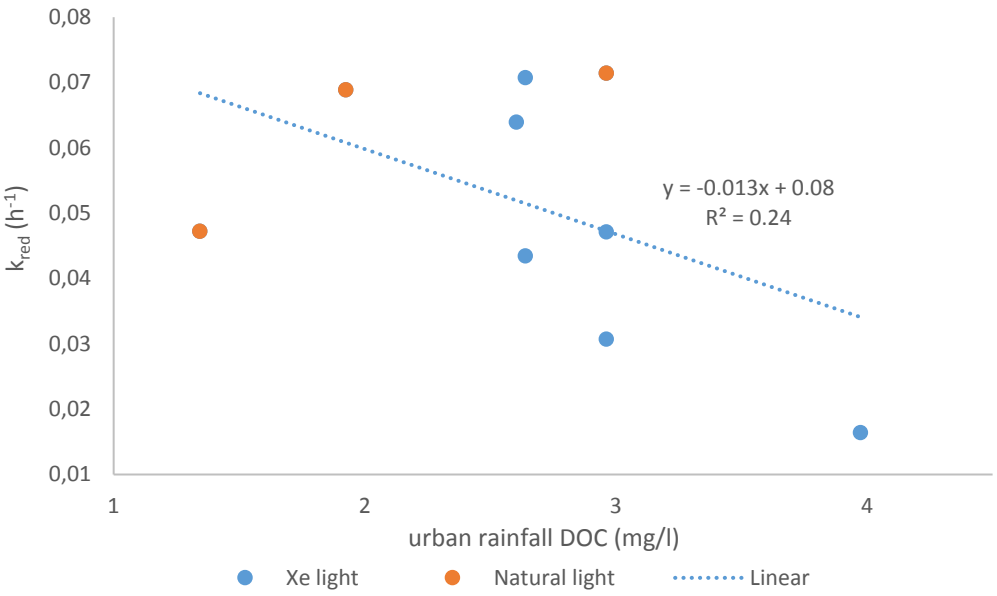

Figure 12 *photoreduction rates, k_{red} plotted as a function of urban toulouse rainfall DOC in the urban rainwater*

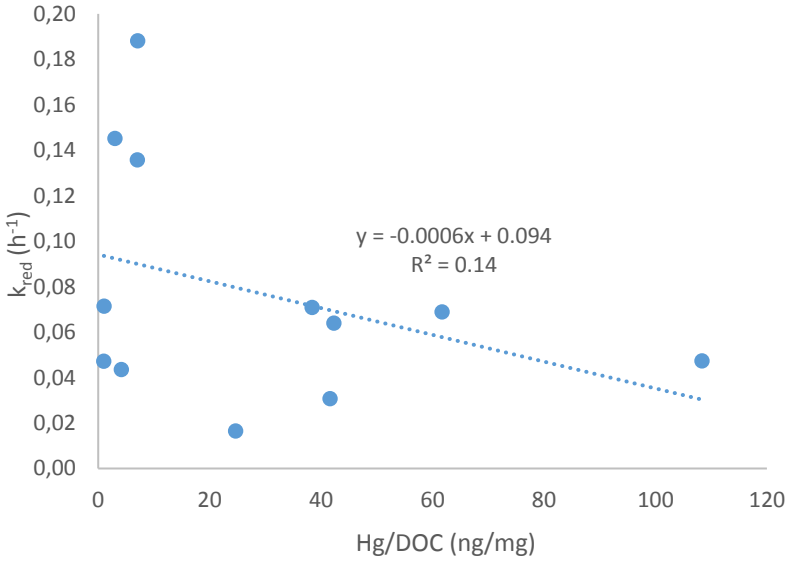

Figure 13 *photoreduction rates, k_{red} plotted as a function of Hg versus DOC in the rainwater.*

Table 4 *Summary of photoreduction experiments of artificial Hg solution (NIST 3133, 100ppb) for light and dark control experiments (A1-A3) and in the presence of different types of halides (A4-A6), in the presence of different Br^-/DOC ratios (A7-A12), in the presence of different types of halide/DOC (A13-A14). Hg concentrations in italics are included in kinetic rate constants analysis. Pseudo first-order reduction rate constants were calculated based on total Hg(II) concentration.*

experiment no.		A1	A2	A3	A4	A5	A6	A7	A8	A9	A10	A11	A12	A13	A14
pH		4.1	4.1	4.1	4.2	4.2	4.0	7.0	4.1	4.1	4.1	4.1	4.1	4.2	7.0
argon gas	ml/min	80	80	80	80	80	80	80	80	80	80	80	80	80	80
gross or net		gross	gross	gross	gross	gross	gross	gross	gross	gross	gross	gross	gross	gross	gross
light source		Xe	dark control	dark control	Xe	Xe	Xe	Xe	Xe	Xe	Xe	Xe	Xe	Xe	Xe
UVB	W/m²	25	/	/	25	25	25	25	25	25	25	25	25	25	25
UVA	W/m²	186	/	/	186	186	186	186	186	186	186	186	186	186	186
visible light	W/m²	242	/	/	242	242	242	242	242	242	242	242	242	242	242
Hg conc.	ng/l	100	100	100	100	100	100	100	100	100	100	100	100	100	100
DOC conc.	mg/l	/	/	/	/	/	/	1.00	1.00	1.00	1.00	1.00	1.00	1.00	1.00
matrix type		/	/	KBr	KCl	KBr	KI	/	KBr	KBr	KBr	KBr	KBr	KCl	KI
matrix conc.	mM	/	/	0.20	0.10	0.20	0.10	0.00	0.001	0.01	0.10	1.00	10.00	0.10	0.10
k_{red}	h^{-1}	0.022	0.009	0.001	0.016	0.004	0.0018	0.23	0.137	0.046	0.011	0.0055	0.001	0.158	0.0023
	h	ng/ml	ng/ml	ng/ml	ng/ml	ng/ml	ng/ml	ng/ml	ng/ml	ng/ml	ng/ml	ng/ml	ng/ml	ng/ml	ng/ml
Hg conc.	0	***86***	***85***	***113***	***101***	***101***	***100***	***92***	***100.5***	***102***	***109***	***105***	***114***	***107***	***119***
	0.17		***73***						***89.4***	***95***	***99***				
	0.25	***86***			***102***		***100***							***103***	
	0.50	***88***	***74***		***101***		***99***		***84.1***		***102***			***94***	
	0.67									***94***					
	0.75	***87***			***100***		***98***							***98***	
	1	***86***	***70***		***101***		***99***		***78***	***92***	***96***			***91***	
	2	***85***	***69***		***100***		***99***		***65***	***88***	***99***			***79***	
	3	***84***	***66***		***95***		***99***		***55***	***85***	***96***			***71***	
	4	***82***	***63***		***91***		***99***		***51***	***81***	***99***			***62***	
	5	***83***	***64***				***100***		***45***	***78***	***97***				
	6	***79***	***63***		***90***		***99***		***41***	***74***	***102***	***99***	***109***	***44***	
	12	**75**	***61***				***97***	***6***	***16***	***56***	***95***				
	19					***92.2***									
	24	**59**	***54***	***110***	***69***		97	3.8	***4***	26	***78***	***89***	***109***	***2.4***	***116***
	36	**42**	***50***				97	2.6	2.2	5.8					
	43					***86.1***									
	48	**29**	***51***	***106***			99	2.1	1.8	2.5	***61***	***80***	***106***		***106***

Table 5 *Measurement of natural UV and visible light intensities of outdoor photochemical experiments. Solar light PMA 2200 radiometer including PMA 2106, PMA 2110 and PMA 2130 employed for UV-B (280-320nm), UVA (320-400nm) and visible light (400-780nm) detector respectively.*

Experiment no.	Experiment name	date	light type	time	UVB	UVA	visible light	experiment time
					280-320 nm	320-400 nm	400-780 nm	
R5	Rain event 4-F-Natural light-TL	4/7/2017	Natural sunlight	10:05	0.600	24.37	97.595	0
				11:05	1.200	36.54	126.718	1
				12:20	1.750	44.52	149.16	2.25
				13:05	2.010	51.58	155.571	3
				14:05	2.040	51.88	165.487	4
				15:05	1.900	46.52	160.229	5
				16:30	1.530	39.51	131.985	6
				17:05	0.950	32.32	116.568	7
				18:05	0.510	22.73	89.029	8
R6	Rain event 5-F-Natural light-TL	5/7/2017	Natural sunlight	9:23	0.38	18.32	69.575	0
				10:23	0.77	28.25	103.967	1
				11:23	1.28	37.63	127.156	2
				12:23	1.66	44.77	147.202	3
				13:23	1.81	48.12	161.099	4
				14:23	1.78	46.33	154.710	5
				15:23	1.52	43.10	143.031	6
				16:23	1.13	35.67	123.698	7
				17:23	0.67	26.20	99.251	8
				18:23	0.31	17.18	71.396	9
				19:23	0.11	8.58	37.998	10
				20:23	0.02	2.78	10.648	11
R8	Rain event 8-U-Natural light-TL	31/8/2017	Natural sunlight	14:53	0.950	26.28	67.366	0
				15:08	0.830	33.79	167.210	0.25
				15:23	0.85	22.79	79.887	0.50
				15:38	0.37	10.13	24.658	0.75
				15:53	0.41	13.52	35.166	1
				16:53	0.140	6.03	16.319	2
				17:53	0.07	4.58	12.769	3
		1/9/2017	Natural sunlight	10:27	0.49	22.12	81.995	3
				11:27	0.97	32.93	110.323	4
				12:27	1.23	41.36	141.488	5
				13:27	1.43	46.25	154.211	6
				14:27	1.49	38.58	181.882	7
				15:27	0.67	18.49	43.545	8
				16:27	0.36	10.91	23.268	9
				17:27	0.15	8.81	24.532	10

Chapter 4. Photoreduction of gaseous oxidized mercury changes global atmospheric mercury speciation, transport and deposition (published coauthor article in Nature Communications)

4.1. article

Photoreduction of gaseous oxidized mercury changes global atmospheric mercury speciation, transport and deposition

Alfonso Saiz-Lopez[1,*], Sebastian P. Sitkiewicz[2], Daniel Roca-Sanjuán[3], Josep M. Oliva-Enrich[1], Juan Z. Dávalos[1], Rafael Notario[1], Martin Jiskra[4], Yang Xu[4], Feiyue Wang[5], Colin P. Thackray[6], Elsie M. Sunderland[6], Daniel J. Jacob[6], Oleg Travnikov[7], Carlos A. Cuevas[1], A. Ulises Acuña[1], Daniel Rivero[1], John M. C. Plane[8], Douglas E. Kinnison[9] and Jeroen E. Sonke[4]

[1]Department of Atmospheric Chemistry and Climate, Institute of Physical Chemistry Rocasolano, CSIC, Madrid 28006, Spain.

[2]Kimika Fakultatea, Euskal Herriko Unibertsitatea UPV/EHU and Donostia International Physics Center (DIPC), P.K. 1072, 20080 Donostia, Euskadi, Spain.

[3]Institut de Ciencia Molecular, Universitat de Valencia, Valencia 46071, Spain.

[4]Géosciences Environnement Toulouse, CNRS/OMP/Université de Toulouse, 31400 Toulouse, France.

[5]Centre for Earth Observation Science, Department of Environment and Geography, University of Manitoba, Winnipeg, MB R3T 2N2, Canada.

[6]Harvard John A. Paulson School of Engineering and Applied Sciences, Harvard University, Cambridge, Massachusetts 02138, USA.

[7]Meteorological Synthesizing Centre – East of EMEP, Moscow, Russia.

[8]School of Chemistry, University of Leeds, Leeds, UK.

[9]Atmospheric Chemistry Observations and Modelling, NCAR, Boulder, Colorado USA.

[*]Correspondence to: a.saiz@csic.es

Abstract

Anthropogenic mercury (Hg(0)) emissions oxidize to gaseous Hg(II) compounds, before deposition to Earth surface ecosystems. Atmospheric reduction of Hg(II) competes with deposition, thereby modifying the magnitude and pattern of Hg deposition. Global Hg models have postulated that Hg(II) reduction in the atmosphere occurs through aqueous-phase photoreduction that may take place in clouds. Here we report that experimental rainfall Hg(II) photoreduction rates are much slower than modeled rates. We compute novel absorption cross sections of gaseous Hg(II) compounds and show that fast Hg(II) photolysis can dominate atmospheric mercury reduction and lead to a substantial increase in modelled, global atmospheric Hg lifetime by a factor two. Models with Hg(II) photolysis show enhanced Hg deposition to land, which may prolong recovery of aquatic ecosystems long after Hg emissions are lowered, due to the longer residence time of Hg in soils than in oceans. These results call for a reassessment of atmospheric cycling and its impact on ecosystem health.

Introduction

Atmospheric mercury, a contaminant of global concern, is primarily emitted in the gaseous elemental Hg(0) form, with smaller contributions of gaseous oxidized Hg(II) and particle-bound Hg(II). Gaseous oxidized Hg(II)XY compounds may contain a variety of X,Y halogen atoms or oxygen-containing species, including Br, BrO, Cl, I, O, OH, HO_2, NO_2, and organic groups. Due to the low ambient concentration (pg m^{-3}), gaseous oxidized Hg(II) compounds have only been identified as $HgCl_2$ and $HgBr_2$ in urban and indoor air(Deeds et al. 2015b) and as $HgCl_2$ in power plant plumes(Ernest et al. 2014a). The atmospheric Hg(0) and Hg(II) forms have markedly different water solubility, chemical reactivity and lifetime against deposition. The lifetime of Hg(0) against deposition is in the range of several months to over a year, whereas that of Hg(II) compounds is on the order of days to weeks(Ariya et al. 2015b). Eventually, Hg(0) is oxidized to Hg(II) compounds, which are soluble, partition into aerosol, and deposit readily both by dry and wet mechanisms. Direct assimilation of Hg(0) by plants and oceans is also thought to be important(Horowitz et al. 2017a, Jiskra et al. 2018a). The long lifetime of Hg(0) leads to Hg deposition far from its emission sources to remote ecosystems, including the open oceans and polar regions. In aquatic ecosystems, Hg(II) is methylated and may be biomagnified up the food chain to levels that induce toxic effects in wildlife and humans(Sonke 2011).

The development of atmospheric chemistry and transport models (CTMs), an important tool for understanding global Hg cycling and predicting future Hg exposure, has drawn much attention to the mechanistic aspects of Hg(0) oxidation. While gas-phase O_3, OH, HO_2, H_2O_2, and NO_3 are all potential Hg(0) oxidants(Horowitz et al. 2017a, Dibble, Zelie and Mao 2012b, Lin and Pehkonen 1999a, Wang et al. 2014a), the oxidation process under atmospheric conditions is thought to be initiated primarily via photolytically produced atomic bromine by a two-stage mechanism (Fig. 1)(Horowitz et al. 2017a, Wang et al. 2014a, Goodsite, Plane and Skov 2004, Holmes, Jacob and Yang 2006a). In the first step, the dominant reaction to produce gaseous oxidized Hg(II) compounds is thought to be the oxidation of Hg(0) by bromine atoms, yielding the unstable intermediate HgBr. This radical can be readily dissociated back to Hg(0), but HgBr can also be competitively oxidized by other

major radical oxidant species in the atmosphere (e.g. OH, Br, I, Cl, NO_2, HO_2, BrO, IO and ClO) to a series of currently-assumed stable Hg(II) compounds, as shown in Figure 14:

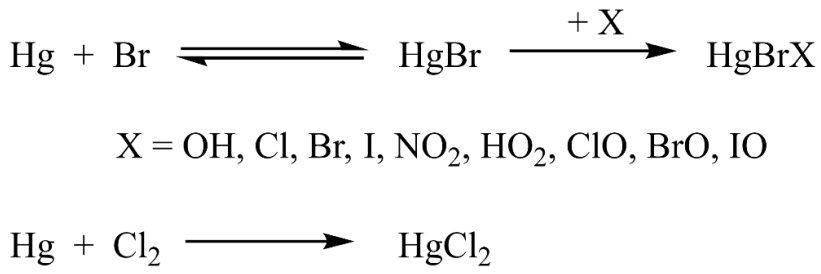

Figure 14 *Current understanding of the formation of oxidized Hg(II) compounds from atmospheric gaseous elemental mercury initiated by different oxidant species. This scheme also includes other secondary oxidation mechanisms involving single-step reactions with Cl_2, O_3, BrO and ClO.*

Much less is known about the reduction of Hg(II) compounds to Hg(0) in the atmosphere. Global Hg CTMs, based on Hg(0) oxidation alone, predict an unrealistically short residence time of Hg(0), and the simulated spatiotemporal Hg(0) variations would not match observations(Horowitz et al. 2017a). To reconcile such differences, these models need to include an adjustable term to account for Hg(II) reduction in the atmosphere. Such reduction has been presumed to occur in the aqueous phase of clouds(Horowitz et al. 2017a, Lin and Pehkonen 1999a, Shia et al. 1999b). Faster gas-phase Hg(0) oxidation kinetics has led to the need of these models to employ ever faster in-cloud Hg(II) reduction(Horowitz et al. 2017a), with maximum rate constants > ~1-3 h^{-1}, corresponding to in-cloud Hg(II) lifetimes < 1 hour on a global mean basis (see SI). Although aqueous Hg(II) photoreduction in Earth's surface waters is a well-documented process(Qureshi et al. 2011a), little experimental or observational evidence exists in the case of atmospheric liquid water(Pehkonen and Lin 1998b). Earlier studies suggested that Hg(II) reduction could proceed via aqueous SO_3 and HO_2 reaction pathways(Pehkonen and Lin 1998b, Seigneur, Vijayaraghavan and Lohman 2006a), but these pathways are now considered irrelevant at the global scale(Horowitz et al. 2017a). Therefore, the relevance of atmospheric aqueous Hg(II) reduction and the validity of their inclusion in the global mercury CTMs has been questioned(Horowitz et al. 2017a, Seigneur et al. 2006a, Gårdfeldt et al. 2003).

None of the global mercury models has tested the possibility of an alternative explicit gas-phase photoreduction of Hg(II) compounds, due to the poor understanding of its mechanism and reaction rates(Horowitz et al. 2017a). The most recent studies – albeit 27 years ago - suggested no gas-phase photoreduction for $HgCl_2$ and $Hg(CN)_2$ and slow photoreduction rates(Lindqvist et al. 1991, Strömberg, Strömberg and Wahlgren 1991) for $Hg(OH)_2$ and $Hg(SH)_2$, despite an earlier study of the UV absorption cross sections which suggested that $HgBr_2$ and HgI_2 could undergo relatively fast photolysis(Wadt 1980, Maya 1977). As far as we are aware there have been no further experimental or theoretical studies on the photolytic properties of Hg(II) compounds of atmospheric relevance.

Here, we revisit the photoreduction pathways of atmospheric Hg(II) compounds. First, we show that irradiation experiments with boundary layer and free tropospheric rainwater do not support fast aqueous-phase Hg(II) photoreduction. We then compute the UV-VIS absorption cross sections of the following Hg(II) compounds: $HgCl_2$, $HgBr_2$, HgBrI, HgBrOBr, HgBrOI, $HgBrNO_2$, HgBrONO, HgBrOH, HgBrOOH and HgO, using high-level quantum chemical methods, and infer the corresponding atmospheric photoreduction rates. Our results show for the first time that gas-phase Hg(II) photoreduction can proceed at relevant timescales, and is more important than in-cloud Hg(II) photoreduction. Inclusion of this new gaseous-phase Hg(II) photoreduction mechanism in two state-of-the-art global Hg models reveals major implications for our understanding of Hg cycling in the atmosphere, and its deposition to the surface environment.

Results

Laboratory rainfall Hg(II) photoreduction experiments. To study aqueous phase Hg(II) photoreduction, ten rainfall events were sampled in sub-urban Toulouse and at the high altitude (2877m) Pic du Midi Observatory (PDM, France) in the summer of 2017. Rainfall samples were irradiated in a quartz reactor with natural sunlight or with a solar simulator (see Methods). We observe (Supplementary Figure 1a and 1b, Supplementary Data and Supplementary Table 1) no statistically significant differences between rainfall Hg(II) reduction rates under natural (0.063 ± 0.013 h^{-1}) and simulated sunlight (0.037 ± 0.016 h^{-1}), and for filtered (0.058 ± 0.011 h^{-1}) and unfiltered (0.039 ± 0.020 h^{-1}) suburban rainwater (t-test, all $p>0.05$). The mean photochemical reduction rate of suburban rainfall was 0.08 ± 0.05 h^{-1} (σ, n=10). The mean rate at the remote PDM samples was two-fold higher, 0.15 ± 0.01 h^{-1} (σ, n=3), than that of the suburban Toulouse samples, and three times slower than the median photoreduction rate of 0.41 h^{-1} (n=24) for inland and marine waters(Qureshi et al. 2011a). Our experimental rainwater photoreduction rates, under fully sunlit conditions, are an order of magnitude slower that the optimized maximum in-cloud photoreduction rate(Horowitz et al. 2017a, Selin et al. 2007b) in global Hg CTMs of >1.0 h^{-1}.

Quantum chemical computation of gaseous Hg(II) absorption cross sections. We now turn to the computation of electronic spectra and absorption cross sections of gas-phase Hg(II) compounds which are required to estimate the corresponding photoreduction rates. A summary of the novel UV-VIS spectra and absorption cross sections, computed at the CASSCF/MS–CASPT2/SO–RASSI level of theory (Methods), is presented in Figure 15 for the 170 to 600 nm wavelength range. The calculated spectra of $HgCl_2$ and $HgBr_2$ are in very good agreement with previous experimental(Maya 1977, Roxlo and Mandl 1980, Schimitschek, Celto and Trias 1977, Frantom, Bletzinger and Garscadden 1980) and computed spectra(Wadt 1980) (Figure 16), thus providing strong support for the theoretical method applied here. The majority of the spectra consist of well-defined absorption bands in the 200-350 nm range, which are red-shifted when Cl is replaced with Br and I atoms. Note that three different

isomers could form from the reaction of HgBr with NO_2: $HgBrNO_2$, and *syn*- and *anti*-HgBrONO. However, high-level quantum chemical computations indicate that *syn*-HgBrONO is the most thermodynamically stable species(Jiao and Dibble 2017b).

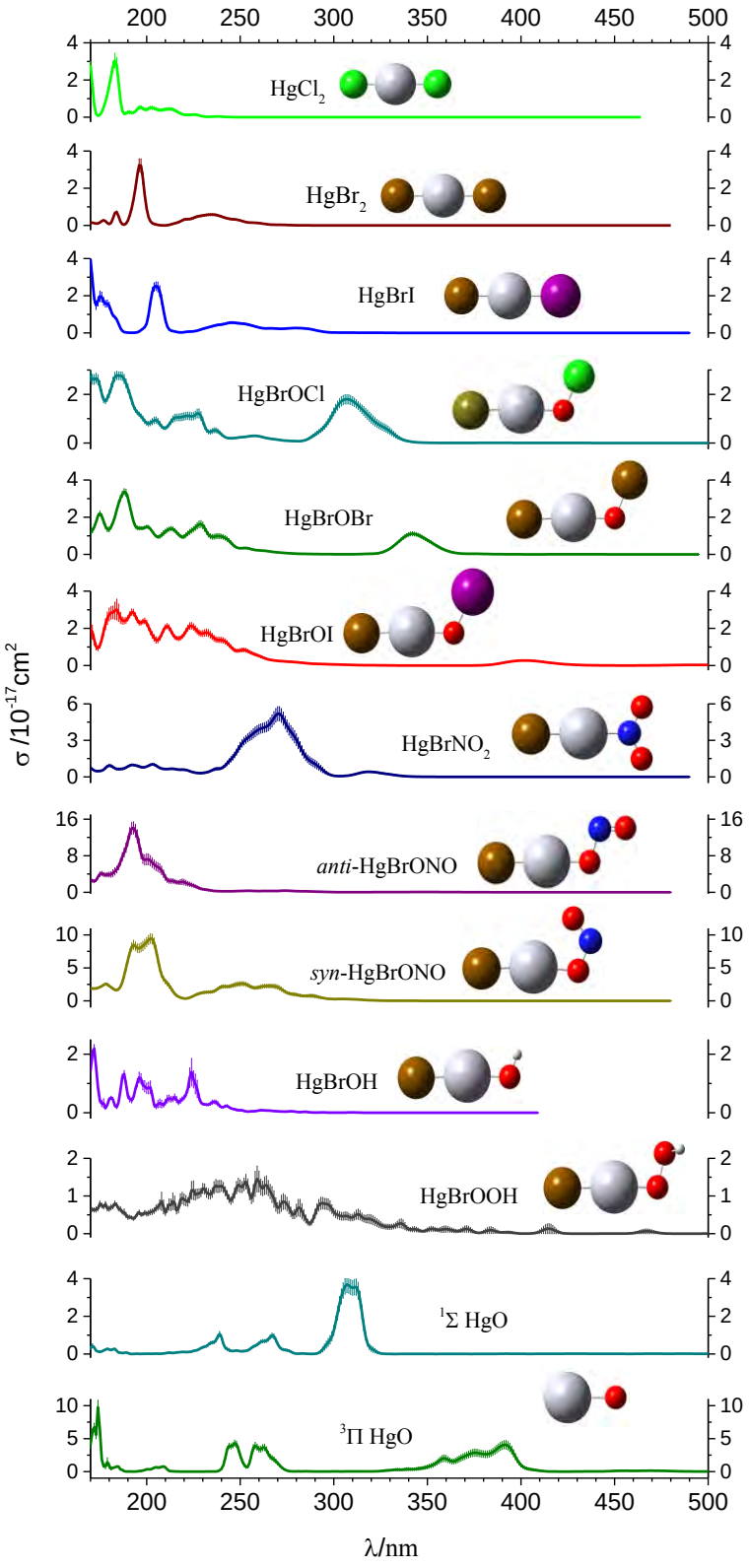

Figure 15 *Ball-and-stick representation and computed UV-VIS absorption spectra and cross sections (σ, cm^2) of the Hg(II) compounds studied in the present work. The light-coloured areas correspond to the uncertainty of the cross section due to the statistical sampling. Note the different range of σ values*

for some of the spectra. Also note that only wavelengths >290 nm are relevant for ambient tropospheric conditions.

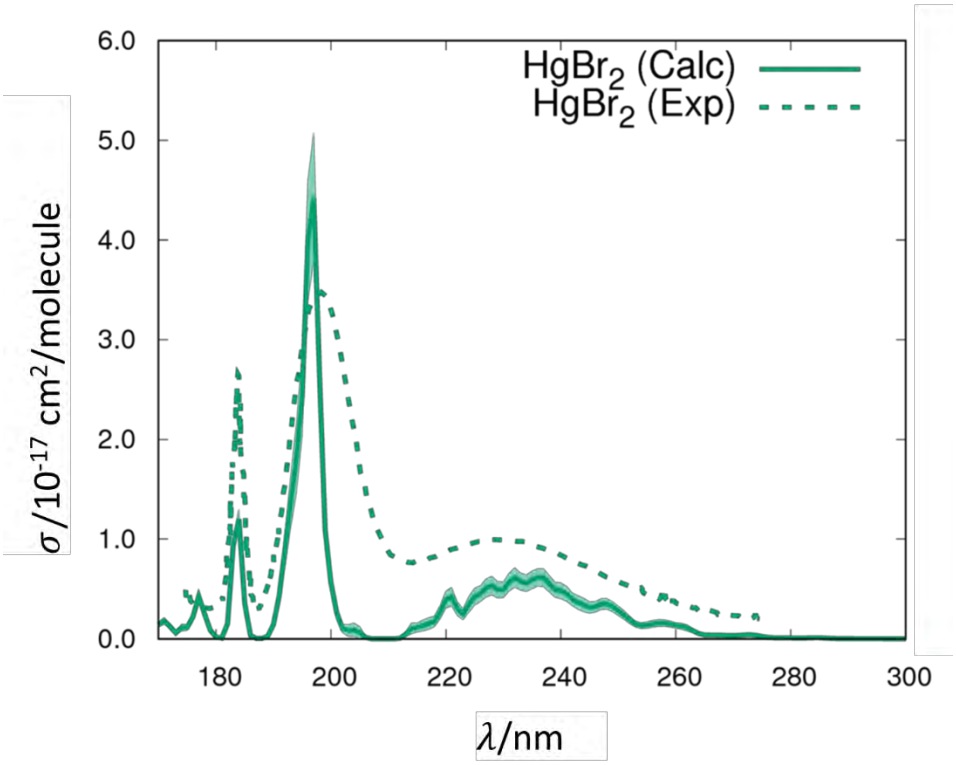

Figure 16 *Calculated and experimental(Frantom et al. 1980) cross section of gas-phase $HgBr_2$. The calculated spectrum was obtained at the CASSCF/MS–CASPT2/SO–RASSI level of theory with the ANO-RCC-VTZP basis set. The light coloured areas correspond to the numerical error of absorption cross sections due to the statistical sampling*

Computation of photolysis rates and atmospheric lifetime of Hg(II) compounds. The annually averaged atmospheric lifetime against photolysis in the troposphere for the Hg(II) compounds studied here are presented in Figure 17 (see also Supplementary Table 2 and Supplementary Figure 2 for zonal-averaged atmospheric lifetimes). The species with the longest lifetime is $HgCl_2$ (48 years), and the species with the shortest lifetime is HgBrOBr (< 1 second). These lifetimes were calculated by assuming a complete UV-Visible driven photodissociation to HgBr under atmospheric conditions. In the case of the parent $HgBr_2$ compound it is well known that irradiation with ~200 nm UV light yields the monohalide (HgBr) with nearly 100% efficiency(Schimitschek et al. 1977, Erlandson and Cool 1983, Whitehurst and King 1987, Wilcomb, Burnham and Djeu 1980). Moreover, detailed quantum-

chemical computations of the Cl- and Br-dihalides predict further efficient photodissociation at wavelengths(Wadt 1980) longer than 200 nm. There are no comparable experimental or calculated photolysis data for the other HgBr-X compounds studied here. Nevertheless, a similar very efficient photodissociation step is to be expected for these mercury halides considering the even lower dissociation energies of the HgBr-X bond, as compared with that of the parent HgBr-Br dihalide (Supplementary Table 3)(Dibble et al. 2012b, Jiao and Dibble 2017b). In addition to this primary photolysis reaction to HgBr, it has been shown that Hg(0) is also generated in the $HgBr_2$ photodissociation through direct or secondary channels, although to a much lesser extent(Baker and Seddon 1988, Schilowitz and Wiesenfeld 1982). Based on this evidence, we consider in the atmospheric modelling below that HgBr is the main product of HgBrX photodissociation, although we also ran one scenario where HgBrX photodissociation results in Hg(0) production.

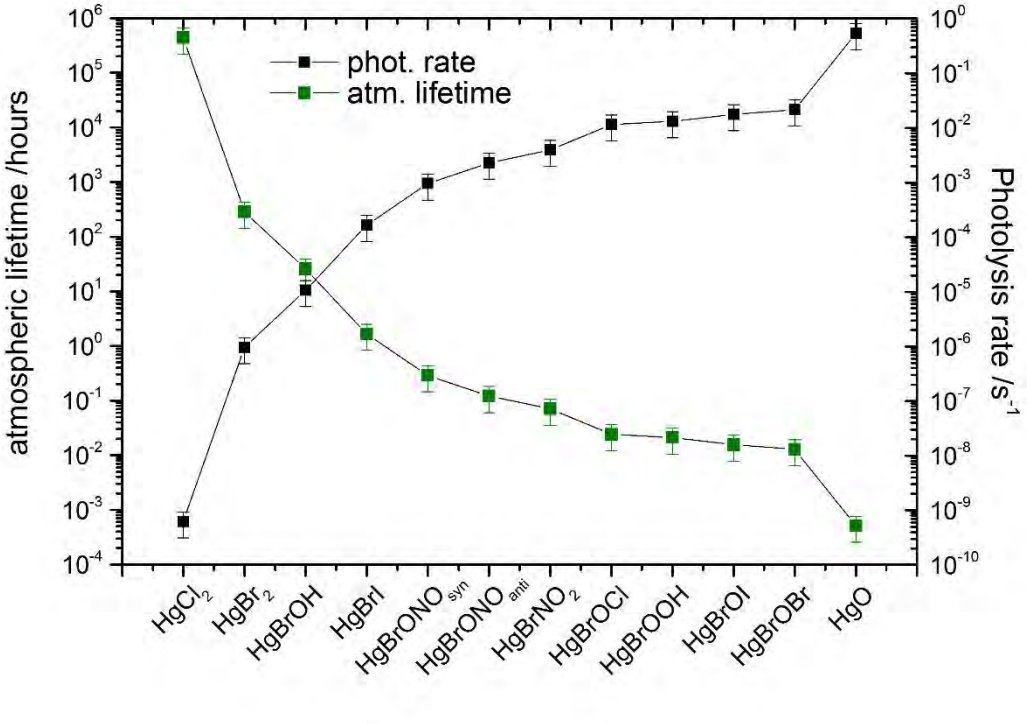

Figure 17 *Annually- and globally-averaged photolysis rate (s^{-1}) and lifetime (h) of Hg(II) compounds in the troposphere.*

Table 6 *Model test runs for different atmospheric Hg(II) reduction scenarios in the GLEMOS model.*

Run ID	Scenario
Run #1	No Hg(II) reduction
Run #2	Hg(II) reduction in aqueous phase using the experimentally derived rate constant (0.15 h^{-1}) in this study
Run #3	Gas phase Hg(II) photoreduction to Hg(0)
Run #4	Gas phase Hg(II) photoreduction to $Hg^{I}Br$

The absorption cross sections of *syn*-HgBrONO, HgBrOOH, HgBrOH, $HgBr_2$, HgBrOCl and HgBrOBr were implemented into the GEOS-Chem(Horowitz et al. 2017a) and GLEMOS(Travnikov 2005, Travnikov et al. 2017) global Hg chemistry and transport models (Methods), since these Hg(II) species are the most likely to be formed in the atmosphere(Horowitz et al. 2017a, Wang et al. 2014a, Jiao and Dibble 2017b). GEOS-Chem simulates Hg(II) as a single tracer, whereas GLEMOS simulates Hg(II) species individually. In GEOS-Chem the rapidly photolyzing Hg(II) species (HgBr-[ONO, OOH, OCl, OBr]) are calculated to be at pseudo-steady-state with $Hg^{I}Br$ to prevent over-reduction. *syn*-HgBrONO and HgBrOOH generally dominate the production of Hg(II) in both models (Supplementary Figure 3), whilst $HgBr_2$ becomes the prevalent Hg(II) species in the troposphere (Supplementary Figure 4) due to its longer lifetime against photolysis. Note that direct photoreduction to Hg(0) produces unrealistically long Hg lifetimes >19 months in both models. Therefore, photoreduction was considered to produce $Hg^{I}Br$ in all cases. Indeed, intensive photolysis of *syn*-HgBrONO and HgBrOOH causes $Hg^{I}Br$ to be a relevant species in the free troposphere (Supplementary Figure 5 and Fig. 5). $Hg^{I}Br$ can then be re-oxidized to gaseous Hg(II), or decay to Hg(0) by thermal dissociation, which is strongly dependent on pressure and temperature(Horowitz et al. 2017a, Dibble et al. 2012b). Atmospheric aqueous Hg(II) reduction parameterizations in both models were capped with an upper limit that corresponds to our observed rainfall photoreduction rate constant, $k_{red} = 0.15$ (h^{-1}). Published model runs with fast aqueous phase Hg(II) reduction and without the gas-phase photoreduction(Horowitz et al. 2017a, Travnikov 2005, Travnikov et al. 2017) yield total atmospheric Hg lifetimes of 5.2 and 4.6 months against deposition. Our new results show that

gaseous Hg(II) photoreduction increases the Hg lifetime to 13 and 10 months in GEOS-Chem and GLEMOS model Run#4, respectively. We find that gas-phase photoreduction is the dominant reduction pathway. GLEMOS does not include the highly uncertain reduction reaction(Horowitz et al. 2017a) $HgBr + NO_2 \rightarrow Hg(0) + BrNO_2$. Omitting this reaction in GEOS-Chem lowers the Hg lifetime from 13 to 8 months in model Run#4.

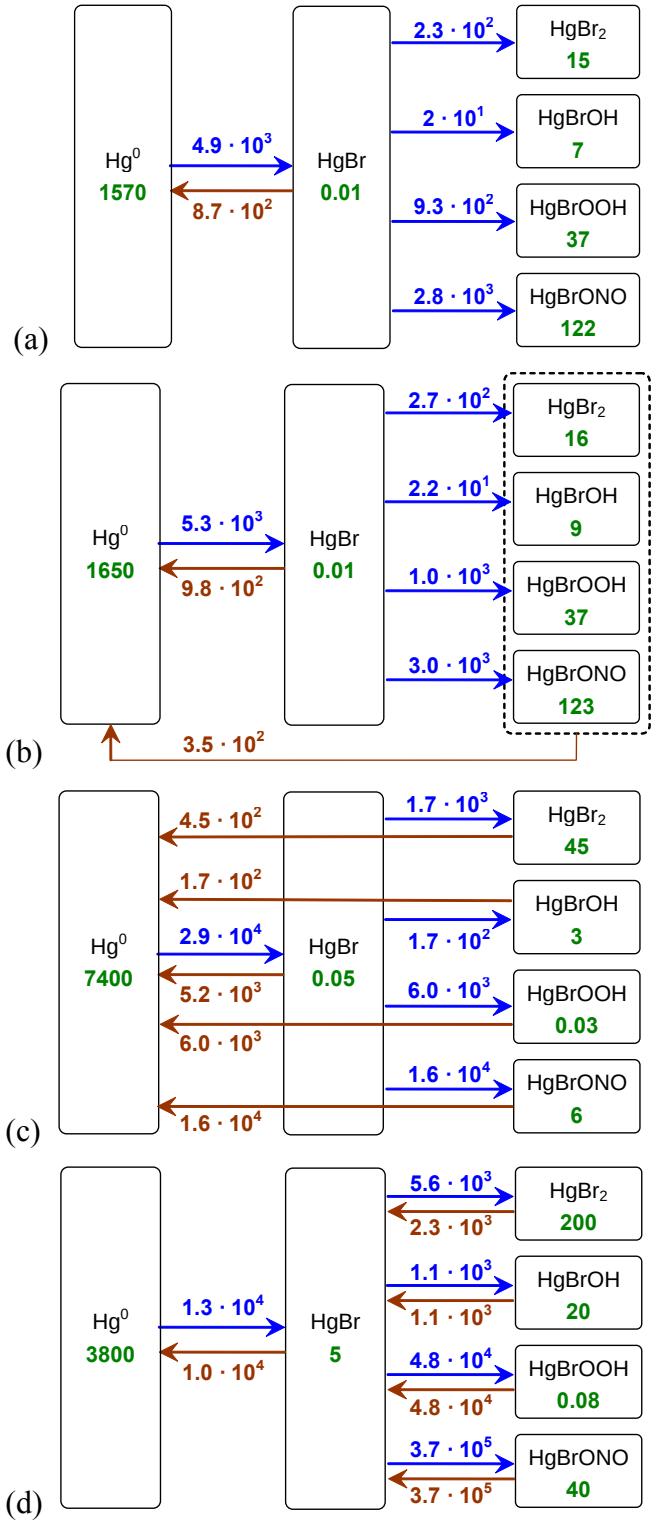

Figure 18 *Global budget of Hg chemical cycling covering the troposphere and lower stratosphere (up to ca. 30 kms) for different tests in GLEMOS: (a) – Run #1; (b) – Run #2; (c) – Run #3; (d) – Run #4. The mass estimates are in Mg, the fluxes are in Mg* a^{-1}.

We further examined the global atmospheric Hg(0) and Hg(II) distribution in GLEMOS. The different model simulated scenarios for atmospheric Hg(II) reduction are shown in Table 1. Figs. 6-7

show the effect of the new photoreduction scheme on the global distribution of Hg(0) surface concentration. All these simulations were made with the previously assumed aqueous photoreduction mechanism removed. We find that simulations without the gaseous photoreduction lead to 35-40% underestimation of observed Hg(0) (Runs #1 and #2). The gas phase Hg(II) photoreduction to Hg(0) (Run #3) results in unrealistically high Hg(0) concentrations with almost two-fold overestimation of the observations and strong underestimation of wet deposition. The model run with incorporation of the gas phase photoreduction to HgBr (Run #4) shows that Hg(0) levels are 18% overestimated, and model Hg(II) wet deposition 20% underestimated with respect to observations (Fig. 6, Supplementary Table 4). The results of test Run#4 are closest to the observations which suggest that gas phase reduction processes are important but also that re-oxidation via the HgBr intermediate is important. An additional step in the evaluation of model results can be made by examining the variability of modelled and observed Hg concentrations. Previous studies indicated that longer Hg(0) lifetimes lead to lower simulated Hg(0) variability, as represented by the standard deviation (1σ) of mean Hg(0) concentrations(Horowitz et al. 2017a, Travnikov et al. 2017). Here, gas-phase photoreduction leads to simulated Hg(0) levels at the measurement sites (1.62±0.36 ng/m^3, 1σ, STP) that have a larger standard deviation than observed Hg(0) (1.38±0.25 ng/m^3, 1σ, STP). This indicates that the longer Hg(0) lifetime estimates of 8-13 months resulting from model Run#4 are broadly compatible with observed Hg(0) variability (1σ). The resulting global zonal distribution of Hg(0) and speciated Hg(II) (*syn*-HgBrONO, HgBrOOH, HgBrOH, HgBr, $HgBr_2$) reveals the major effects of gas-phase Hg(II) photoreduction in the global budget of atmospheric oxidized mercury (Supplementary Figures 4-9) and in the global patterns of mercury surface deposition (Fig. 8 and Supplementary Figure 10). In particular, it leads to strong decrease of free tropospheric concentrations of *syn*-HgBrONO and HgBrOOH, which were previously considered as dominant Hg^{II} species. In contrast, concentrations of HgBrOH and $HgBr_2$ increase drastically due to the lower photolysis rates. The incorporation of gas-phase photoreduction leads to an increase in global Hg(0) deposition from 11% (Run#1) to 24% (Run#4) at the expense of Hg(II) deposition (down by 13%, Fig. 8 and Supplementary Figure 10). We

further observe a reduction of Hg deposition (dry and wet) to the ocean (down by 15%, Fig. 8 and Supplementary Figure 10). and an increase of Hg(0) dry deposition to the land surface (22%), particularly to vegetation in line with the recent findings that foliar uptake by vegetation drives continental Hg(0) seasonality(Jiskra et al. 2018a). Global chemical budget diagrams (Fig. 5) summarize the Hg(0), Hg(I) and Hg(II) cycling in different model runs.

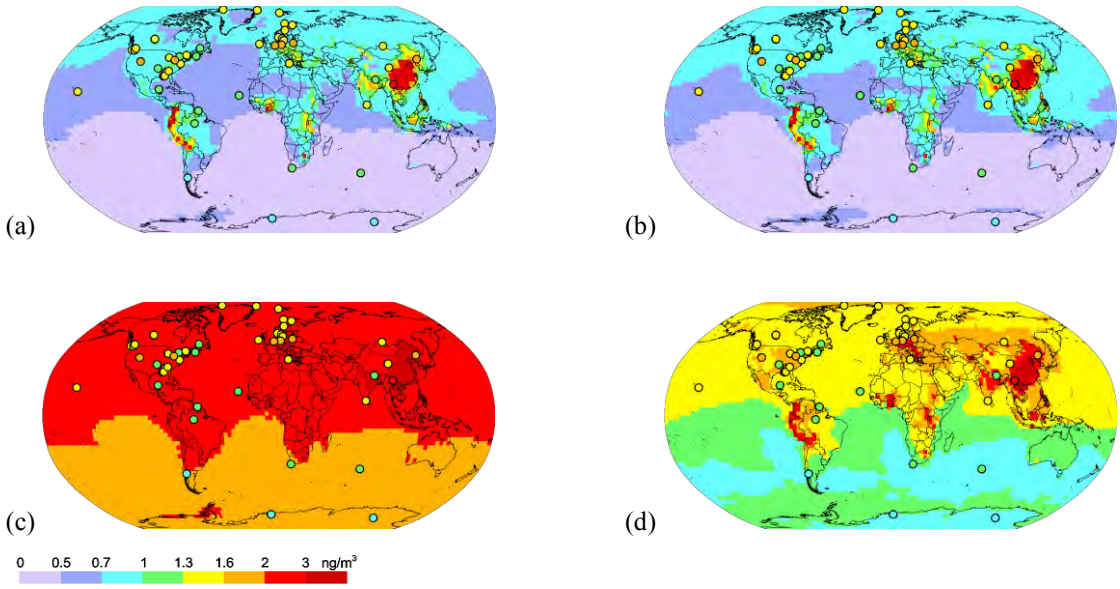

Figure 19 *Spatial distribution of Hg(0) surface concentration for different atmospheric Hg(II) reduction simulations in the GLEMOS model: (a) Run #1; (b) Run #2; (c) Run #3; (d) Run #4. Circles show observed values in the same color scale. The measurement dataset is the same as in ref (Travnikov et al. 2017).*

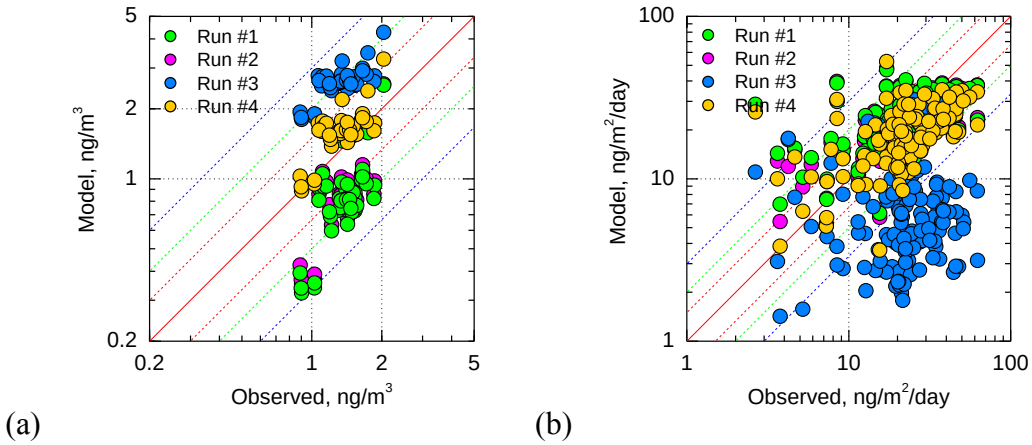

Figure 20 Comparison of simulated Hg(0) air concentration (a) and Hg(II) wet deposition (b) from the GLEMOS model with measurements for the year 2013. The measurement dataset is the same as in ref (Travnikov et al. 2017).

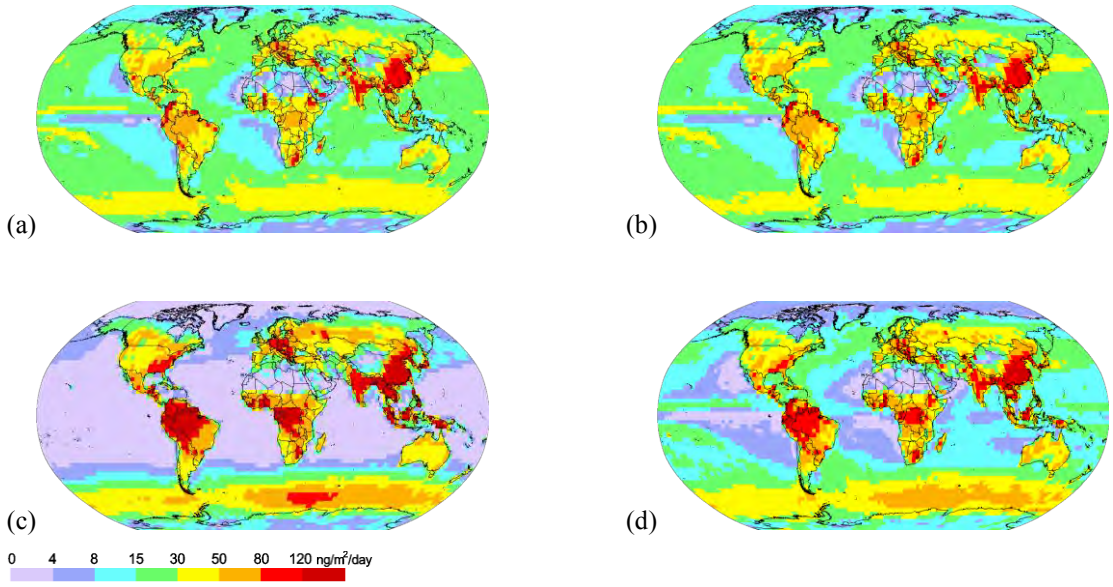

Figure 21 *Spatial distribution of total Hg (i.e. Hg^0 + Hg^{II}) deposition for different tests in GLEMOS: (a) – Run #1; (b) – Run #2; (c) – Run #3; (d) – Run #4. Circles show observed values in the same color scale. The measurement dataset is the same as in ref 32 in the main text.*

This work shows that the presence of an efficient gaseous phase Hg(II) photoreduction challenges our understanding of Hg cycling in the atmosphere and its deposition to the surface environment. We show that the new gas-phase Hg(II) photoreduction mechanism is likely the dominant reduction pathway for atmospheric mercury which changes the concept of the speciation of

Hg(II) in the atmosphere. Its inclusion in state-of-the-art global models leads to significant modifications in the local scale deposition of Hg to the Earth's surface. As a result, enhanced deposition to land surfaces may prolong recovery of aquatic ecosystems long after Hg emissions are curbed, due to the longer residence time of Hg in soils than in oceans(Schuster et al. 2018).

Methods

1. Computation of UV-Vis absorption spectra and cross sections

A set of theoretical methods previously calibrated(Sitkiewicz et al. 2016b) were used for calculating the electronic absorption spectra and cross-sections of $HgCl_2$, $HgBr_2$, HgBrI, HgBrOBr, HgBrOI, HgBrOCl, $HgBrNO_2$, HgBrONO, HgBrOH, HgBrOOH and HgO. Specifically, the highly accurate multireference CASSCF/MS-CASPT2 method(Finley et al. 1998), with the ANO-RCC-VTZP basis set(Roos et al. 2004) was applied, taking into account scalar relativistic and spin-orbit coupling (SOC) effects (see below section 1.1 and 1.2, and Supplementary Table 5 for further details). Scalar relativistic effects were included by means of the third-order Douglas-Kroll and Hess (DKH3) Hamiltonian, and the spin-orbit coupling (SOC) was computed using the restricted active space state interaction (RASSI) method, as implemented in the Molcas 8 program(Aquilante et al. 2016).

Vertical transition energies from the ground to electronically excited states and the corresponding oscillator strengths, expressed as absorption cross-sections (cm^2), were determined as described previously(Sitkiewicz et al. 2016b). The agreement between computed and experimental transition energies was in the range of 5-10%, for those few cases in which gas-phase experimental data were available, namely for mercury compounds $HgCl_2$ and $HgBr_2$ (Figure 2). The corresponding uncertainty in the calculated cross-section values is ±25% for the most intense transitions (see Figure 2), similar to the actual dispersion of the experimental values(Maya 1977, Roxlo and Mandl 1980, Schimitschek et al. 1977, Frantom et al. 1980).

The atmospheric modelling methods used in the present work require as input data the absorption spectrum of any compound that may undergo photolysis under atmospheric conditions. Therefore, absorption spectra were generated for all the compounds studied here by sampling the nuclear coordinates of the ground-state equilibrium structure and frequencies according to a Wigner distribution, as described in refs(Barbatti, Aquino and Lischka 2010, Crespo-Otero and Barbatti 2012). The Wigner distribution of geometries was obtained with the Newton-X 1.4 program(Barbatti et al. 2007, Barbatti et al. 2014), and an in-house program was used to compute the cross sections from the

energies and oscillator strengths generated by the Molcas program. The ground-state structures and frequencies needed to generate the Wigner distribution were obtained by using the PBE0 functional(Adamo and Barone 1999) with the Def2QZVP basis set(Andrae et al. 1990, Peterson et al. 2003, Weigend and Ahlrichs 2005) as implemented in the Gaussian 09 package(Frisch et al. 2009). The minor differences (see section 1.1 and 1.2) observed in the simulated spectra due to ground-state geometries generated using either CASPT2, CCSD or DFT functionals are presented in Supplementary Figure 11.

1.1 Details on the selected active spaces

In this section, the selected active spaces for the CASSCF/CASPT2 computations are briefly discussed. First general details are given and next we discuss those aspects which refer to each group of compounds.

According to our first paper on benchmarking the methodology for the representative $HgBr_2$ molecule(Sitkiewicz et al. 2016a) and on the basis of several test CASSCF computations with distinct active spaces for the whole set of molecules, some rules regarding the selection of the active spaces could be established:

1) For all the systems, s-subshell orbitals (and electrons) are not relevant in the studied energy range (up to 170 nm) and therefore were kept inactive and doubly occupied, except for the 6s orbital of Hg, which has a key role in the transitions.

2) The 5d orbitals of Hg are neither involved in the transitions within the energy region of our interest, and therefore were not correlated in CASSCF/CASPT2 simulations for any system with the exception of the $1^1\Sigma$ and $1^3\Pi$ states of HgO. For this system, tests showed a small contribution of the 5d orbitals for high-energy transitions close to 170 nm.

3) The 6p orbitals of Hg, especially those perpendicular to σ orbitals of Hg-X, namely $6p_x$ and $6p_y$, should be correlated at the CASSCF level. On the other hand, test calculations have shown that the

Hg atomic orbital of $6p_z$-type, colinear with mercury covalent bonds, have not any significance in the transitions relevant for this study, and were not included in the active spaces for the larger systems.

3) The two last NOs of non-bonding character, consisted of Br $4d_{xz/yz}$ + Br $4d_{xz/yz}$ AOs and used in our first benchmark study, were not necessary for the computations and were omitted in the di- and triatomic systems, in order to reduce computational effort.

For each particular compound, the following criteria were adopted:

$HgCl_2$ $HgBr_2$ and HgBrI – CAS(12,10). For these systems, the optimal active spaces consisted of 12 electrons distributed over 10 NOs of the following character: σ/σ^*-type(Hg 6s ± Cl $3p_z$ / Br $4p_z$ / I $6p_z$ and Hg $6p_z$ ± Cl $3p_z$ / Br $4p_z$ / I $5p_z$), σ^{nb}-type (Cl $3p_z$ / Br $4p_z$ / I $5p_z$), and π^{nb}-type (Cl $3p_{x/y}$ / Br $4p_{x/y}$ / I $5p_{x/y}$ and Hg $6p_{x/y}$). Although included in the active space, the σ^* orbital, Hg $6p_z$ ± Cl $3p_z$ / Br $4p_z$ / I $5p_z$ (NO 10) was not occupied due to the excitations.

$^1\Sigma$ HgO and $^3\Pi$ HgO. The optimal active spaces consisted of 16 electrons distributed over 12 NOs. For these systems only, the active space additionally had to include 10 electrons belonging the Hg 5d-subshell, where the remaining NOs were of the following type: σ/σ^*-type (Hg 6s ± O $2p_z$ and Hg $6p_z$ ± O $2p_z$), and π^{nb}-type (O $2p_{x/y}$ and Hg $6p_{x/y}$). In contrast to the other systems studied, σ^* Hg $6p_z$ + O $2p_z$ had observable contribution in the excitations.

HgBrOBr and HgBrOI. The optimal active spaces consisted of 16 electrons distributed over 12 NOs. It consisted of the NOs formed by Hg 6s and the AOs of p-type: O $2p_{x/y/z}$, Br $4p_{x/y/z}$ / I $5p_{x/y/z}$ and Hg $6p_{x/y}$. Tests have shown that for the relevant energy region in the UV-VIS range, there are no relevant transitions to the Hg $6p_z$ orbital, and therefore it was not included in the active space due to the computational limits.

syn-HgBrONO and anti-HgBrONO. For these two isomers, the optimal active spaces consisted of 16 electrons distributed over 12 NOs. It consisted of the NOs formed by Hg 6s and the AOs of p-type: O $2p_{x/y/z}$, Br $4p_{x/y/z}$ / I $5p_{x/y/z}$ and Hg $6p_{x/y}$. Several orbitals from the full valence space had to be omitted

due to the computational limits. Tests have shown that for the relevant wavelength region in the UV-VIS, one σ-type bonding NO between O-N-O group of atoms remain doubly occupied (and moved to the inactive space), whereas the Hg $6p_z$ orbital and the higher σ^*-type virtual orbitals are not active and therefore were kept in the secondary space.

HgBrOH and HgBrOOH. In the case of HgBrOOH, the optimal active spaces were similar to those of HgBrOBr and HgBrOI. They consisted of 16 electrons distributed over 12 NOs formed by Hg 6s and the AOs of p-type: O $2p_{x/y/z}$, Br $4p_{x/y/z}$ / I $5p_{x/y/z}$ and Hg $6p_{x/y}$. Tests have shown that for the selected energy region in the UV-VIS there are no relevant transitions to the Hg $6p_z$ orbital, and therefore it was not included in the active space due to the computational limits. In the case of HgBrOH, full valence active space (12,11) with additional p-type orbitals of Hg was selected.

$HgBrNO_2$. For this compound, the selected active space is chemically the same as of the syn- and anti-HgBrONO, the optimal active spaces consisted of 16 electrons distributed over 12 NOs. It consisted of the NOs formed by Hg 6s and the AOs of p-type: O $2p_{x/y/z}$, Br $4p_{x/y/z}$ / I $5p_{x/y/z}$ and Hg $6p_{x/y}$. Several orbitals from the full valence space had to be omitted due to the computational limits. Tests have shown that for the relevant energy region in the UV-VIS, one σ-type bonding NO between O-N-O group of atoms remain doubly occupied (and moved to the inactive space), whereas the Hg $6p_z$ orbital and the higher σ^*-type virtual orbitals are not active and therefore were kept in the secondary space.

For the di- and triatomic systems, the highest possible symmetries, which enabled for every possible displacement of atoms, were used in the calculations – C_{2v} in HgO and C_s in $HgCl_2$, $HgBr_2$ and HgBrI. For other studied systems, no symmetry was adapted (C_1 group). For a particular system, number of SF states to account for in the CASSCF/CASPT2 calculations was selected accordingly to the energy criteria, in such way to include all relevant SF transitions up to 170 nm (and later apply SOC effects). All of the parameters of the carried simulations of the spectra, such the number of sampled geometries N_p, broadening of the Gaussian shape functions δ, and the numbers of included states per symmetry, are presented in detail in Supplementary Table 5.

1.2. Test of geometry distribution used for simulations (DFT vs CASPT2 vs CCSD distribution)

The comparison of the simulated UV-VIS spectra when using differently generated sets of geometries is presented in Supplementary Figure 11 for the representative $HgBr_2$ molecule. The optimization of the geometry of the ground state and the frequencies of normal modes were obtained (and further used in Wigner distribution) using three different quantum-chemical methods:

- PBE0/Def2QZVP (presented in paper),
- CCSD/Def2QZVP
- SS-CASPT2(12,10)/ANO-RCC-VTZP

The computations of the electronic structure of the excited states were done at the same level of theory: SOC-DKH3-MS-CASPT2(12,10)/ANO-RCC-VTZP. The number of sampled geometries N_p and broadening of the Gaussian shape functions δ, were the same for all of the optimization methods: N_p=100 and δ=0.05 eV, as shown in Supplementary Table 5.

2. Computation of the photolysis rates

In this study we employ the global 3D chemistry-climate model CAM-Chem (Community Atmospheric Model with chemistry, version 4.0)(Gent et al. 2011), to estimate the photolysis rate (J), and therefore the atmospheric lifetime (τ=1/J), of the different Hg(II) species according to their computed absorption cross section. The model includes a comprehensive chemistry scheme to simulate the evolution of trace gases and aerosols in the troposphere and the stratosphere(Ordóñez et al. 2012). The model runs with the chlorine, iodine and bromine chemistry schemes from previous studies(Fernandez et al. 2014, Saiz-Lopez et al. 2014, Saiz-Lopez et al. 2015), including the photochemical breakdown of bromo- and iodo-carbons emitted from the oceans(Ordóñez et al. 2012) and abiotic oceanic sources(Prados-Roman et al. 2015) of HOI and I_2. We have included all the Hg(II) species ($HgCl_2$, $HgBr_2$, HgBrI, HgBrOCl, HgBrOBr, HgBrOI, $HgBrNO_2$, HgBrONO (*syn* and *anti*), HgBrOH, HgBrOOH and HgO) and their computed absorption cross sections. CAM-Chem has been configured in this work with a horizontal resolution of 1.9º latitude by 2.5º longitude and 26 vertical

levels, from the surface to ~40 km altitude. The model run in this study was performed in the specified dynamics mode(Ordóñez et al. 2012) using offline meteorological fields instead of an online calculation. This offline meteorology consists of a high frequency meteorological input from a previous free running climatic simulation.

3. Description of the GEOS-Chem model

In this study, we use the GEOS-Chem Hg simulation from ref(Horowitz et al. 2017a) using the surface slab ocean boundary parametrization(Soerensen et al. 2010). The model calculates the transport and chemistry of tracer species Hg(0) and Hg(II). The parametrization of gas-particle partitioning of Hg(II) is from ref(Amos et al. 2012a), and the mercury redox chemistry (described in detail in Supplementary Table 6) includes Br- and Cl-initiated oxidation. Radical concentrations for Hg redox chemistry are from ref(Schmidt et al. 2016) with a diurnal cycle based on solar zenith angle imposed on top of monthly averages. Photolysis of HgBr-X species is calculated using the GEOS-Chem implementation(Eastham, Weisenstein and Barrett 2014) of the Fast-JX code(Bian and Prather 2002).

4. Description of the GLEMOS model

For evaluation of the new Hg chemical mechanisms under the atmospheric conditions we apply the 3D multi-scale chemical transport model GLEMOS (Global EMEP Multi-media Modelling System). The model simulates atmospheric transport, chemical transformations and deposition of Hg species(Travnikov 2005, Travnikov and Ilyin 2009, Travnikov et al. 2017). In this study the model grid has a horizontal resolution 3°×3° and covers troposphere and lower stratosphere up to 10 hPa (ca. 30 km) with 20 irregular terrain-following sigma layers. The atmospheric transport of the tracers is driven by meteorological fields generated by the Weather Research and Forecast modelling system (WRF)(Skamarock et al. 2005) fed by the operational analysis data from the European Centre for Medium-Range Weather Forecasts (ECMWF) (*ECMWF*, 2018)(ECMWF: European Centre for Medium-Range Weather Forecasts (datasets available from http://www.ecmwf.int/en/forecasts/dataset). In the current version the model transports Hg(0) and four

Hg(II) species ($HgBr_2$, HgBrOH, HgBrOOH, $HgBrNO_2$) as separate species. Gas-particle partitioning of Hg(II) is parameterized following ref(Amos et al. 2012a)[55]. A two-step mechanism of Hg(0) oxidation by Br in gas phase is included (ref (Horowitz et al. 2017a)[5]):

$$Hg(0) + X + M \rightarrow Hg^{I}X + M \quad \text{(R1)}$$

$$Hg^{I}X + M \rightarrow Hg(0) + X + M \quad \text{(R2)}$$

$$Hg^{I}X + Y \rightarrow Hg(0) + XY \quad \text{(R3)}$$

$$Hg^{I}X + Y + M \rightarrow Hg^{II}XY + M, \quad \text{(R4)}$$

The full reaction scheme is listed in Supplementary Table 6. Briefly, X ≡ Br is the first-step Hg(0) oxidant, Y is the second-step Hg(I) oxidant, and M is a molecule of air. The reaction rate constants are from: ref (Donohoue et al. 2006b) for R1; ref (Dibble et al. 2012b) for R2; ref (Balabanov, Shepler and Peterson 2005b) for Y ≡ Br in R3; ref (Goodsite et al. 2004) for Y ≡ Br and OH in R4; ref (Jiao and Dibble 2017b) for Y ≡ HO_2 and NO_2 in R4. Six-hourly concentration fields of Br are archived from a GEOS-Chem simulation(Parrella et al. 2012), whereas OH, HO_2, NO_2 and particulate matter ($PM_{2.5}$) fields are imported from MOZART(Emmons et al. 2010). The aqueous-phase chemistry includes oxidation(Lin and Pehkonen 1999a, Gårdfeldt et al. 2001, Munthe 1992b) of Hg(0) by dissolved O_3, OH and $Cl(I)^I$. We have included the gas-phase photoreduction of $HgBr_2$, HgBrOH, HgBrOOH, *syn*-HgBrONO using the rates calculated by CAM-Chem and the aqueous-phase photoreduction in cloud droplets with the photolysis rate constant 0.15 h^{-1} estimated in this study. We perform simulations for the period 2007-2013 using anthropogenic emissions for 2010 (AMAP/UNEP 2013b, AMAP/UNEP 2013a). Prescribed fluxes of Hg natural and secondary emissions from soil and seawater are generated depending on Hg concentration in soil, soil temperature and solar radiation for emissions from land and proportional to the primary production of organic carbon in seawater for emissions from the ocean(Travnikov and Ilyin 2009). The first 6 years of the period are used for the model spin up to achieve the steady-state Hg concentrations in the troposphere. The model results are presented as annual averages for 2013.

5. Description of rainfall Hg(II) gross reduction rate experiments

Ten rainfall events were sampled in sub-urban Toulouse and at the high mountaintop Pic du Midi Observatory (Sprovieri et al.) in the summer of 2017 using ultra-clean methods(Enrico et al. 2016b). Rainfall samples were transferred to a 0.5L quartz reactor and illuminated with natural sunlight outdoors (up to 8h), or with a solar simulator indoors (up to 48h). Filtered samples were passed through a 0.45 micro-m quartz filter membrane to remove particles, in un-filtered samples this step was left out. Total Hg concentration of selected rainfall samples was augmented 10x with a NIST 3133 standard Hg solution, and equilibrated 24 h before light exposure. During light exposure, the quartz reactor was purged with Hg-free argon gas to remove product Hg(0). Reactant Hg(II) concentrations were measured in duplicate by cold vapor atomic fluorescence spectroscopy (CV-AFS) in 5mL aliquots recovered from the reactor at fixed time steps and acidified to 0.04 M HCl, and 0.1 M BrCl. CV-AFS analysis accuracy was evaluated by regular analysis of the NRC ORMS-6 certified (25.6 ng L^{-1}) reference material with good results (24.8 ± 1.6 ng L^{-1}, 1σ, n=33). Five out of twelve experiments showed increasing or constant reactant Hg(II) levels during the initial 2-4 hours, followed by a gradual decreasing in the final 24 hours (Supplementary Material). These initial observations, tentatively explained by Hg(II)-DOM interaction with the quartz reactor wall, were not included in the rate constant calculation. This simplification did not affect the main outcome of this study. For further discussion on in-cloud Hg photoreduction see Supplementary Note.

Code and data availability

The code and data that support the findings of this study are available upon request.

Acknowledgments: This work was supported by the Consejo Superior de Investigaciones Científicas (CSIC) Spain. The National Center for Atmospheric Research (Sprovieri et al.) is funded by the National Science Foundation (NSF). Computing resources were provided by the Climate Simulation Laboratory at NCAR's Computational and Information Systems Laboratory (CISL), sponsored by the NSF, provided computing resources. The CESM project (which includes CAM-Chem) is supported by the NSF and the office of Science (BER) of the US Department of Energy. This study has received funding from the European Research Council Executive Agency under the European Union´s Horizon 2020 Research and innovation programme (Projects 'ERC-2016-COG 726349 CLIMAHAL' to ASL and 'ERC-2010-STG 258537' to JES), and from H2020 ERA-PLANET 689443. We thank the UMS 831 Pic du Midi Observatory team for help with rainwater sampling.

Author contribution

A.S.-L and J.E.S conceived the experiments. S.P.S. and D.R-S. performed the quantum-chemical simulations. C.A.C and D.E.K. performed the global photolysis rate calculations. M.J., and Y.X. conducted the aqueous photoreduction experiments. C.P.T., E.M.S., D.J.J. and O.T. performed the mercury chemical transport model simulations. A.S.-L., S.P.S., D.R-S. J.M.O., J.Z.D., R.N., J.M.C.P., C.A.C., D.E.K., F.W., D.R., A.U.A., J.E.S., C.P.T., E.M.S., D.J.J. and O.T. analysed and interpreted both the quantum-chemical and atmospheric results. All authors contributed to paper writing.

Competing interests

The authors declare no competing interests.

4.2. Supporting Information

SUPPLEMENTARY INFORMATION:

Atmospheric photoreduction of gaseous oxidized mercury requires a rethink of the global mercury cycle

Saiz-Lopez et al.,

This file contains:

1. **Supplementary Figures 1-11**
2. **Supplementary Tables 1-6**
3. **Supplementary Note: text for in-cloud Hg photoreduction**
4. ***Supplementary Information References.***

1. Supplementary Figures

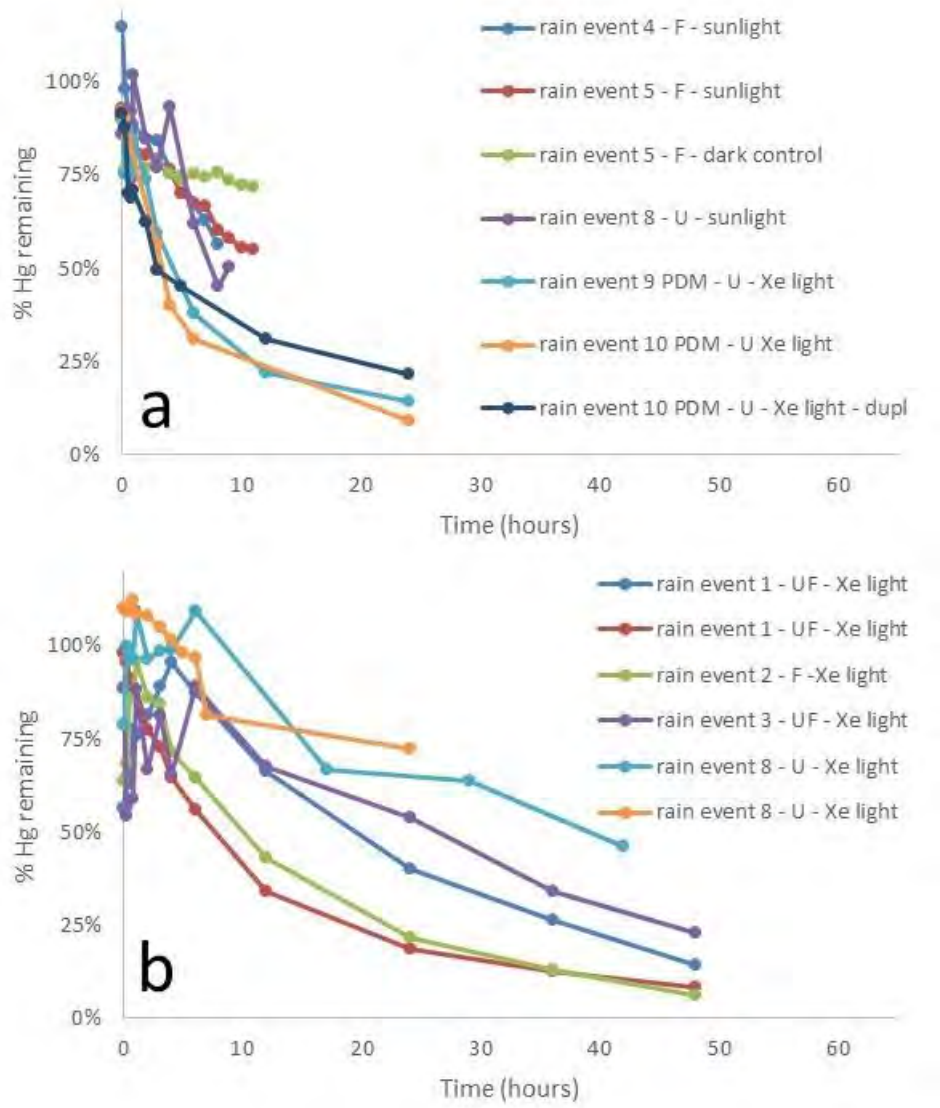

Figure 22 *Experimental Hg^{II} photoreduction rates for a) short outdoors exposure of Toulouse rainfall to sunlight (events 4, 5, 8), to no light conditions (event 8 dark control), and Pic du Midi rainfall to simulated light conditions (events 9, 10), b) controlled exposure of Toulouse rainfall to simulated sunlight. (events 1, 2, 3, 8). UF and F indicate unfiltered and filtered rainfall. The combined analysis uncertainty of Hg concentration measurements was 13% (2σ level).*

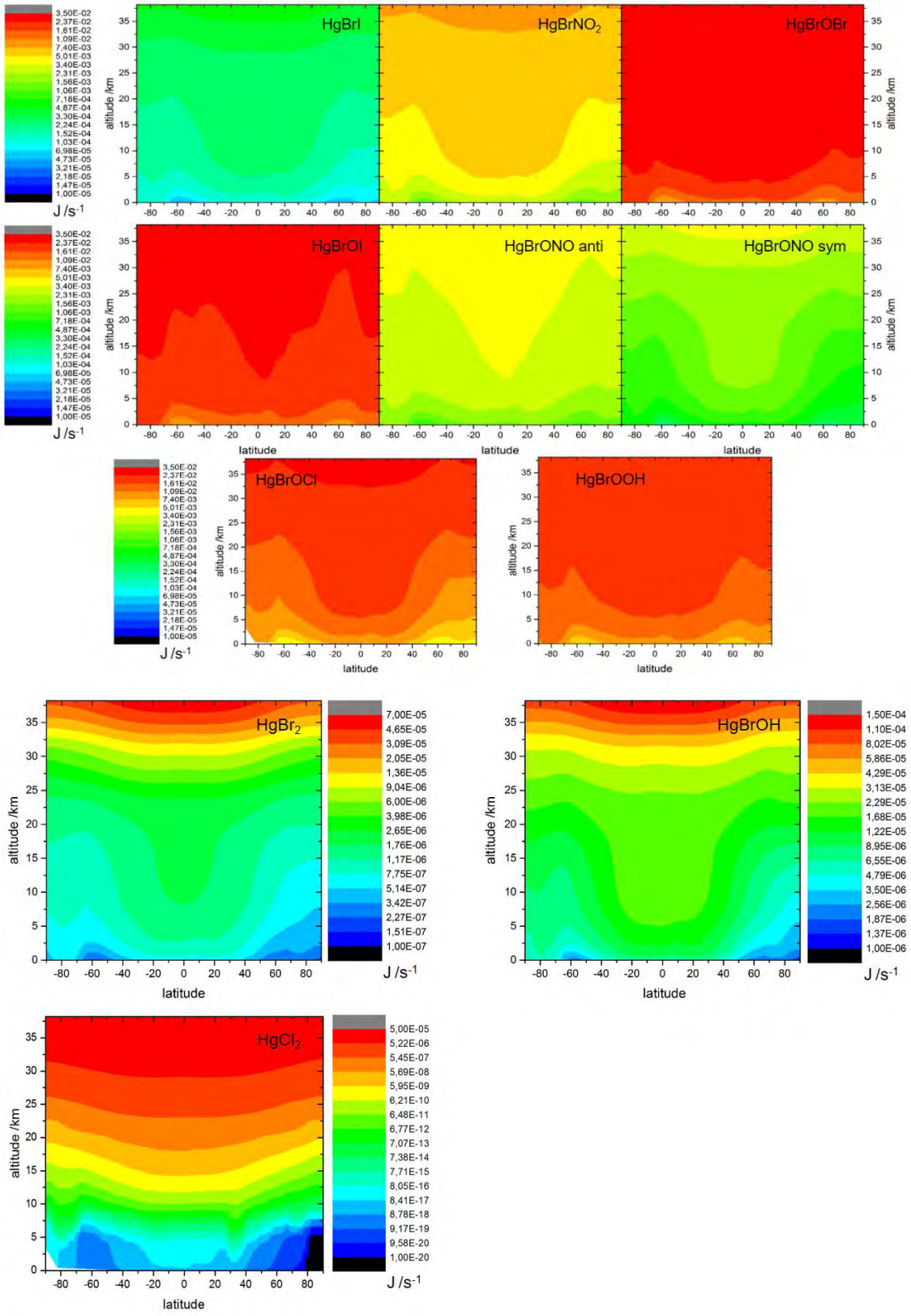

Figure 23 *Photolysis rates (J, s^{-1}) zonal-averaged along all longitudes for the studied Hg^{II} compounds, computed with global 3D chemistry-climate model CAM-Chem.*

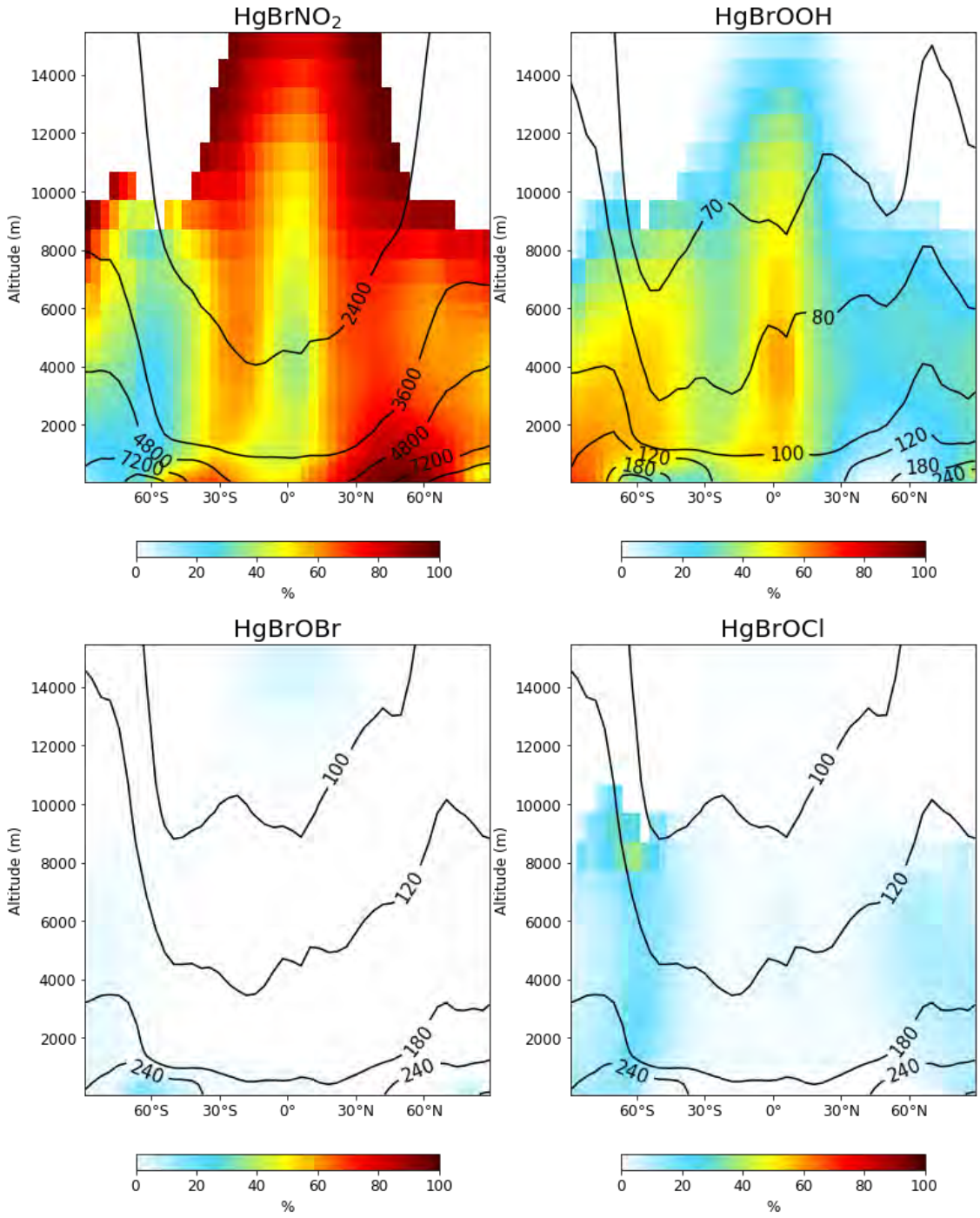

Figure 24 *Fraction of HgBrX (X = BrO, ClO, syn-ONO, HO_2) in colours and photolysis lifetimes (seconds) in contours modelled by GEOS-Chem. Note that HgBrOH and $HgBr_2$ are both very small fractions of HgBrX and are not shown.*

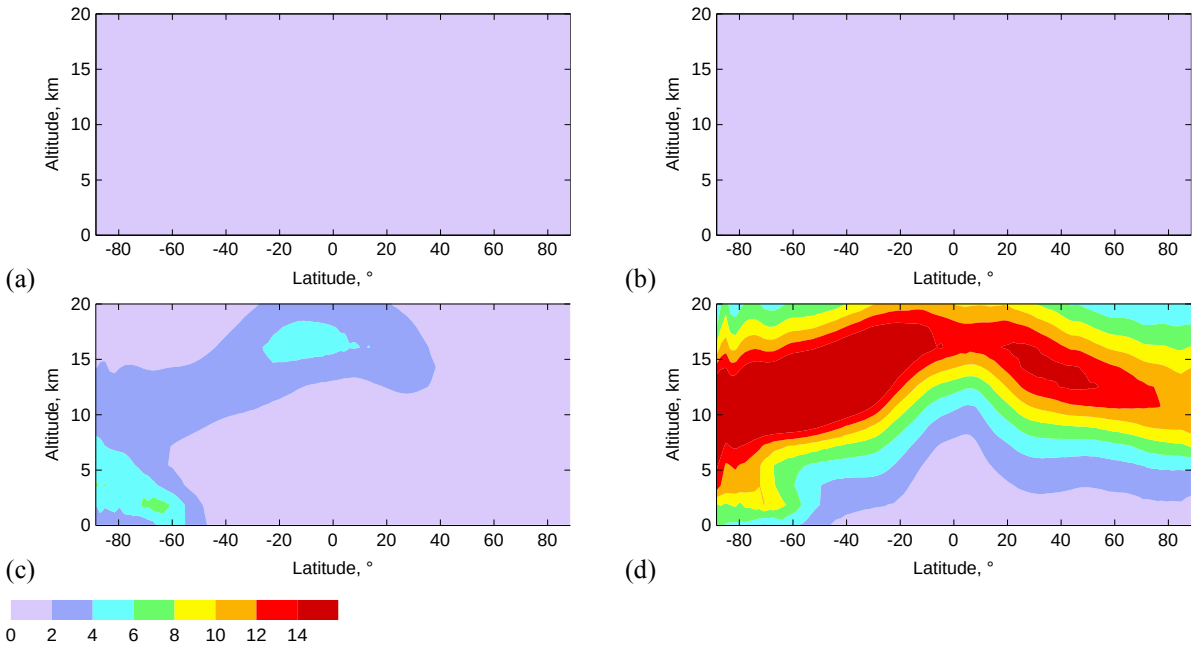

Figure 25 *Annual zonal mean volume mixing ratios of $HgBr_2$ (ppqv Hg) for different tests in GLEMOS: (a) – Run #1; (b) – Run #2; (c) – Run #3; (d) – Run #4.*

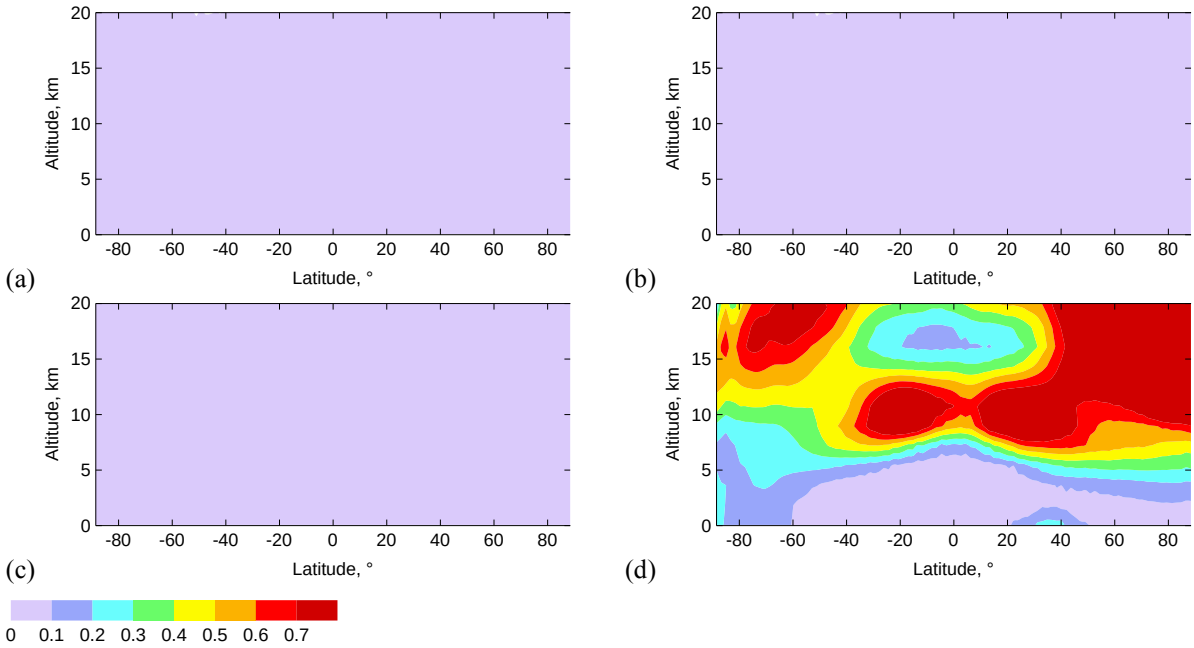

Figure 26 *Annual zonal mean volume mixing ratios of HgBr (ppqv Hg) for different tests in GLEMOS: (a) – Run #1; (b) – Run #2; (c) – Run #3; (d) – Run #4.*

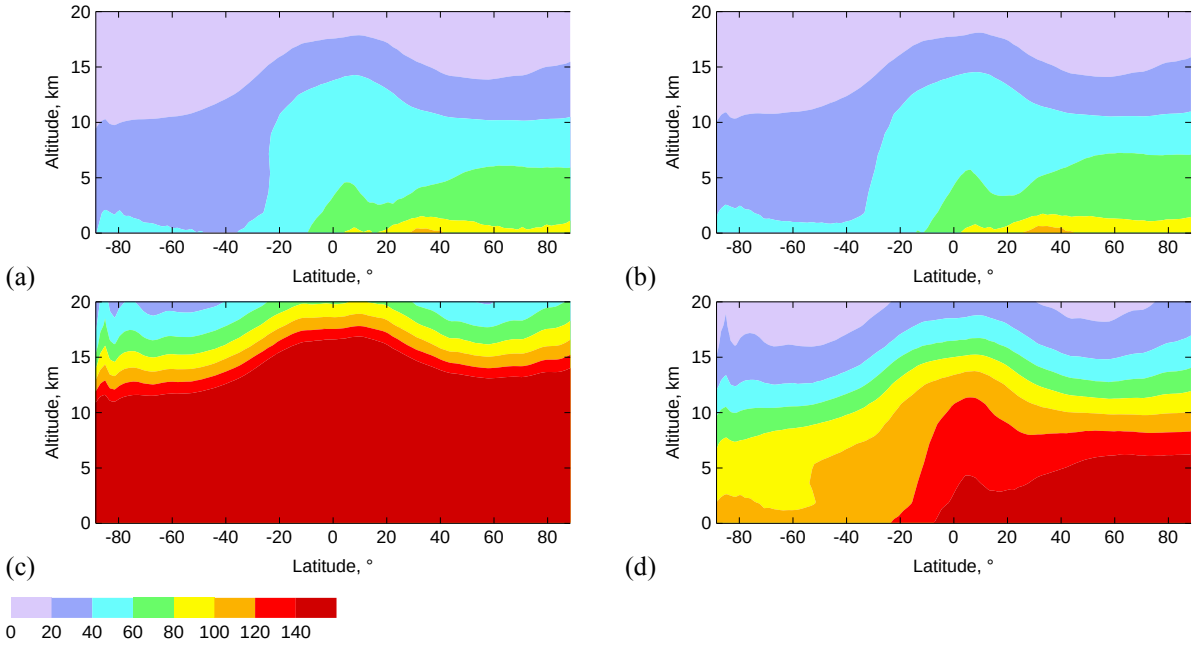

Figure 27 Annual zonal mean volume mixing ratios of Hg^0 (ppqv) for different tests in GLEMOS: (a) – Run #1; (b) – Run #2; (c) – Run #3; (d) – Run #4.

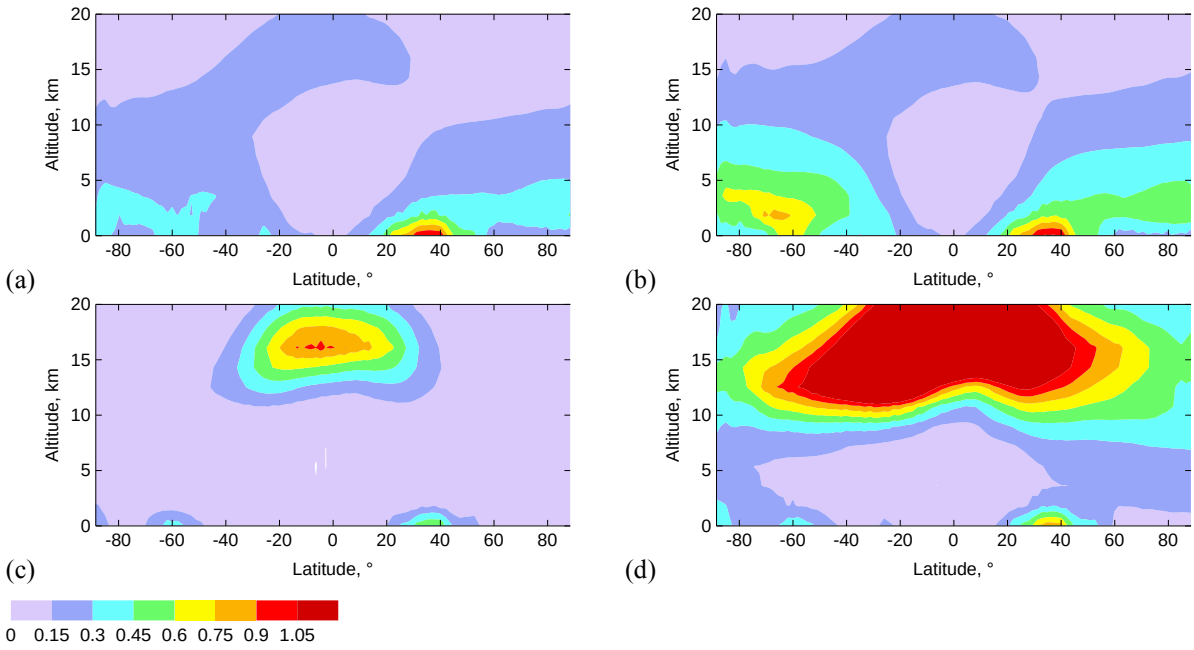

Figure 28 *Annual zonal mean volume mixing ratios of HgBrOH (ppqv Hg) for different tests in GLEMOS: (a) – Run #1; (b) – Run #2; (c) – Run #3; (d) – Run #4.*

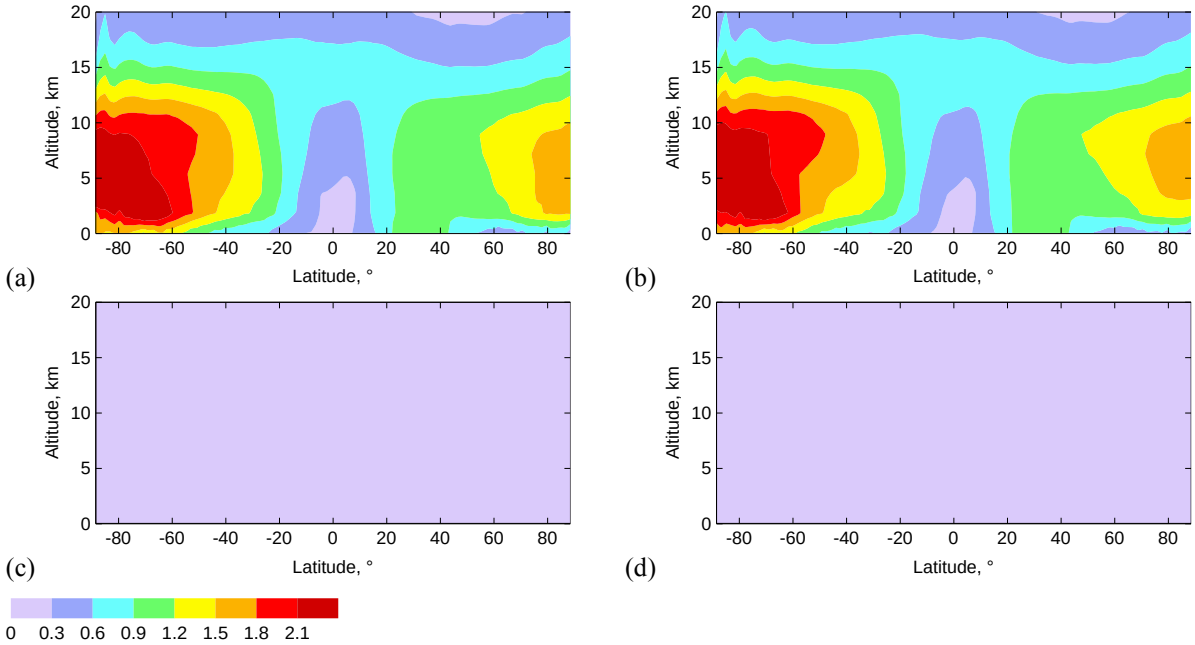

Figure 29 *Annual zonal mean volume mixing ratios of HgBrOOH (ppqv Hg) for different tests in GLEMOS: (a) – Run #1; (b) – Run #2; (c) – Run #3; (d) – Run #4.*

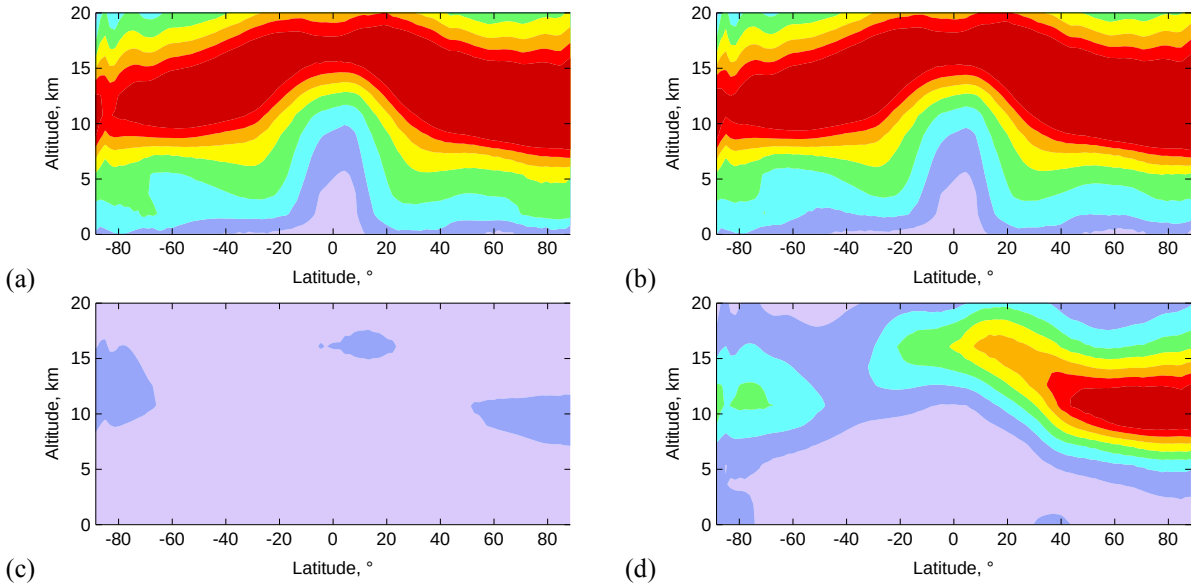

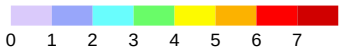

Figure 30 *Annual zonal mean volume mixing ratios of syn-HgBrONO (ppqv Hg) for different tests in GLEMOS: (a) – Run #1; (b) – Run #2; (c) – Run #3; (d) – Run #4.*

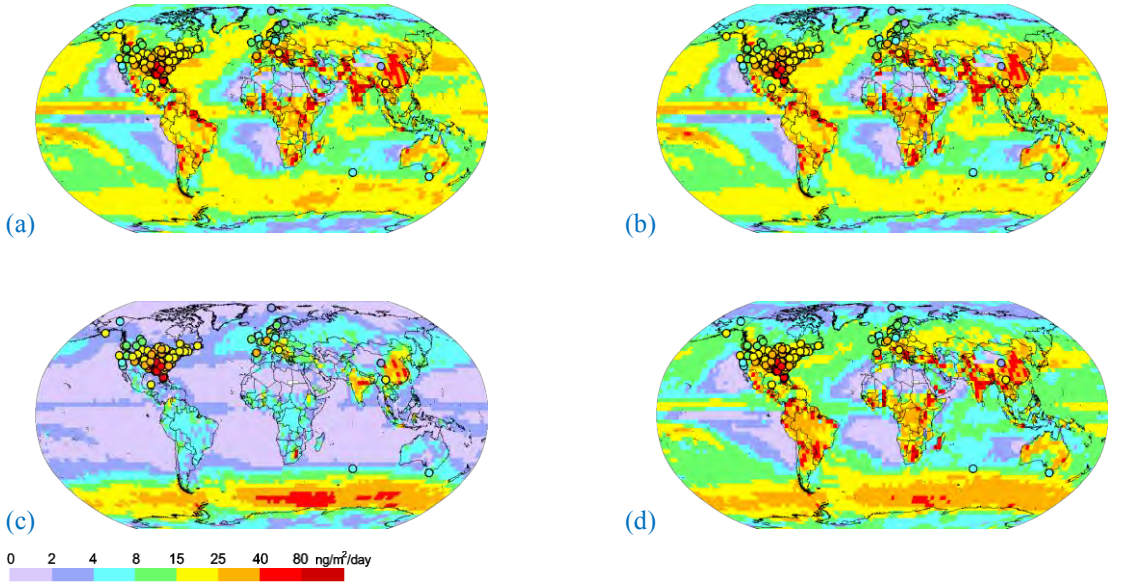

Figure 31 *Spatial distribution of Hg^{II} wet deposition for different tests in GLEMOS: (a) – Run #1; (b) – Run #2; (c) – Run #3; (d) – Run #4. Circles show observed values in the same color scale. The measurement dataset is the same as in ref Tranikov et al., 2017(Travnikov et al. 2017) in the main text.*

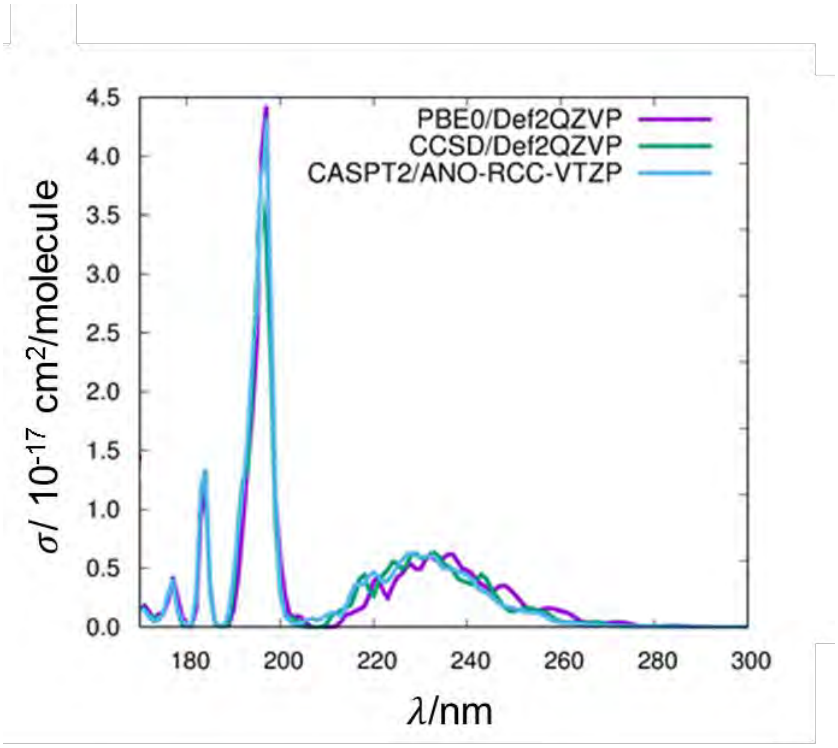

Figure 32 *Calculated spectra of $HgBr_2$ using different ensembles of geometries generated at different level of theory. Electronic structure computations were done at the CASSCF/MS–CASPT2/SO–RASSI level with the ANO-RCC-VTZP basis set.*

2. Supplementary Tables

***Table** 7 Summary of Hg^{II} photoreduction experiments for rainfall collected in suburban Toulouse (events 1-8) and in the free troposphere of the Pic du Midi Observatory (PDM, 2877m altitude). UF, unfiltered; F, filtered; Xe, xenon solar simulator. Legends are referred to Supplementary Data.*

Experiment name	Figure legend	k_{red} (h^{-1})
PC-R1U1XL	rain event 1 - UF - Xe light	0.043
PC-R1U2S2XL	rain event 1 - UF - Xe light	0.071
PC-R2F1S1XL	rain event 2 - F -Xe light	0.064
PC-R3U1S1XL	rain event 3 - UF - Xe light	0.016
PC-R4F1S1NL	rain event 4 - F - sunlight	0.069
PC-R5F1S1NL	rain event 5 - F - sunlight	0.047
R5F2S1DC	rain event 5 - F - dark control	0.007
PC-R8U1NL	rain event 8 - U - sunlight	0.071
PC-R8U2XL	rain event 8 - U - Xe light	0.047
PC-R8U3S1XL	rain event 8 - U - Xe light	0.031
mean		**0.077**
σ		0.052
PC-9	PDM rain event 9 – U – Xe light	0.145
PC-10	PDM rain event 10 – U – Xe light	0.188
PC-10 duplicate	PDM rain event 10 - U - Xe light	0.136
mean		**0.153**
σ		0.012
Selin et al., 2007(Selin et al. 2007b)	GEOS-Chem vs 7-04	2.9
Horowitz et al., 2017(Horowitz et al. 2017a)	GEOS-Chem vs 9-02	1.0

Table 8 *Photolysis rate (J) and annually averaged lifetime in the troposphere* (τ) *of the* Hg^{II} *compounds.*

Compound	**J/s^{-1}**	**τ /s**
$HgCl_2$	6.28E-10	1.59E+09
$HgBr_2$	9.70E-07	1.03E+06
HgBrI	1.67E-04	5.99E+03
HgBrONO_*syn*	9.60E-04	1.04E+03
HgBrONO_*anti*	2.31E-03	4.34E+02
$HgBrNO_2$	3.95E-03	2.53E+02
HgBrOOH	1.32E-02	7.57E+01
HgBrOI	1.78E-02	5.60E+01
HgBrOBr	2.17E-02	4.61E+01
HgO	5.42E-01	1.84E+00
HgBrOH	1.07E-05	9.34E+04

Table 9 *Calculated bond dissociation energies D_0 (at 0K) for BrHg–X species. All values in kJ·mol^{-1}.*

	D_0
BrHg–Br	305.4(Balabanov and Peterson 2003), 303.8(Shepler, Balabanov and Peterson 2007)
BrHg–NO_2	138.9(Dibble, Zelie and Jiao 2014), 149.0(Jiao and Dibble 2015), 142.7(Jiao and Dibble 2017a), 139.3(Dibble et al. 2012b)
anti-BrHg–ONO	156.1(Dibble et al. 2014), 160.7(Jiao and Dibble 2015), 151.9(Jiao and Dibble 2017a), 150.2(Dibble et al. 2012b)
syn-BrHg–ONO	177.0(Dibble et al. 2014), 182.2(Jiao and Dibble 2015), 177.4(Jiao and Dibble 2017a), 176.1(Dibble et al. 2012b)
BrHg–OOH	177.4(Jiao and Dibble 2015), 167.4(Dibble et al. 2012b)
BrHg–OBr	232.6(Dibble et al. 2012b), 223.8(Jiao and Dibble 2015)
BrHg–OCl	220.6(Dibble et al. 2012b), 211.7(Jiao and Dibble 2015)

Table 10 *Statistics of the model evaluation against measurements*

Run ID	*Hg^0 concentration*		*Hg wet deposition*	
	Correlation [(a)]	*Relative bias, % [(b)]*	*Correlation [(a)]*	*Relative bias, % [(b)]*
Run #1	0.63	-39	0.51	-6.8
Run #2	0.63	-35	0.53	-8.5

Run #3	0.71	91	0.11	-78
Run #4	0.68	18	0.52	-21

(a) Pearson's correlation coefficient:

$$R_{corr} = \frac{\sum_i (M_i - \overline{M})(O_i - \overline{O})}{\sqrt{\sum_i (M_i - \overline{M})^2 \sum_i (O_i - \overline{O})^2}};$$

(b) Relative bias:

$$RBIAS = \frac{\overline{M} - \overline{O}}{\overline{O}} 100\%.$$

Table 11 *Summary of the computational details used in the quantum-chemical calculation of spectra and cross sections of mercury compounds: geometry optimization and vibrational analysis, computation of the excited states, symmetry constraints, active space used in the CASSCF/CASPT2*

calculations, number of the sampled geometries (Monperrus et al.), number of states for each irreducible representation including ground state (N_{fs}), phenomenological broadening δ.

Table 12 *Chemical schemes used in the GLEMOS and GEOS-Chem models.*

System	$HgCl_2$, $HgBr_2$, HgBrI		$^1\Sigma$ HgO, $^3\Pi$ HgO		syn-, anti-HgBrONO, $HgBrNO_2$		HgBrOBr, HgBrOI		HgBrOH, HgBrOOH	
Geom. opt. and vibr. analysis	Method: PBE0 Basis set: Def2QZVP									
Comp. of the excited states	Method: SOC-DKH3-MSCASPT2 Basis set: ANO-RCC-VTZP									
Symmetry	C_s		C_{2v}		C_1		C_1		C_1	
Active space	(12,10)		(16,12)		(16,12)		(16,12)		HgBrOH: (12,11) HgBrOOH: (16,12)	
N_p	100		100		200		150		HgBrOH: 150 HgBrOOH: 200	
N_{fs} (per Irrep)	$^1A'$: 10 $^1A''$: 10	$^3A'$: 10 $^3A''$: 10	$^1A_1$: 8 $^1A_2$: 8 $^1B_1$: 8 $^1B_2$: 8	$^3A_1$: 8 $^3A_2$: 8 $^3B_1$: 8 $^3B_2$: 8	^1A: 25	^3A : 25	^1A: 25	^3A : 25	^1A: 20	^3A : 20
δ [eV][7]	0.05									

GLEMOS:

N	Reaction	Rate, molecule cm^{-3} s^{-1}	Reference
R1	$Hg^0 + Br + M \rightarrow HgBr + M$	$1.5 \times 10^{-32} (T/298)^{-1.86}$ $[Hg^0][Br][M]$	Donohoue et al. (2006)(Donohoue et al. 2006a)
R2	$HgBr + M \rightarrow Hg^0 + Br + M$	1.6×10^{-9} exp(-7801/T) [HgBr][M]	Dibble et al. (2012)(Dibble et al. 2012b)
R3	$HgBr + Br \rightarrow Hg^0 + Br_2$	3.9×10^{-11} [HgBr][Br]	Balabanov et al. (2005)(Balabanov, Shepler and Peterson 2005a)
R4	$HgBr + Br \xrightarrow{M} HgBr_2$	$2.5 \times 10^{-10} (T/298)^{-0.57}$ [HgBr][Br]	Goodsite et al. (2004)(Goodsite et al. 2004)
R5	$HgBr + OH \xrightarrow{M} HgBrOH$	$2.5 \times 10^{-10} (T/298)^{-0.57}$ [HgBr][OH]	Goodsite et al. (2004)(Goodsite et al. 2004)
R6	$HgBr + NO_2 \xrightarrow{M} HgBrNO_2$	$k_{NO2}([M],T)[HgBr][NO_2]$	Jiao and Dibble (2017)(Jiao and Dibble 2017a)
R7	$HgBr + HO_2 \xrightarrow{M} HgBrHO_2$	$k_{HO2}([M],T)[HgBr][HO_2]$	Jiao and Dibble (2017)(Jiao and Dibble 2017a)
R8	$HgBrY \xrightarrow{h\nu} Hg^0 + products$, $Y = Br, OH, NO_2, HO_2$	$k_{photo}([M],T)[HgBrY]$	This study
R9	$HgBrY \xrightarrow{h\nu} HgBr + products$, $Y = Br, OH, NO_2, HO_2$	$k_{photo}([M],T)[HgBrY]$	This study
R10	$Hg^{II}(aq) + h\nu \rightarrow Hg^0(aq)$	4.25×10^{-5} s^{-1}	This study

GEOS-Chem:

	Reaction	Rate expression	Ref
R1	$Hg^0 + Br + M \rightarrow HgBr + M$	1.46×10^{-32} (T/298)$^{-1.86}$[Hg^0][Br][M]	(Donohoue et al., 2006)(Donohoue et al. 2006a)
R2	$HgBr + M \rightarrow Hg^0 + Br + M$	1.6×10^{-9} (T/298)$^{-1.86}$ exp(-7801/T)[HgBr][M]	(Dibble et al., 2012) (Dibble et al. 2012b)
R3	$HgBr + Br \rightarrow Hg^0 + Br_2$	3.9×10^{-11} [HgBr][Br]	(Balabanov et al., 2005)(Balabanov et al. 2005a)
R4	$HgBr + NO_2 \rightarrow Hg^0 + BrNO_2$	3.4×10^{-12} exp(391/T)[HgBr][NO_2]	(Jiao & Dibble 2017)(Jiao and Dibble 2017a)
R5	$HgBr + Br \overset{M}{\rightarrow} HgBr$	3.0×10^{-11} [HgBr][Br]	(Balabanov et al., 2005)(Balabanov et al. 2005a)
R6	$HgBr + NO_2 \overset{M}{\rightarrow} HgBrNO_2$	k_{NO_2}([M],T)[HgBr][NO_2]	(Jiao & Dibble 2017)(Jiao and Dibble 2017a)
R7	$HgBr + Y \overset{M}{\rightarrow} HgBrY$ $Y = HO_2, ClO, BrO, OH, Br_2$	k_{HO_2}([M],T)[HgBr][Y]	(Jiao & Dibble 2017)(Jiao and Dibble 2017a)
R8	$Hg^0 + Cl + M \rightarrow HgCl + M$	2.2×10^{-22} exp(680(1/T – 1/298))[Hg^0][Cl][M]	(Donohoue et al., 2005)(Donohoue, Bauer and Hynes 2005)
R9	$HgCl + Cl \rightarrow Hg^0 + Cl_2$	1.20×10^{-11}exp(-5942/T)[HgCl][Cl]	(Wilcox 2009)(Wilcox 2009)
R10	$HgCl + Br \overset{M}{\rightarrow} HgBrCl$	3.0×10^{-11} [HgCl][Br]	(Balabanov et al., 2005)(Balabanov et al. 2005a)
R11	$HgCl + NO_2 \overset{M}{\rightarrow} HgClNO_2$	k_{NO_2}([M],T)[HgBr][NO_2]	(Jiao & Dibble 2017)(Jiao and Dibble 2017a)
R12	$HgCl + Y \overset{M}{\rightarrow} HgClY$ $Y = HO_2, ClO, BrO, OH, Br_2$	k_{HO_2}([M],T)[HgBr][Y]	(Jiao & Dibble 2017)(Jiao and Dibble 2017a)
R13	$Hg^0_{(aq)} + O_{3(aq)} \rightarrow Hg^{II}_{(aq)} + products$	4.7×10^7 [$Hg^0_{(aq)}$][$O_{3(aq)}$]	(Munthe 1992)(Munthe 1992a)
R14	$Hg^0_{(aq)} + HOCl_{(aq)} \rightarrow Hg^{II}_{(aq)} + OH^-_{(aq)} + Cl^-_{(aq)}$	2×10^6 [$Hg^0_{(aq)}$][$HOCl_{(aq)}$]	(Lin & Pehkonen 1998)(Lin and Pehkonen 1998),(Wang & Pehkonen 2004)(Wang and Pehkonen 2004)
R15	$Hg^0_{(aq)} + OH_{(aq)} \rightarrow Hg^{II}_{(aq)} + products$	2.0×10^9 [$Hg^0_{(aq)}$][$OH_{(aq)}$]	(Lin & Pehkonen 1997)(Lin and Pehkonen 1997),(Buxton et al., 1998)(Buxton et al. 1988)
R16	$Hg^{II}_{(aq)} + h\nu \rightarrow Hg^0_{(aq)}$	$6.5 \times 10^{-2}\ j_{NO_2}$[OA][$Hg^{II}_{(aq)}$]	(Buxton et al., 1998)(Buxton et al. 1988)
R17	$HgBrX + h\nu \rightarrow HgBr + X$ $X = NO_2, HO_2, ClO, BrO, OH, Br$	j_Y [HgBrX]	This study

3. Supplementary Note: text for in-cloud Hg photoreduction

The first global Hg CTM(Shia et al. 1999b) included Hg(II) reduction in the aqueous phase by sulfite (SO_3^{2-}), with k_{red} of 0.6 s^{-1} (2160 h^{-1}) based on work by Munthe et al.1991(Munthe, Xiao and Lindqvist 1991b)

$HgSO_3^0{}_{(aq)} \rightarrow Hg^0{}_{(aq)}$ with $d[HgSO_3^0]/dt = k_{red} \times [HgSO_3^0]$ (Eq.1)

$Hg(SO_3)_2^{2-}{}_{(aq)} \rightarrow Hg^0{}_{(aq)}$ with $d[Hg(SO_3)_2]/dt = k_{red} \times [Hg(SO_3)_2]$ (Eq.2)

A later study that directly measured the reactant $HgSO_3$ put into question the previously proposed reduction mechanism and rate constant, reporting k_{red} of 0.0106 s^{-1} (38.2 h^{-1}) at pH=3 and regardless of Hg, SO_3, and O_2 concentrations (though not independent of other competing ligands).(Van Loon, Mader and Scott 2000a) Shia et al.'s CTM(Shia et al. 1999b) also included aqueous phase reduction of Hg(II) by hydroperoxyl, HO_2, radicals, based on Lin and Pehkonen (1998):(Lin and Pehkonen 1998)

$Hg^{2+}{}_{(aq)} + HO_{2(aq)} \rightarrow Hg^0{}_{(aq)}$ with $d[Hg^{2+}]/dt = k_{red} \times [Hg^{2+}] \times [HO_2]$ (Eq.3)

with k_{red} of 1.7 10^4 M^{-1} s^{-1}. This reaction, which proceeds by a Hg(I) intermediate step has been questioned by Gardfeldt and Jonsson(Gårdfeldt and Jonsson 2003) based on the rapid oxidation of the Hg(I) form back to Hg(II). It is also important to note that the reaction rate expressions Eq.1 and 2 depend on free Hg^{2+} or $HgSO_3^0$ ion concentrations, which cannot be measured and have to be estimated based on equilibrium speciation calculations. In the 1990's and early 2000's it was generally assumed that inorganic ligands such as Cl- were among the dominant Hg binding ligands in atmospheric waters, or that high SO_3 concentrations in polluted areas inhibited Hg reduction via the slower Eq. 2. The subsequent gradual acceptance of simple and complex (humics) dissolved organic ligands as dominant Hg binding ligand in natural waters, including rainfall(Bash et al. 2014a) results in low $HgSO_3$, $Hg(SO_3)_2$ and even lower free Hg^{2+} ion concentrations.(Haitzer, Aiken and Ryan

2002a),(Tipping 2007) Consequently these aqueous phase Hg(II) reduction mechanisms have been gradually abandoned in Hg CTMs.

The uncertainty in atmospheric Hg(II) reduction pathways has led subsequent models to adopt a fitting approach (e.g. CTM-Hg, GEOS-Chem) to aqueous phase Hg(II) reduction.(Seigneur et al. 2006a),(Selin et al. 2007c) GEOS-Chem provides the most explicit parameterization that is well suited for comparison to our experimental results. Selin et al. (2007)(Selin et al. 2007c) optimized in-cloud Hg(II) photoreduction in the GEOS-Chem CTM as k_{red} = 8 10^{-10} [OH] (s^{-1}) where [OH] is the gas phase concentration in units of molecules cm^{-3}. [OH] serves as a proxy for the actinic flux in the VIS region. For a typical [OH] of 10^6 , k_{red} is 8 10^{-4} s^{-1} (2.9 h^{-1}) which resulted in a mean lifetime of 20 min for dissolved Hg^{II} in cloud in the model. Note that the associated rate expression, $d[Hg^{II}]/dt=k_{red}$ x $[Hg^{II}]$ is expressed relative to total divalent Hg^{II} concentration in cloud water. Horowitz et al. (2017),(Horowitz et al. 2017a) using the most recent two-step fast Hg^0 oxidation scheme in GEOS-Chem, extended atmospheric Hg^{II} reduction to aqueous-phase Hg^{II}–organic complexes in both aqueous aerosols and clouds. k_{red} (s^{-1}) is parameterized as $\alpha j NO_2[OA]$, were α is a scaling factor, jNO_2 the NO_2 photolysis frequency, a proxy for the UV actinic flux, [OA] the local concentration of organic aerosol. If we take generic values of $jNO2 = 10^{-2}$ s^{-1} and maximum [OA] = 1 ug m^{-3} (STP), we obtain a maximum rate constant of 1 h^{-1}.

Following an experimental study on aqueous Hg(II) reduction by dicarboxylic acids (Hg^{2+}_{aq} + DCA_{aq} + hv → Hg^0_{aq}) by Si and Ariya (2008),(Si and Ariya 2008a) Bash et al. (2014)(Bash et al. 2014a) recently incorporated this reaction into the CMAQ model using a rate of 1.2×10^4 $M^{-1} \cdot s^{-1}$ (the highest rate observed for oxalic acid). Global oxalic acid concentrations in rainfall and cloud water are on the order of 5 μeq/L (2.5 μM), yielding an approximate maximum k_{red} of 1.2 10^4 x 2.5 10^{-6} = 0.03 s^{-1} (108 h^{-1}) for the reaction rate expression $d[Hg^{2+}]/dt=k_{red}[Hg^{2+}]$. As argued above, free Hg^{2+} (likely < 10^{-15} mol/L) is only a very small fraction of the total Hg^{II} concentration.

Therefore, a conditional rate constant relative to total Hg^{II} will be orders of magnitude slower.

Supplementary Data summarizes the rainfall events, rainfall pH and incubation conditions (filtration, UVA, UVA, VIS) used in this study. pH was measured using an Orion pH electrode, calibrated against NIST traceable standards of pH 4 and 7. UVA, UVB, VIS intensity of outdoors sunlight and of the solar simulator (xenon lamp) were measured with a Solar Light PMA2200 Radiometer with specific UVB (PMA2106), UVA (PMA2110) and Visible (PMA2130) detectors. Additional details can be found in the Methods section. Photoreduction rates were generally 1^{st} order with respect to total Hg concentrations during the first 12 hours. Duplicate incubations of rainfall samples 1, 8 and 10 indicate a mean RSD of 29% on k_{red}.

Chapter 5. Conclusions and perspectives

5.1. conclusions

Redox reactions of atmospheric Hg influence Hg transport and deposition, and determine oxidation states of Hg, which play a key role in biogeochemical cycle of Hg (Ariya et al. 2015a). It has been reported that atmospheric Hg(0) is oxidized to Hg(II) dominantly by a Br-induced two-stage reaction and results in formation of a series of end products of Hg(II)XY complexes (e.g., $HgCl_2$, HgBrOH, $HgBr_2$, HgBrI, HgBrCl, $HgBrNO_2$, HgBrONO, HgBrOOH, HgBrOBr, HgBrOI, HgBrOCl) and oxygen-containing species (HgO) (Saiz-Lopez et al. 2018, Horowitz et al. 2017b). Atmospheric Hg(II) photoreduction to Hg(0) changes solubility, chemical reactivity and lifetime of atmospheric Hg, and is an important pathway to modify the magnitude and pattern of atmospheric Hg deposition. At the start of this PhD research, photoreduction of atmospheric Hg(II) was thought to take place in the atmospheric aqueous phase (i.e clouds, rainfall, hydrated aerosols), but not in the gas phase. Due to the lack of experimental observations for both aqueous and gaseous phase photoreduction of atmospheric Hg(II), fast in-cloud aqueous phase Hg(II) photoreduction rates were assumed and optimized in global Hg models such as GEOS-Chem and GLEMOS to balance fast Hg(0) oxidation and reproduce global variability in observed Hg(0). (Travnikov and Ryaboshapko 2002, Selin et al. 2007a, Horowitz et al. 2017b). The fitted model k_{red} are typically on the order of 1.0 h^{-1}, which corresponds to Hg(II) lifetimes in clouds and aqueous aerosol of ~20 minutes (Selin et al. 2007a).

In order to partly fill the missing data gap, we conducted the first aqueous phase photoreduction experiments of Hg(II) in rainfall. Our experimental observations for rainfall Hg(II) photoreduction show that there is no statistically significant differences between rainfall Hg(II) reduction rates under natural ($0.063 \pm 0.013 h^{-1}$) and simulated sunlight ($0.037 \pm 0.016 h^{-1}$), and for filtered ($0.058 \pm 0.011 h^{-1}$) and unfiltered ($0.039 \pm 0.020 h^{-1}$) suburban rainwater (t-test, all $p > 0.05$). The mean photochemical reduction rate of suburban rainfall was $0.051 \pm 0.019\ h^{-1}$ (σ, $n = 10$). The mean rate at the remote Pic du Midi (PDM) samples was two-fold higher, $0.15 \pm 0.01\ h^{-1}$ (σ, $n = 3$), than

that of the suburban Toulouse samples, and three times slower than the median photoreduction rate of 0.41 h^{-1} (n = 24) for previously published inland and marine waters. Our experimental rainwater photoreduction rates, under fully sunlit conditions, are an order of magnitude slower than the optimized maximum in-cloud photoreduction rate of > 1.0 h^{-1} in global Hg models. Photoreduction experiments of simulated rainfall solutions containing known amounts of Hg, halides (Cl, Br, I) and DOC were also performed and combined with equilibrium speciation calculations using the Visual Minteq program. The ensemble of observations suggests that atmospheric gaseous $HgBr_2$, $HgCl_2$, $HgBrNO_2$, $HgBrHO_2$ forms (Figure 1-1), scavenged by aqueous aerosols and cloud droplets, are converted to Hg(II)-DOC forms in rainfall due to abundant organic carbon in aerosols and cloud water. Aqueous phase photoreduction of Hg(II)-DOC complexes is the dominant reduction pathway in the atmospheric system and proceeds at reaction rates that are slower than in terrestrial and marine waters, likely due to different origin and molecular structure of atmospheric DOC.

Aqueous phase reduction of atmospheric Hg(II) was simulated by GEOS-Chem and GLEMOS models using the experimentally derived rate constant for free tropospheric rainfall at the PDM (0.15 h^{-1}). The model results indicated that the slow atmospheric reduction leads to a simulated imbalance in the atmospheric Hg(0) pool which is biased low (1650Mg in figure 4-b, chapter 4), compared to Hg(0) observations (3500Mg in Figure 1-1). As a result, photoreduction of Hg(II)-DOC in aqueous aerosols and clouds is too slow to balance fast oxidation of atmospheric Hg. As a result of this the model description of the atmospheric Hg cycle has become incomplete. Either some reactions are missing or some of the reaction rates included in the model are incorrect.

Our collaborators at the Spanish CSIC have proposed, as part of our studies at the PDM, the possibility that gaseous Hg(II) compounds may directly photolyse to the Hg(I)Br intermediate. By using high-level quantum-chemical computation they have been able to estimate gas phase photolysis rate constants for a dozen Hg(II) compounds, which have been included in the global Hg models GEOS-Chem and GLEMOS. The results of our combined studies show that gas phase photolysis of Hg(II) compounds can be fast, and is fast enough to rebalance the modeled atmospheric Hg cycle.

Figure 4-d in chapter 4 shows that including gas phase Hg(II) photolysis leads to an unbiased global Hg(0) inventory of 3800Mg, similar to observations (3500Mg).

5.2. Perspectives

Even if we have achieved initial experimental observation data for aqueous phase photoreduction of atmospheric Hg, further research are needed to be done to address the effects of environmental factors (e.g., different wavelengths and intensities of sunlight, inorganic and organic ligands) on photoreduction rates and for the development of global atmospheric Hg model. The following research needs can be identified:

1) The relationship of reduction rates and mechanisms between photoreduction of dissolved Hg(II) in the aquatic system and rainfall are not clearly described in Chapter 3. More research need to be done to understand the differences in aqueous photoreduction of dissolved Hg(II)-DOM complexes between atmospheric system and terrestrial and marine aquatic systems.

2) Aqueous $HgBr_2$ can be partially reduced to monohalide (HgBr) in the presence of ~200nm UV light. Aqueous phase reduction of Hg(II) by hydroperoxyl radicals ($HO_2\cdot$) including the production of an intermediate of Hg(I)Br has been proposed and implemented in the early Hg models (Pehkonen and Lin 1998a, Shia et al. 1999a). Previous studies on Hg(II)-halide photochemistry suggested that ligand to metal charge transfer due to UV absorption in the 200-300nm wavelength range can result in Hg(0) or Hg(I) products depending on Hg/halide ratio and presence of oxygen (Horvath and Vogler 1993). Is it possible that aqueous phase reduction of Hg(II)-halide to Hg(I)-halide occurs in the atmosphere in the presence of a range of UV light wavelength?

3) Based on theoretical chemistry computation of k_{red}, we proposed that gas phase photoreduction of Hg(II)BrX to Hg(I)Br increase the Hg lifetime to 13 and 10 months in GEOS-Chem and GELOS models, and is a dominant reduction pathway for atmospheric Hg(II). However, there are no observational data to support this findings, and further experiments are needed on gas phase Hg(II) photolysis, and on heterogeneous Hg(II) photolysis on aersols.

4) Hg stable isotopes have proven useful to understand Hg reduction mechanisms. The next challenge is the perform similar Hg isotope analyses on gaseous Hg(II) compound photolysis.

Chapitre 5. Conclusions et perspectives

5.1. Conclusions

Les réactions d'oxydoréduction du mercure dans l'atmosphère influencent le transport et le dépôt de mercure et déterminent les états d'oxydation du mercure, qui jouent un rôle clé dans le cycle biogéochimique du mercure (Ariya et al. 2015). Il a été rapporté que le Hg(0) atmosphérique est oxydé en Hg(II) principalement par une réaction en deux étapes induite par le Br et aboutit à la formation d'une série de produits finaux de complexes Hg(II)XY (par exemple, $HgCl_2$, HgBrOH, $HgBr_2$, HgBrI, HgBrCl, $HgBrNO_2$, HgBrONO, HgBrOOH, HgBrOBr, HgBrOI, HgBrOCl) et les espèces contenant de l'oxygène (HgO) (Saiz-Lopez et al. 2018, Horowitz et al. 2017). La photoréduction du Hg(II) atmosphérique en Hg(0) modifie la solubilité, la réactivité chimique et la durée de vie du Hg atmosphérique. Elle constitue un moyen important de modifier l'ampleur et la structure du dépôt de Hg dans l'atmosphère. Au début de cette thèse, on pensait que la photoréduction du Hg(II) atmosphérique avait lieu dans la phase aqueuse atmosphérique (nuages, précipitations, aérosols hydratés), mais pas dans la phase gazeuse. En raison du manque d'observations expérimentales sur la photoréduction à la fois en phase aqueuse et gazeuse du Hg(II) atmosphérique, des vitesses de photoréduction rapides en phase aqueuse dans les nuages ont été supposées et optimisées dans des modèles globaux de mercure tels que GEOS-Chem et GLEMOS. (Travnikov et Ryaboshapko 2002, Selin et al. 2007, Horowitz et al. 2017). Les modèles ajustés ont des constantes de photoreduction, k_{red}, qui sont typiquement de l'ordre de $1{,}0h^{-1}$, ce qui correspond aux durées de vie du Hg(II) dans les nuages et aérosols aqueux d'environ 20 minutes (Selin et al. 2007).

Afin de combler en partie le manque de données manquantes, nous avons mené les premières expériences de photoréduction en phase aqueuse du Hg(II) dans les précipitations. Nos observations expérimentales sur la photoréduction des précipitations au Hg(II) montrent qu'il n'existe aucune différence statistiquement significative entre les taux de réduction du Hg(II) observes sous la lumière du soleil naturelle ($0{,}063 \pm 0{,}013h^{-1}$) et la lumière solaire simulée par une lampe a Xe ($0{,}037 \pm 0{,}016h^{-1}$), ni entre l'eau de pluie suburbaine filtrée ($0{,}058 \pm 0{,}011h^{-1}$) et non filtrée ($0{,}039 \pm 0{,}020h^{-1}$) (test t,

toutes p> 0,05). Le taux moyen de réduction photochimique des précipitations en périphérie urbaine était de 0,051 ± 0,019 h^{-1} (σ, n =10). Le taux moyen des échantillons distants du Pic du Midi (PDM) était trois fois plus élevé, soit 0,15 ± 0,01 h^{-1} (σ, n = 3), que celui des échantillons de Toulouse de banlieue et trois fois plus lent que le taux de photoreduction médian 0,41 h^{-1} (n = 24) pour les eaux continentales et marines publiées antérieurement. Les vitesses de photoreduction du Hg dans les eaux de pluie, dans des conditions d'ensoleillement total, sont inférieurs d'un ordre de grandeur aux taux optimisés de photoreduction dans les nuages, >1.0 h^{-1} dans les modèles globaux de mercure.

Des expériences de photoréduction de solutions pluviométriques simulées contenant des quantités connues de Hg, d'halogénures (Cl, Br, I) et de carbone organique dissoute (DOC) ont également été réalisées et combinées avec des calculs de spéciation à l'équilibre à l'aide du programme Visual Minteq. L'ensemble des observations suggère que les formes $HgBr_2$, $HgCl_2$, $HgBrNO_2$, $HgBrHO_2$ gazeuses dans l'atmosphère (Figure 1-1), absorbes par des aérosols aqueux et des gouttelettes de nuages, sont converties en formes Hg(II)-DOC dans les précipitations en raison de l'abondance de carbone organique dans les aérosols et les eaux de nuages. La photoréduction en phase aqueuse des complexes Hg(II)-DOC est la principale voie de réduction dans le système atmosphérique. Elle s'effectue à une vitesse de réaction plus lente que dans les eaux terrestres et marines, probablement en raison de l'origine et de la structure moléculaire différentes du COD atmosphérique.

La réduction en phase aqueuse du Hg(II) atmosphérique a été simulée par les modèles GEOS-Chem et GLEMOS en utilisant la constante de vitesse observée expérimentalement pour les précipitations troposphériques libres au PDM (0,15 h^{-1}). Les résultats du modèle indiquent que la lente réduction du Hg(II) dans les eaux atmosphériques entraînait un déséquilibre simulé dans le réservoir de Hg(0) atmosphérique, qui est biaisé (1650Mg dans la Figure 4-b, chapitre 4), par rapport aux observations de Hg(0) (3500Mg dans la Figure 1-1). En conséquence, la photoréduction du Hg(II)-DOC dans les aérosols et les nuages aqueux est trop lente pour permettre l'équilibrage de l'oxydation rapide du Hg atmosphérique. En conséquence, la description du modèle du cycle atmosphérique du

mercure est devenue incomplète. Certaines réactions manquent ou certaines des vitesses de réaction incluses dans le modèle sont incorrectes.

Nos collaborateurs à la CSIC espagnole ont proposé, dans le cadre de nos études au PDM, la possibilité que des composés gazeux du Hg(II) puissent se photolyser directement vers l'intermédiaire Hg(I)Br. En utilisant un calcul quantique chimique de haut niveau, ils ont pu estimer les constantes de vitesse de photolyse en phase gazeuse pour une douzaine de composés de Hg(II), qui ont été inclus dans les modèles globaux de mercure GEOS-Chem et GLEMOS. Les résultats de nos études combinées montrent que la photolyse en phase gazeuse de composés de mercure(II) peut être suffisamment rapide pour rééquilibrer le cycle de mercure atmosphérique modélisé. La figure 4-d de chapitre 4 montre que l'inclusion de la photolyse du Hg(II) en phase gazeuse conduit à un stock global non biaisé de Hg(0) de 3800 Mg, similaire aux observations (3500 Mg).

5.2. Perspectives

Même si nous avons obtenu des données d'observation expérimentales initiales sur la photoréduction en phase aqueuse du Hg atmosphérique, des recherches supplémentaires sont nécessaires pour examiner les effets des facteurs environnementaux (par exemple, différentes longueurs d'onde et intensités de la lumière solaire, présence d'autres ligands inorganiques et organiques) sur les vitesses de photoréduction et pour le développement du modèle global de Hg atmosphérique. Les besoins de recherche suivants peuvent être identifiés:

1) La relation entre les taux de réduction et les mécanismes de photoréduction du Hg(II) dissous dans les précipitations n'est pas clairement décrite au chapitre 3. Il est nécessaire de poursuivre les recherches pour comprendre les différences de vitesses de photoréduction entre les systèmes atmosphériques et les systèmes aquatiques terrestres et marins. Particulièrement la structure moléculaire du DOC et les sites de complexation impliques doit être mieux comprise, et paramétrisé.

2) Le $HgBr_2$ aqueux peut être partiellement réduit en monohalogénure (HgBr) en présence d'environ 200 nm de rayons ultraviolets. La réduction en phase aqueuse de Hg(II) par les radicaux hydroperoxyle ($HO_2\cdot$), y compris la production d'un intermédiaire de Hg(I)Br, a été proposée et mise en œuvre dans les premiers modèles de mercure (Pehkonen et Lin 1998, Shia et al. 1999). Des études antérieures sur la photochimie des halogénures de Hg(II) suggéraient que le transfert de charge ligand-métal dû à l'absorption UV dans la plage de longueurs d'onde de 200 à 300 nm pouvait donner lieu à des produits de Hg(0) ou de Hg(I), en fonction du rapport Hg/ halogénure et de la présence de l'oxygène (Horvath et Vogler 1993). Est-il possible qu'une réduction en phase aqueuse de l'halogénure de Hg(II) en halogénure de Hg(I) ait lieu dans l'atmosphère en présence d'une plage de longueurs d'onde de la lumière ultraviolette?

3) Sur la base du calcul théorique en chimie de k_{red}, nous avons proposé que la photoréduction en phase gazeuse de Hg(II)BrX à Hg(I)Br augmente la durée de vie du mercure à 13 et 10 mois dans les modèles GEOS-Chem et GELOS et constitue une voie de réduction dominante pour le Hg(II)

atmosphérique. Cependant, il n'y a pas de données d'observation pour étayer ces résultats et d'autres expériences sont nécessaires, cette fois ci en phase gazeuse, et en phase d'aerosol.

4) Les isotopes stables du mercure se sont révélés utiles pour comprendre les mécanismes de réduction du mercure. Le prochain défi consiste à effectuer des analyses isotopiques du mercure similaires sur la photolyse du composé gazeux du Hg(II).

List of figures

List of tables

References

Adamo, C. & V. Barone (1999) Toward reliable density functional methods without adjustable parameters: The PBE0 model. *The Journal of chemical physics,* 110**,** 6158-6170.

Agency, U. S. E. P. (2002) Method 1631, Revision E: Mercury in Water by Oxidation, Purge and Trap, and Cold Vapor Atomic Fluorescence Spectrometry.

Allard, B. & I. Arsenie (1991) ABIOTIC REDUCTION OF MERCURY BY HUMIC SUBSTANCES IN AQUATIC SYSTEM - AN IMPORTANT PROCESS FOR THE MERCURY CYCLE. *Water Air and Soil Pollution,* 56**,** 457-464.

AMAP/UNEP (2013a) Technical Background Report for the Global Mercury Assessment 2013. *Arctic Monitoring and Assessment Programme*.

--- (2013b) Technical Background Report for the Global Mercury Assessment 2013.

Amos, H. M., D. J. Jacob, C. Holmes, J. A. Fisher, Q. Wang, R. M. Yantosca, E. S. Corbitt, E. Galarneau, A. Rutter & M. Gustin (2012a) Gas-particle partitioning of atmospheric Hg (II) and its effect on global mercury deposition. *Atmospheric Chemistry and Physics,* 12**,** 591-603.

Amos, H. M., D. J. Jacob, C. D. Holmes, J. A. Fisher, Q. Wang, R. M. Yantosca, E. S. Corbitt, E. Galarneau, A. P. Rutter, M. S. Gustin, A. Steffen, J. J. Schauer, J. A. Graydon, V. L. St Louis, R. W. Talbot, E. S. Edgerton, Y. Zhang & E. M. Sunderland (2012b) Gas-particle partitioning of atmospheric Hg(II) and its effect on global mercury deposition. *Atmospheric Chemistry and Physics,* 12**,** 591-603.

Amos, H. M., D. J. Jacob, D. G. Streets & E. M. Sunderland (2013) Legacy impacts of all-time anthropogenic emissions on the global mercury cycle. *Global Biogeochemical Cycles,* 27**,** 410-421.

Amyot, M., G. A. Gill & F. M. M. Morel (1997) Production and loss of dissolved gaseous mercury in coastal seawater. *Environmental Science & Technology,* 31**,** 3606-3611.

Amyot, M., D. R. S. Lean, L. Poissant & M. R. Doyon (2000) Distribution and transformation of elemental mercury in the St. Lawrence River and Lake Ontario. *Canadian Journal of Fisheries and Aquatic Sciences,* 57**,** 155-163.

Amyot, M., G. Mierle, D. R. S. Lean & D. J. McQueen (1994) SUNLIGHT-INDUCED FORMATION OF DISSOLVED GASEOUS MERCURY IN LAKE WATERS. *Environmental Science & Technology,* 28**,** 2366-2371.

Amyot, M., G. Southworth, S. E. Lindberg, H. Hintelmann, J. D. Lalonde, N. Ogrinc, A. J. Poulain & K. A. Sandilands (2004) Formation and evasion of dissolved gaseous mercury in large enclosures amended with (HgCl2)-Hg-200. *Atmospheric Environment,* 38**,** 4279-4289.

Andrae, D., U. Haeussermann, M. Dolg, H. Stoll & H. Preuss (1990) Energy-adjustedab initio pseudopotentials for the second and third row transition elements. *Theoretical Chemistry Accounts: Theory, Computation, and Modeling (Theoretica Chimica Acta),* 77**,** 123-141.

Aquilante, F., J. Autschbach, R. K. Carlson, L. F. Chibotaru, M. G. Delcey, L. De Vico, N. Ferré, L. M. Frutos, L. Gagliardi & M. Garavelli (2016) Molcas 8: New capabilities for multiconfigurational quantum chemical calculations across the periodic table. *Journal of computational chemistry,* 37**,** 506-541.

Ariya, P. A., M. Amyot, A. Dastoor, D. Deeds, A. Feinberg, G. Kos, A. Poulain, A. Ryjkov, K. Semeniuk, M. Subir & K. Toyota (2015a) Mercury Physicochemical and Biogeochemical Transformation in the Atmosphere and at Atmospheric Interfaces: A Review and Future Directions. *Chemical Reviews,* 115**,** 3760-3802.

Ariya, P. A., M. Amyot, A. Dastoor, D. Deeds, A. Feinberg, G. Kos, A. Poulain, A. Ryjkov, K. Semeniuk, M. Subir & K. Toyota (2015b) Mercury physicochemical and biogeochemical transformation in the atmosphere and at atmospheric interfaces: A review and future directions. *Chem. Rev.,* 115**,** 3760–3802.

Baker, H. & N. Seddon (1988) Transient absorption processes in a mercury bromide laser discharge. *Journal of Physics D: Applied Physics,* 21**,** 1347.

Balabanov, N. B. & K. A. Peterson (2003) Mercury and reactive halogens: the thermochemistry of Hg+{Cl2, Br2, BrCl, ClO, and BrO}. *J. Phys. Chem. A,* 107**,** 7465-7470.

Balabanov, N. B., B. C. Shepler & K. A. Peterson (2005a) Accurate global potential energy surface and reaction dynamics for the ground state of HgBr2. *J. Phys. Chem. A,* 109**,** 8765-8773.

--- (2005b) Accurate global potential energy surface and reaction dynamics for the ground state of HgBr2. *The Journal of Physical Chemistry A,* 109**,** 8765-8773.

Barbatti, M., A. J. Aquino & H. Lischka (2010) The UV absorption of nucleobases: semi-classical ab initio spectra simulations. *Physical Chemistry Chemical Physics,* 12**,** 4959-4967.

Barbatti, M., G. Granucci, M. Persico, M. Ruckenbauer, M. Vazdar, M. Eckert-Maksić & H. Lischka (2007) The on-the-fly surface-hopping program system Newton-X: Application to ab initio simulation of the nonadiabatic photodynamics of benchmark systems. *Journal of Photochemistry and Photobiology A: Chemistry,* 190**,** 228-240.

Barbatti, M., M. Ruckenbauer, F. Plasser, J. Pittner, G. Granucci, M. Persico & H. Lischka (2014) Newton‐X: a surface‐hopping program for nonadiabatic molecular dynamics. *Wiley Interdisciplinary Reviews: Computational Molecular Science,* 4**,** 26-33.

Bash, J., A. Carlton, W. Hutzell & O. Bullock Jr. (2014a) Regional Air Quality Model Application of the Aqueous-Phase Photo Reduction of Atmospheric Oxidized Mercury by Dicarboxylic Acids. *Atmosphere,* 5**,** 1.

Bash, J. O., A. G. Carlton, W. T. Hutzell & O. R. Bullock (2014b) Regional Air Quality Model Application of the Aqueous-Phase Photo Reduction of Atmospheric Oxidized Mercury by Dicarboxylic Acids. *Atmosphere,* 5**,** 1-15.

Bergquist, B. A. & J. D. Blum (2007) Mass-dependent and -independent fractionation of hg isotopes by photoreduction in aquatic systems. *Science,* 318**,** 417-20.

Bian, H. & M. J. Prather (2002) Fast-J2: Accurate simulation of stratospheric photolysis in global chemical models. *Journal of Atmospheric Chemistry,* 41**,** 281-296.

Buxton, G. V., C. L. Greenstock, W. P. Helman & A. B. Ross (1988) Critical Review of rate constants for reactions of hydrated electrons, hydrogen atoms and hydroxyl radicals (·OH/·O− in Aqueous Solution. *Journal of Physical and Chemical Reference Data,* 17**,** 513-886.

Costa, M. & P. S. Liss (1999) Photoreduction of mercury in sea water and its possible implications for Hg(0) air-sea fluxes. *Marine Chemistry,* 68**,** 87-95.

Crespo-Otero, R. & M. Barbatti (2012) Spectrum simulation and decomposition with nuclear ensemble: formal derivation and application to benzene, furan and 2-phenylfuran. *Theoretical Chemistry Accounts,* 131**,** 1237.

Deeds, D. A., A. Ghoshdastidar, F. Raofie, E.-A. Guerette, A. Tessier & P. A. Ariya (2015a) Development of a Particle-Trap Preconcentration-Soft Ionization Mass Spectrometric Technique for the Quantification of Mercury Halides in Air. *Analytical Chemistry,* 87**,** 5109-5116.

Deeds, D. A., A. Ghoshdastidar, F. Raofie, E. l.-A. e. Guérette, A. Tessier & P. A. Ariya (2015b) Development of a particle-trap preconcentration-soft ionization mass spectrometric technique for the quantification of mercury halides in air. *Analytical chemistry,* 87**,** 5109-5116.

Del Vecchio, R. & N. V. Blough (2002) Photobleaching of chromophoric dissolved organic matter in natural waters: kinetics and modeling. *Marine Chemistry,* 78**,** 231-253.

Dibble, T. S., M. J. Zelie & Y. Jiao (2014) Quantum Chemistry Guide to PTRMS Studies of As-Yet Undetected Products of the Bromine-Atom Initiated Oxidation of Gaseous Elemental Mercury. *J. Phys. Chem. A,* 118**,** 7847-7854.

Dibble, T. S., M. J. Zelie & H. Mao (2012a) Thermodynamics of reactions of ClHg and BrHg radicals with atmospherically abundant free radicals. *Atmospheric Chemistry and Physics,* 12**,** 10271-10279.

Dibble, T. S., M. J. Zelie & H. Mao (2012b) Thermodynamics of reactions of ClHg and BrHg radicals with atmospherically abundant free radicals. *Atmos. Chem. Phys. ,* 12**,** 10271-10279.

Donohoue, D. L., D. Bauer, B. Cossairt & A. J. Hynes (2006a) Temperature and pressure dependent rate coefficients for the reaction of Hg with Br and the reaction of Br with Br: A pulsed laser photolysis-pulsed laser induced fluorescence study. *J. Phys. Chem. A,* 110**,** 6623-6632.

--- (2006b) Temperature and pressure dependent rate coefficients for the reaction of Hg with Br and the reaction of Br with Br: A pulsed laser photolysis-pulsed laser induced fluorescence study. *The Journal of Physical Chemistry A,* 110**,** 6623-6632.

Donohoue, D. L., D. Bauer & A. J. Hynes (2005) Temperature and Pressure Dependent Rate Coefficients for the Reaction of Hg with Cl and the Reaction of Cl with Cl: A Pulsed Laser Photolysis−Pulsed Laser Induced Fluorescence Study. *The Journal of Physical Chemistry A,* 109**,** 7732-7741.

Eastham, S. D., D. K. Weisenstein & S. R. Barrett (2014) Development and evaluation of the unified tropospheric–stratospheric chemistry extension (UCX) for the global chemistry-transport model GEOS-Chem. *Atmospheric Environment,* 89**,** 52-63.

ECMWF: European Centre for Medium-Range Weather Forecasts (datasets available from http://www.ecmwf.int/en/forecasts/dataset, a. F.

Emmons, L. K., S. Walters, P. G. Hess, J.-F. Lamarque, G. G. Pfister, D. Fillmore, C. Granier, A. Guenther, D. Kinnison & T. Laepple (2010) Description and evaluation of the Model for Ozone and Related chemical Tracers, version 4 (MOZART-4).

Enrico, M., G. Le Roux, N. Marusczak, L. E. Heimburger, A. Claustres, X. W. Fu, R. Y. Sun & J. E. Sonke (2016a) Atmospheric Mercury Transfer to Peat Bogs Dominated by Gaseous Elemental Mercury Dry Deposition. *Environmental Science & Technology,* 50**,** 2405-2412.

Enrico, M., G. l. L. Roux, N. Marusczak, L.-E. Heimb rger, A. Claustres, X. Fu, R. Sun & J. E. Sonke (2016b) Atmospheric mercury transfer to peat bogs dominated by gaseous elemental mercury dry deposition. *Environmental science & technology,* 50**,** 2405-2412.

Erlandson, A. C. & T. A. Cool (1983) On the regeneration mechanism of HgBr/2 in HgBr/HgBr2 dissociation lasers. *Chemical Physics Letters,* 96**,** 685-689.

Ernest, C. T., D. Donohoue, D. Bauer, A. T. Schure & A. J. Hynes (2014a) Programmable thermal dissociation of reactive gaseous mercury, a potential approach to chemical speciation: Results from a field study. *Atmosphere,* 5**,** 575-596.

Ernest, C. T., D. Donohoue, D. Bauer, A. Ter Schure & A. J. Hynes (2014b) Programmable Thermal Dissociation of Reactive Gaseous Mercury, a Potential Approach to Chemical Speciation: Results from a Field Study. *Atmosphere,* 5**,** 575-596.

Feng, X. & G. Qiu (2008) Mercury pollution in Guizhou, southwestern China - an overview. *Sci Total Environ,* 400**,** 227-37.

Fernandez, R. P., R. J. Salawitch, D. E. Kinnison, J. F. Lamarque & A. Saiz-Lopez (2014) Bromine partitioning in the tropical tropopause layer: implications for stratospheric injection. *Atmos. Chem. Phys.,* 14**,** 13391-13410.

Finley, J., P.-Å. Malmqvist, B. O. Roos & L. Serrano-Andrés (1998) The multi-state CASPT2 method. *Chemical physics letters,* 288**,** 299-306.

Frantom, G., P. Bletzinger & A. Garscadden (1980) Measurement of the ultraviolet absorption cross-section of mercuric bromide. *Bull. Am. Phys. Soc.,* 25**,** 461.

Frisch, M., G. Trucks, H. B. Schlegel, G. Scuseria, M. Robb, J. Cheeseman, G. Scalmani, V. Barone, B. Mennucci & G. Petersson. 2009. Gaussian 09, revision D. 01. Gaussian, Inc., Wallingford CT.

Fu, X., N. Marusczak, L.-E. Heimbuerger, B. Sauvage, F. Gheusi, E. M. Prestbo & J. E. Sonke (2016a) Atmospheric mercury speciation dynamics at the high-altitude Pic du Midi Observatory, southern France. *Atmospheric Chemistry and Physics,* 16**,** 5623-5639.

Fu, X. W., N. Marusczak, L. E. Heimburger, B. Sauvage, F. Gheusi, E. M. Prestbo & J. E. Sonke (2016b) Atmospheric mercury speciation dynamics at the high-altitude Pic du Midi Observatory, southern France. *Atmospheric Chemistry and Physics,* 16**,** 5623-5639.

Futsaeter, G. & S. Wilson. 2013. The UNEP Global Mercury Assessment: Sources, Emissions and Transport. In *Proceedings of the 16th International Conference on Heavy Metals in the Environment,* ed. N. Pirrone.

Garcia, E., A. J. Poulain, M. Amyot & P. A. Ariya (2005) Diel variations in photoinduced oxidation of Hg0 in freshwater. *Chemosphere,* 59**,** 977-981.

Gårdfeldt, K. & M. Jonsson (2003) Is Bimolecular Reduction of Hg(II) Complexes Possible in Aqueous Systems of Environmental Importance. *The Journal of Physical Chemistry A,* 107**,** 4478-4482.

Gårdfeldt, K., J. Sommar, R. Ferrara, C. Ceccarini, E. Lanzillotta, J. Munthe, I. Wängberg, O. Lindqvist, N. Pirrone & F. Sprovieri (2003) Evasion of mercury from coastal and open waters of the Atlantic Ocean and the Mediterranean Sea. *Atmospheric Environ.,* 37**,** 73-84.

Gardfeldt, K., J. Sommar, R. Ferrara, C. Ceccarini, E. Lanzillotta, J. Munthe, I. Wangberg, O. Lindqvist, N. Pirrone, F. Sprovieri, E. Pesenti & D. Stromberg (2003) Evasion of mercury from coastal and open waters of the Atlantic Ocean and the Mediterranean Sea. *Atmospheric Environment,* 37**,** S73-S84.

Gårdfeldt, K., J. Sommar, D. Strömberg & X. Feng (2001) Oxidation of atomic mercury by hydroxyl radicals and photoinduced decomposition of methylmercury in the aqueous phase. *Atmospheric Environment,* 35**,** 3039-3047.

Gardfeldt, K., J. Sommar, D. Stromberg & X. B. Feng (2001) Oxidation of atomic mercury by hydroxyl radicals and photoinduced decomposition of methylmercury in the aqueous phase. *Atmospheric Environment,* 35**,** 3039-3047.

Gent, P. R., G. Danabasoglu, L. J. Donner, M. M. Holland, E. C. Hunke, S. R. Jayne, D. M. Lawrence, R. B. Neale, P. J. Rasch & M. Vertenstein (2011) The community climate system model version 4. *Journal of Climate,* 24**,** 4973-4991.

Goodsite, M. E., J. Plane & H. Skov (2004) A theoretical study of the oxidation of Hg0 to HgBr2 in the troposphere. *Environ. Sci. Technol.,* 38**,** 1772-1776.

Gustafsson, J. P. (2001) Modeling the Acid–Base Properties and Metal Complexation of Humic Substances with the Stockholm Humic Model. *Journal of Colloid and Interface Science,* 244**,** 102-112.

Haitzer, M., G. R. Aiken & J. N. Ryan (2002a) Binding of Mercury(II) to Dissolved Organic Matter: The Role of the Mercury-to-DOM Concentration Ratio. *Environmental Science & Technology,* 36**,** 3564-3570.

Haitzer, M., G. R. Aiken & J. N. Ryan (2002b) Binding of mercury(II) to dissolved organic matter: The role of the mercury-to-DOM concentration ratio. *Environmental Science & Technology,* 36**,** 3564-3570.

Holmes, C. D., D. J. Jacob & X. Yang (2006a) Global lifetime of elemental mercury against oxidation by atomic bromine in the free troposphere. *Geophys. Res. Lett.,* 33.

Holmes, C. D., D. J. Jacob & X. Yang (2006b) Global lifetime of elemental mercury against oxidation by atomic bromine in the free troposphere. *Geophysical Research Letters,* 33.

Horowitz, H. M., D. J. Jacob, Y. Zhang, T. S. Dibble, F. Slemr, H. M. Amos, J. A. Schmidt, E. S. Corbitt, E. A. Marais & E. M. Sunderland (2017a) A new mechanism for atmospheric mercury redox chemistry: Implications for the global mercury budget. *Atmos. Chem. Phys.,* 17**,** 6353–6371.

Horowitz, H. M., D. J. Jacob, Y. X. Zhang, T. S. Dibble, F. Slemr, H. M. Amos, J. A. Schmidt, E. S. Corbitt, E. A. Marais & E. M. Sunderland (2017b) A new mechanism for atmospheric mercury redox chemistry: implications for the global mercury budget. *Atmospheric Chemistry and Physics,* 17**,** 6353-6371.

Horvath, O. & A. Vogler (1993) Photoredox chemistry of chloromercurate(II) complexes in acetonitrile. *Inorganic Chemistry,* 32**,** 5485-5489.

Jiang, T., U. Skyllberg, S. Wei, D. Wang, S. Lu, Z. Jiang & D. C. Flanagan (2015) Modeling of the structure-specific kinetics of abiotic, dark reduction of Hg(II) complexed by O/N and S

functional groups in humic acids while accounting for time-dependent structural rearrangement. *Geochimica Et Cosmochimica Acta,* 154**,** 151-167.

Jiao, Y. & T. S. Dibble (2015) Quality Structures, Vibrational Frequencies, and Thermochemistry of the Products of Reaction of BrHg• with NO2, HO2, ClO, BrO, and IO. *J. Phys. Chem. A,* 119**,** 10502-10510.

--- (2017a) First kinetic study of the atmospherically important reactions BrHg˙+ NO 2 and BrHg˙+ HOO. *Phys. Chem. Chem. Phys.,* 19**,** 1826-1838.

--- (2017b) First kinetic study of the atmospherically important reactions BrHg˙+ NO 2 and BrHg˙+ HOO. *Physical Chemistry Chemical Physics,* 19**,** 1826-1838.

Jiskra, M., J. E. Sonke, D. Obrist, J. Bieser, R. Ebinghaus, C. L. Myhre, K. A. Pfaffhuber, I. Wängberg, K. Kyllönen & D. Worthy (2018a) A vegetation control on seasonal variations in global atmospheric mercury concentrations. *Nat. Geosci.***,** 1.

Jiskra, M., J. E. Sonke, D. Obrist, J. Bieser, R. Ebinghaus, C. L. Myhre, K. A. Pfaffhuber, I. Wangberg, K. Kyllonen, D. Worthy, L. G. Martin, C. Labuschagne, T. Mkololo, M. Ramonet, O. Magand & A. Dommergue (2018b) A vegetation control on seasonal variations in global atmospheric mercury concentrations. *Nature Geoscience,* 11**,** 244-+.

Kessler, R. (2013) The Minamata Convention on Mercury: A First Step toward Protecting Future Generations. *Environmental Health Perspectives,* 121**,** A304-A309.

Lalonde, J. D., M. Amyot, J. Orvoine, F. M. M. Morel, J. C. Auclair & P. A. Ariya (2004) Photoinduced oxidation of Hg-0 (aq) in the waters from the St. Lawrence estuary. *Environmental Science & Technology,* 38**,** 508-514.

Lin, C.-j. & S. O. Pehkonen (1997) Aqueous free radical chemistry of mercury in the presence of iron oxides and ambient aerosol. *Atmospheric Environment,* 31**,** 4125-4137.

--- (1998) Two-phase model of mercury chemistry in the atmosphere. *Atmospheric Environment,* 32**,** 2543-2558.

Lin, C.-J. & S. O. Pehkonen (1999a) The chemistry of atmospheric mercury: a review. *Atmospheric Environment,* 33**,** 2067-2079.

Lin, C. J. & S. O. Pehkonen (1999b) The chemistry of atmospheric mercury: a review. *Atmospheric Environment,* 33**,** 2067-2079.

Lindqvist, O., K. Johansson, L. Bringmark, B. Timm, M. Aastrup, A. Andersson, G. Hovsenius, L. Håkanson, Å. Iverfeldt & M. Meili (1991) Mercury in the Swedish environment—recent research on causes, consequences and corrective methods. *Water Air Soil Pollut.,* 55**,** xi-261.

Liu, G., Y. Cai & N. O'Driscoll. 2012. *Environmental chemistry and toxicology of mercury*. Hoboken: John Wiley & Sons, Inc.

Maizel, A. C. & C. K. Remucal (2017) Molecular Composition and Photochemical Reactivity of Size-Fractionated Dissolved Organic Matter. *Environ Sci Technol,* 51**,** 2113-2123.

Marusczak, N., J. E. Sonke, X. W. Fu & M. Jiskra (2017) Tropospheric GOM at the Pic du Midi Observatory-Correcting Bias in Denuder Based Observations. *Environmental Science & Technology,* 51**,** 863-869.

Mason, R. P., A. L. Choi, W. F. Fitzgerald, C. R. Hammerschmidt, C. H. Lamborg, A. L. Soerensen & E. M. Sunderland (2012) Mercury biogeochemical cycling in the ocean and policy implications. *Environmental Research,* 119**,** 101-117.

Mason, R. P., F. M. M. Morel & H. F. Hemond (1995) THE ROLE OF MICROORGANISMS IN ELEMENTAL MERCURY FORMATION IN NATURAL-WATERS. *Water Air and Soil Pollution,* 80**,** 775-787.

Maya, J. (1977) Ultraviolet absorption cross sections of HgI2, HgBr2, and tin (II) halide vapors. *The Journal of Chemical Physics,* 67**,** 4976-4980.

Monperrus, M., E. Tessier, D. Amouroux, A. Leynaert, P. Huonnic & O. F. X. Donard (2007) Mercury methylation, demethylation and reduction rates in coastal and marine surface waters of the Mediterranean Sea. *Marine Chemistry,* 107**,** 49-63.

Munthe, J. (1992a) The aqueous oxidation of elemental mercury by ozone. *Atmospheric Environ.,* 26**,** 1461-1468.

--- (1992b) The aqueous oxidation of elemental mercury by ozone. *Atmospheric Environment. Part A. General Topics,* 26**,** 1461-1468.

Munthe, J., Z. F. Xiao & O. Lindqvist (1991a) The aqueous reduction of divalent mercury by sulfite *Water Air and Soil Pollution,* 56**,** 621-630.

--- (1991b) The aqueous reduction of divalent mercury by sulfite. *Water Air & Soil Pollution,* 56**,** 621-630.

O'Driscoll, N. J., S. D. Siciliano, D. R. S. Lean & M. Amyot (2006) Gross photoreduction kinetics of mercury in temperate freshwater lakes and rivers: Application to a general model of DGM dynamics. *Environmental Science & Technology,* 40**,** 837-843.

Obrist, D., J. L. Kirk, L. Zhang, E. M. Sunderland, M. Jiskra & N. E. Selin (2018) A review of global environmental mercury processes in response to human and natural perturbations: Changes of emissions, climate, and land use. *Ambio,* 47**,** 116-140.

Ordóñez, C., J. F. Lamarque, S. Tilmes, D. E. Kinnison, E. L. Atlas, D. R. Blake, G. Sousa Santos, G. Brasseur & A. Saiz-Lopez (2012) Bromine and iodine chemistry in a global chemistry-climate model: description and evaluation of very short-lived oceanic sources. *Atmos. Chem. Phys.,* 12**,** 1423-1447.

Parrella, J., D. J. Jacob, Q. Liang, Y. Zhang, L. J. Mickley, B. Miller, M. Evans, X. Yang, J. Pyle & N. Theys (2012) Tropospheric bromine chemistry: implications for present and pre-industrial ozone and mercury. *Atmospheric Chemistry and Physics,* 12**,** 6723-6740.

Pehkonen, S. O. & C.-J. Lin (1998a) Aqueous photochemistry of mercury with organic acids. *Journal of the Air & Waste Management Association,* 48**,** 144-150.

--- (1998b) Aqueous photochemistry of mercury with organic acids. *J. Air. Waste. Manag. Assoc.,* 48**,** 144-150.

Peleg, M., E. Tas, D. Obrist, V. Matveev, C. Moore, M. Gabay & M. Luria (2015) Observational Evidence for Involvement of Nitrate Radicals in Nighttime Oxidation of Mercury. *Environmental Science & Technology,* 49**,** 14008-14018.

Peterson, K. A., D. Figgen, E. Goll, H. Stoll & M. Dolg (2003) Systematically convergent basis sets with relativistic pseudopotentials. II. Small-core pseudopotentials and correlation consistent basis sets for the post-d group 16–18 elements. *The Journal of chemical physics,* 119**,** 11113-11123.

Prados-Roman, C., C. A. Cuevas, R. P. Fernandez, D. E. Kinnison, J. F. Lamarque & A. Saiz-Lopez (2015) A negative feedback between anthropogenic ozone pollution and enhanced ocean emissions of iodine. *Atmos. Chem. Phys.,* 15**,** 2215-2224.

Qureshi, A., M. MacLeod, E. Sunderland & K. Hungerbühler. 2011a. Exchange of Elemental Mercury between the Oceans and the Atmosphere. In *Environmental Chemistry and Toxicology of Mercury*, 389-421. John Wiley & Sons, Inc.

Qureshi, A., M. MacLeod, E. M. Sunderland & H. Konrad. 2011b. Exchange of Elemental Mercury between the Oceans and the Atmosphere. In *In Environmental Chemistry and Toxicology of Mercury; Liu, G.; Cai, Y.; O'Driscoll, N. J., Eds.; John Wiley & Sons, Inc: Hoboken, NJ*, PP 389-421.

Ravichandran, M. (2004) Interactions between mercury and dissolved organic matter--a review. *Chemosphere,* 55**,** 319-31.

Richard, J. H., C. Bischoff & H. Biester (2016) Comparing Modeled and Measured Mercury Speciation in Contaminated Groundwater: Importance of Dissolved Organic Matter Composition. *Environmental Science & Technology,* 50**,** 7508-7516.

Rolfhus, K. R. & W. F. Fitzgerald (2004) Mechanisms and temporal variability of dissolved gaseous mercury production in coastal seawater. *Marine Chemistry,* 90**,** 125-136.

Roos, B. O., R. Lindh, P.-Å. Malmqvist, V. Veryazov & P.-O. Widmark (2004) Main group atoms and dimers studied with a new relativistic ANO basis set. *The Journal of Physical Chemistry A,* 108**,** 2851-2858.

Roxlo, C. & A. Mandl (1980) Vacuum ultraviolet absorption cross sections for halogen containing molecules. *Journal of Applied Physics,* 51**,** 2969-2972.

Saiz-Lopez, A., S. Baidar, C. A. Cuevas, T. K. Koenig, R. P. Fernandez, B. Dix, D. E. Kinnison, J. F. Lamarque, X. Rodriguez-Lloveras, T. L. Campos & R. Volkamer (2015) Injection of iodine to the stratosphere. *Geophys. Res. Lett.,* 42**,** 6852-6859.

Saiz-Lopez, A., R. P. Fernandez, C. Ordóñez, D. E. Kinnison, J. C. Gómez Martín, J. F. Lamarque & S. Tilmes (2014) Iodine chemistry in the troposphere and its effect on ozone. *Atmos. Chem. Phys.,* 14**,** 13119-13143.

Saiz-Lopez, A., S. P. Sitkiewicz, D. Roca-Sanjuan, J. M. Oliva-Enrich, J. Z. Davalos, R. Notario, M. Jiskra, Y. Xu, F. Wang, C. P. Thackray, E. M. Sunderland, D. J. Jacob, O. Travnikov, C. A. Cuevas, A. U. Acuna, D. Rivero, J. M. C. Plane, D. E. Kinnison & J. E. Sonke (2018) Photoreduction of gaseous oxidized mercury changes global atmospheric mercury speciation, transport and deposition. *Nature Communications,* 9.

Schilowitz, A. M. & J. R. Wiesenfeld (1982) Time-resolved study of mercury atom production and removal following the photolysis of HgBr2 at 193 nm. *Chemical Physics Letters,* 89**,** 438-442.

Schimitschek, E., J. Celto & J. A. Trias (1977) Mercuric bromide photodissociation laser. *Applied Physics Letters,* 31**,** 608-610.

Schmidt, J. A., D. Jacob, H. M. Horowitz, L. Hu, T. Sherwen, M. J. Evans, Q. Liang, R. M. Suleiman, D. Oram & M. Le Breton (2016) Modeling the observed tropospheric BrO background: Importance of multiphase chemistry and implications for ozone, OH, and mercury. *Journal of Geophysical Research: Atmospheres,* 121.

Schroeder, W. H. & J. Munthe (1998) Atmospheric mercury - An overview. *Atmospheric Environment,* 32**,** 809-822.

Schuster, P. F., K. M. Schaefer, G. R. Aiken, R. C. Antweiler, J. F. Dewild, J. D. Gryziec, A. Gusmeroli, G. Hugelius, E. Jafarov & D. P. Krabbenhoft (2018) Permafrost stores a globally significant amount of mercury. *Geophys. Res. Lett.,* 45**,** 1463-1471.

Seigneur, C., K. Vijayaraghavan & K. Lohman (2006a) Atmospheric mercury chemistry: Sensitivity of global model simulations to chemical reactions. *J. Geophys. Res. Atmos.,* 111**,** D22306.

--- (2006b) Atmospheric mercury chemistry: Sensitivity of global model simulations to chemical reactions. *Journal of Geophysical Research-Atmospheres,* 111.

Selin, N. E. (2009) Global Biogeochemical Cycling of Mercury: A Review. *Annual Review of Environment and Resources,* 34**,** 43-63.

Selin, N. E., D. J. Jacob, R. J. Park, R. M. Yantosca, S. Strode, L. Jaegle & D. Jaffe (2007a) Chemical cycling and deposition of atmospheric mercury: Global constraints from observations. *Journal of Geophysical Research-Atmospheres,* 112.

Selin, N. E., D. J. Jacob, R. J. Park, R. M. Yantosca, S. Strode, L. Jaeglé & D. Jaffe (2007b) Chemical cycling and deposition of atmospheric mercury: Global constraints from observations. *Journal of Geophysical Research: Atmospheres,* 112.

--- (2007c) Chemical cycling and deposition of atmospheric mercury: Global constraints from observations. *J. Geophys. Res. Atmos.,* 112.

Shepler, B. C., N. B. Balabanov & K. A. Peterson (2007) Hg+ Br→ Hg Br recombination and collision-induced dissociation dynamics. *J. Chem. Phys,* 127**,** 164304.

Shia, R. L., C. Seigneur, P. Pai, M. Ko & N. D. Sze (1999a) Global simulation of atmospheric mercury concentrations and deposition fluxes. *Journal of Geophysical Research-Atmospheres,* 104**,** 23747-23760.

Shia, R. L., C. Seigneur, P. Pai, M. Ko & N. D. Sze (1999b) Global simulation of atmospheric mercury concentrations and deposition fluxes. *J. Geophys. Res. Atmos.,* 104**,** 23747-23760.

Si, L. & P. Ariya (2018) Recent Advances in Atmospheric Chemistry of Mercury. *Atmosphere,* 9**,** 76.

Si, L. & P. A. Ariya (2008a) Reduction of Oxidized Mercury Species by Dicarboxylic Acids (C2−C4): Kinetic and Product Studies. *Environmental Science & Technology,* 42**,** 5150-5155.

Si, L. & P. A. Ariya (2008b) Reduction of oxidized mercury species by dicarboxylic acids (C(2)-C(4)): Kinetic and product studies. *Environmental Science & Technology,* 42**,** 5150-5155.

Siciliano, S. D., N. J. O'Driscoll & D. R. S. Lean (2002) Microbial reduction and oxidation of mercury in freshwater lakes. *Environmental Science & Technology,* 36**,** 3064-3068.

Sitkiewicz, S. P., J. M. Oliva, J. Z. Dávalos, R. Notario, A. Saiz–Lopez, D. R. Alcoba, O. B. Oña & D. Roca-Sanjuán (2016a) Ab initio quantum–chemical computations of the electronic states in HgBr2 and IBr: Molecules of interest on the Earth's atmosphere. *J. Chem. Phys.,* 145**,** 244304.

--- (2016b) Ab initio quantum–chemical computations of the electronic states in HgBr2 and IBr: Molecules of interest on the Earth's atmosphere. *The Journal of chemical physics,* 145**,** 244304.

Skamarock, W. C., J. B. Klemp, J. Dudhia, D. O. Gill, D. M. Barker, W. Wang & J. G. Powers. 2005. A description of the advanced research WRF version 2. National Center For Atmospheric Research Boulder Co Mesoscale and Microscale Meteorology Div.

Smith-Downey, N. V., E. M. Sunderland & D. J. Jacob (2010) Anthropogenic impacts on global storage and emissions of mercury from terrestrial soils: Insights from a new global model. *Journal of Geophysical Research-Biogeosciences,* 115.

Soerensen, A. L., E. M. Sunderland, C. D. Holmes, D. J. Jacob, R. M. Yantosca, H. Skov, J. H. Christensen, S. A. Strode & R. P. Mason (2010) An improved global model for air-sea exchange of mercury: High concentrations over the North Atlantic. *Environmental science & technology,* 44**,** 8574-8580.

Sonke, J. E. (2011) A global model of mass independent mercury stable isotope fractionation. *Geochimica et Cosmochimica Acta,* 75**,** 4577-4590.

Sprovieri, F., N. Pirrone, M. Bencardino, F. D'Amore, H. Angot, C. Barbante, E.-G. Brunke, F. Arcega-Cabrera, W. Cairns & S. Comero (2017) Five-year records of mercury wet deposition flux at GMOS sites in the Northern and Southern hemispheres. *Atmospheric Chemistry and Physics,* 17**,** 2689-2708.

Streets, D. G., H. M. Horowitz, D. Jacob, Z. Lu, L. Levin, A. F. H. ter Schure & E. M. Sunderland (2017) Total Mercury Released to the Environment by Human Activities. *Environmental Science & Technology,* 51**,** 5969-5977.

Strömberg, D., A. Strömberg & U. Wahlgren (1991) Relativistic quantum calculations on some mercury sulfide molecules. *Water Air Soil Pollut.,* 56**,** 681-695.

Suess, E., F. Aemisegger, J. E. Sonke, M. Sprenger, H. Wernli & L. H. E. Winkel (2019) Marine versus Continental Sources of Iodine and Selenium in Rainfall at Two European High-Altitude Locations. *Environmental Science & Technology,* 53**,** 1905-1917.

Tipping, E. (2007) Modelling the interactions of Hg(II) and methylmercury with humic substances using WHAM/Model VI. *Applied Geochemistry,* 22**,** 1624-1635.

Travnikov, O. (2005) Contribution of the intercontinental atmospheric transport to mercury pollution in the Northern Hemisphere. *Atmospheric Environment,* 39**,** 7541-7548.

Travnikov, O., H. Angot, P. Artaxo, M. Bencardino, J. Bieser, F. D'Amore, A. Dastoor, F. De Simone, M. del Carmen Diéguez & A. Dommergue (2017) Multi-model study of mercury dispersion in the atmosphere: atmospheric processes and model evaluation. *Atmospheric Chem. Phys.,* 17**,** 5271.

Travnikov, O. & I. Ilyin. 2009. The EMEP/MSC-E mercury modeling system. In *Mercury Fate and Transport in the Global Atmosphere*, 571-587. Springer.

Travnikov, O. & A. Ryaboshapko (2002) Modelling of mercury hemispheric transport and deposition

Tyndall, G. S. & A. R. Ravishankara (1991) Atmospheric oxidation of reduced sulfur species *International Journal of Chemical Kinetics,* 23**,** 483-527.

UNEP (2013a) Global Mercury Assessment 2013: Sources, Emissions, Releases and Environmental Transport.

--- (2013b) Minamata Convention on Mercury.

Van Loon, L., E. Mader & S. L. Scott (2000a) Reduction of the Aqueous Mercuric Ion by Sulfite: UV Spectrum of HgSO3 and Its Intramolecular Redox Reaction. *The Journal of Physical Chemistry A,* 104**,** 1621-1626.

Van Loon, L., E. Mader & S. L. Scott (2000b) Reduction of the aqueous mercuric ion by sulfite: UV spectrum of HgSO3 and its intramolecular redox reaction. *Journal of Physical Chemistry A,* 104**,** 1621-1626.

Wadt, W. R. (1980) The electronic structure of HgCl2 and HgBr2 and its relationship to photodissociation. *The Journal of Chemical Physics,* 72**,** 2469-2478.

Wang, F., A. Saiz-Lopez, A. S. Mahajan, J. C. Gómez Martín, D. Armstrong, M. Lemes, T. Hay & C. Prados-Roman (2014a) Enhanced production of oxidised mercury over the tropical Pacific Ocean: A key missing oxidation pathway. *Atmos. Chem. Phys.,* 14**,** 1323–1335.

Wang, F., A. Saiz-Lopez, A. S. Mahajan, J. C. G. Martin, D. Armstrong, M. Lemes, T. Hay & C. Prados-Roman (2014b) Enhanced production of oxidised mercury over the tropical Pacific Ocean: a key missing oxidation pathway. *Atmospheric Chemistry and Physics,* 14**,** 1323-1335.

Wang, Z. & S. O. Pehkonen (2004) Oxidation of elemental mercury by aqueous bromine: atmospheric implications. *Atmospheric Environment,* 38**,** 3675-3688.

Weigend, F. & R. Ahlrichs (2005) Balanced basis sets of split valence, triple zeta valence and quadruple zeta valence quality for H to Rn: Design and assessment of accuracy. *Physical Chemistry Chemical Physics,* 7**,** 3297-3305.

Whitehurst, C. & T. King (1987) Emission spectroscopy of mixed photodissociated mercury halides. *Journal of Physics D: Applied Physics,* 20**,** 1577.

Wilcomb, B., R. Burnham & N. Djeu (1980) UV absorption cross section and fluorescence efficiency of HgBr2. *Chemical Physics Letters,* 75**,** 239-242.

Wilcox, J. (2009) A Kinetic Investigation of High-Temperature Mercury Oxidation by Chlorine. *The Journal of Physical Chemistry A,* 113**,** 6633-6639.

Wolfe, M. F., S. Schwarzbach & R. A. Sulaiman (1998) Effects of mercury on wildlife: A comprehensive review. *Environmental Toxicology and Chemistry,* 17**,** 146-160.

Xiao, Z., J. Munthe, D. Strömberg & O. Lindqvist (1994) Photochemical behaviour of inorganic mercury compounds in aqueous solution. *Mercury Pollution; Integration and Synthesis, CJ Watras and JW Huckabee (Eds.)***,** 581-592.

Xiao, Z. F., D. Stromberg & O. Lindqvist (1995) Influence of humic substances on photolysis of divalent mercury in aqueous solution. *Water Air and Soil Pollution,* 80**,** 789-798.

Zhang, H. 2006. Photochemical redox reactions of mercury. In *Recent Developments in Mercury Science,* ed. D. A. Atwood, 37-79.

Zhang, H. & S. E. Lindberg (2001) Sunlight and iron(III)-induced photochemical production of dissolved gaseous mercury in freshwater. *Environmental Science & Technology,* 35**,** 928-935.

Zheng, W. & H. Hintelmann (2009) Mercury isotope fractionation during photoreduction in natural water is controlled by its Hg/DOC ratio. *Geochimica et Cosmochimica Acta,* 73**,** 6704-6715.

Une étude expérimentale de la photoréduction du mercure atmosphérique dans des eaux de pluie et son implication potentielle pour le modèle global de mercure atmosphérique

An experimental study of atmospheric mercury photoreduction in rainfall and its potential implication for global atmospheric mercury model

AUTEUR: Xu YANG

DIRECTEUR: Jeroen SONKE

DISCIPLINE: Géochimie d'Environnement

SOUTENANCE: Le 19 Novembre 2019 au GET

LABORATOIRE: laboratoire Géosciences Environnement Toulouse (GET) UMR 5563,
Université Paul Sabatier/CNRS/IRD, 14 avenue Edouard Belin
31400 Toulouse, France

Résumé:

La photoréduction atmosphérique du Hg pourrait avoir lieu à la fois en phase gazeuse et aqueuse. Les taux de photoréduction du Hg(II) que nous observons dans l'eau de pluie, en condition d'ensoleillement total, sont d'un ordre de grandeur inférieur au taux optimisé de photoréduction dans les nuages >1.0 h^{-1} dans les modèles globaux de mercure. La photoréduction aqueuse de mercure dans l'atmosphère est trop lente pour constituer une voie de réduction dominante. Les formes $HgBr_2$, $HgCl_2$, $HgBrNO_2$, $HgBrHO_2$ gazeuses atmosphériques, balayées par les aérosols aqueux et les gouttelettes de nuages, sont converties en formes de Hg(II)-DOC dans les précipitations en raison de l'abondance de carbone organique dans les aérosols et de l'eau de nuages. Des calculs théoriques montrent que les taux de photolyse en phase gazeuse de composés de mercure(II) peuvent être suffisamment rapide pour rééquilibrer le cycle de mercure atmosphérique modélisé.

Mots clés: Mercure, eau de pluie, taux de photoréduction, phase gazeuse, phase aqueuse, modèle atmosphérique

---

Abstract:

Atmospheric Hg photoreduction could take place in both gas- and aqueous phase. Rainwater Hg(II) photoreduction rates, under fully sunlit conditions, are an order of magnitude slower than the optimized maximum in-cloud photoreduction rate of > 1.0 h^{-1} in global Hg models. Atmospheric aqueous Hg photoreduction is too slow to be dominant reduction pathway. Atmospheric gaseous $HgBr_2$, $HgCl_2$, $HgBrNO_2$, $HgBrHO_2$ forms, scavenged by aqueous aerosols and cloud droplets, are converted to Hg(II)-DOC forms in rainfall due to abundant organic carbon in aerosols and cloud water. Computation of gas phase photolysis rates of Hg(II) compounds can be fast, and is fast enough to rebalance the modeled atmospheric Hg cycle between Hg(0) oxidation and Hg(II) reduction.

Keywords: Mercury, rain water, photoreduction rate, gas phase, aqueous phase, atmospheric model.
